NOTE TO USERS

Impedance-based Detection of DNA Sequences Using A Silicon Transducer with PNA as the Probe Layer

Alvira Macanovic

A Thesis

In

The Department

Of

Chemistry and Biochemistry

Presented in Partial Fulfillment of the Requirements

For the Degree of Doctor of Philosophy at

Concordia University, Montreal, Quebec, Canada

September 2004

Your file Votre référence
ISBN: 0-612-96940-1
Our file Notre référence
ISBN: 0-612-96940-1

Abstract

Impedance-based Detection of DNA Sequences Using A Silicon Transducer with PNA as the Probe Layer

Alvira Macanovic, Ph.D.
Concordia University 2004

Electrochemical impedance measurements were used for the detection of single-strand DNA sequences using a peptide nucleic acid (PNA) probe layer immobilized onto Si/SiO_2 chips. In our approach, the PNA is covalently linked to the surface of Si/SiO_2 chips that have been functionalized with a silane, 3-glycidoxypropyltrimethoxysilane (GPTS). The functionalization procedure has been optimized to ensure maximum available sites for probe attachment. The PNA probe is hybridized with complementary solution-phase target DNA.

Impedance measurements allow for the detection of the changes in charge distribution at the oxide/solution interface following modifications to the oxide surface. Due to these modifications, there are significant shifts in the semiconductor's flat-band potential after immobilization and hybridization. The results obtained using this direct and rapid approach are supported by fluorescence measurements according to classical methods for the detection of nucleic acid sequences.

One of the main challenges to achieving highly reproducible and more sensitive silicon-based sensor devices is the optimization of the probe layer immobilization procedures. Hybridization may be kinetically or sterically hindered at high surface probe densities. Varying the amount of time that the solid support is exposed to the PNA solution and controlling the probe solution concentration can control the probe density of

the probe layer. Fifteen minutes for immobilization appears to be sufficient enough to obtain a single strand layer with a good balance between density and steric hindrance.

The second focus of this thesis is the determination of the melting temperature (T_m) of a complex sequence PNA 10-mer by measuring the impedance of the electrochemical system at different temperatures. The T_m for perfect matched duplexes is 52.2 ± 0.3°C. This compared well to the theoretical one of 50 °C. The introduction of a single base mismatch in the complementary DNA oligomer results in a 13°C lowering of the observed T_m. The T_m for a single base mismatch is 39.7 ± 0.6°C.

Acknowledgements

I would like to thank Dr. Marcus Lawrence for his guidance, help, and support during my Ph.D. I wish to thank the members of my research committee, Dr. P.H. Bird and Dr. S. Robidoux for all of their help.

I would especially like to thank Carole Coutts for all of her help. I cannot express enough how much your kindness is appreciated. I would also like to thank my friends, Rupa, Vina, and Cathy. It is nice to know that I always have friends that I can count on for help and support.

Finally, I would like to thank my mother for everything. Your support and belief in me has always been a constant in my life. I could never have done this without your encouragement.

To my father, Alex Macanovic.

Table of Contents

List of Figures

List of Tables

List of Schemes

List of Abbreviations

A	adenine
AC	alternating current
C	cytosine
DC	direct current
d-d	deionized-distilled
DNA	deoxyribonucleic acid
DPEA	diisopropylethylamine
E_c	conduction band energy
E_f	Fermi level energy
E_g	band gap energy
EIS	electrolyte / insulator / semiconductor
E_v	valence band energy
G	guanine
GPTS	glycidoxypropyltrimethoxysilane
PNA	peptide nucleic acid
QCM	quartz crystal microbalance
RNA	ribonucleic acid
Si/SiO_2	silicon/silicon dioxide
ss	single-stranded
T	thymine
T_m	melting temperature
V_{fb}	flat-band potential

XPS	x-ray photoelectron spectroscopy
Z_I	out-of-phase impedance

CHAPTER 1

INTRODUCTION

1.1 Project Goals and Thesis Outline

Since the advent of biosensors, various fields of research have been revolutionized. The greatest impact of this technology has been in the area of DNA diagnostics. Its potential in medicine is extensive. Biosensors can be used to detect disease-causing and food-contaminating organisms, detect and characterize viruses, bacteria, and parasites, determine identity in forensic and environmental cases, perform assays in the oncogenic field, and DNA sequence determination (1-12). Most specifically, with the completion of the human genome project, the way we treat and diagnose disease will be revolutionized. Biosensors have tremendous promise for the effectiveness in the testing for genetic disease. We now know many of the single nucleotide polymorphisms that are responsible for many inherited diseases such as hypertension and diabetes. By knowing that an individual is at risk to develop any inherited disease, we can treat them in the early stages of illness, or most significantly, prevent the disease.

Major efforts are currently being devoted to the development of devices allowing the direct (non-labelled) and rapid detection of genetic materials in liquid media. These techniques rely on the specific affinity inherent to the hybridization between single-strand DNA (ssDNA) sequences, and their complementary counterparts as probe layer affixed to the surface of a transducer. Approaches to direct signal generation that have received much attention in recent years include surface plasmon resonance (13-21), acoustic network analysis (22-24) and quartz crystal microbalance (QCM) (25-29). In addition,

the feasibility of using electrochemical techniques for the detection of biomolecules (30-36), especially that based on impedance and/or field effect measurements (37-42) is now well established because of their promise for rapid, simple and inexpensive detection systems.

Initial reports by our group in this area describe an electrochemical approach to detecting the hybridization of complementary strands using Si/SiO_2 substrates as transducer, and simple homooligonucleotide sequences as probes (43-46). This particular approach involves measuring variations in electrical impedance. The functionalized Si/SiO_2 /ss-DNA/electrolyte structure allows direct detection of the hybridization process as one monitors the variation in capacitance caused by the changes occurring within the ss-DNA probe layer.

One of the main challenges to achieving highly reproducible and more sensitive silicon-based sensor devices is the optimization of the probe layer immobilization procedures, to achieve probe layer uniformity, and the nature of the probe layer itself. Most DNA biosensors are not capable of the high selectivity necessary for the detection of disease-related point mutations. In recent years, sequence specificity has been achieved using peptide nucleic acid (PNA) probe layers (47, 48). Our biosensor uses the electrochemical impedance approach for the detection of single-strand DNA sequences using a PNA probe layer immobilized onto Si/SiO_2 chips, and the detection of its hybridization with complementary DNA.

This technology will be used to measure a specific DNA sequence melting temperature (T_m). The hybridized oligonucleotide immobilized on the surface of the Si/SiO_2 electrode can be thermally dehybridized. This denaturation will be recorded by

measuring the impedance of the electrochemical system at different temperatures. A rapid determination of the T_m for DNA hybridized with immobilized known sequences can provide a powerful tool to detect base mutations in gene sequences. The reliability of the melting temperature measurements will be studied.

Our detection system has several advantages making it a superior sensor to the traditional DNA sensors. Most significantly, our method allows for direct, in situ detection of specific sequences. Other techniques are not practical in that they require labeled DNA probes (enzymatically labeled with radioisotopes such as ^{32}P or ^{125}I or fluorescent tags) and their reaction and detection steps are separate. These factors make in situ, real-time monitoring impossible. Our detection system provides rapid detection (5-10 minutes per measurement) of oligonucleotides. This is advantageous because this device could help to reduce the time needed for diagnosis. Very simple equipment is needed to perform electrochemical measurements and to determine the melting temperature. As a result, this method provides ease of use by non-expert personnel or as a completely automated system. This method uses Si/SiO_2 semiconductor/oxide chips as working electrodes, based on well developed silicon technology; and allows for miniaturization to then fabricate high density arrays (ease of fabrication). Cost reduction using this sensor is also practicable because it requires inexpensive equipment and materials.

1.2 Biosensors

There are two methods for the detection of specific gene sequences: direct sequencing or DNA hybridization. However, the DNA hybridization method is preferred because of its simplicity.

Biosensors are devices that are small in size and consist of a biological recognition element and transducer (49, 50). The biological recognition element is a probe used to selectively detect the target analyte. The sensitive transducer is used to translate this biorecognition event into an electrical signal. Common transducing elements are optical, electrochemical, and mass-sensitive devices, converting the recognition event into light, current, or frequency signals, respectively (50).

There are two types of biosensors. Bioaffinity devices involve the selective binding of the target analyte to a ligand that is bound to the surface of the transducer (i.e. antibody, oligonucleotide). The biocatalytic sensor consists of an enzyme bound to the transducer surface that recognizes the target. The most common type of biocatalytic sensor is the sensor strips used for monitoring of diabetes that have glucose oxidase bound to them. The glucose oxidase enzyme converts the glucose analyte into hydrogen peroxide. The hydrogen peroxide is electrochemically detected by the electrochemical transducer (50).

1.2.1 Sequence-specific hybridization biosensors

DNA biosensors are of particular interest. The biological recognition element is ssDNA or for our purposes, ssPNA referred to as probe. The probe is immobilized either

covalently or via adsorption onto different signal transducers. The probe most frequently is about 15 to 50 bases long (51). The target gene sequence is recognized by the probe forming a double-stranded hybrid (PNA-DNA) with its complementary nucleic acid (target sequence) in the presence of a mixture of much different, non-complementary nucleic acid. The hybridization of the probe with the target complementary DNA can be detected either by some type of hybridization indicator or by examining the changes that result from the binding. Following hybridization, the transducer converts this event into a signal.

There are two requirements for a DNA biosensor to be considered successful. The sensor must exhibit sensitivity and the probe must bind selectively and specifically (including when there is the introduction of a single base mismatch) with a particular sequence of DNA with high efficiency. This is the advantage to using PNA probes. PNA probes have higher specificity, hybridize faster at room and elevated temperatures, low ionic strengths are required for hybridization, and shorter probes can be used (52).

Immobilization of the probe onto the transducer surface causes a loss in configurational freedom. This affects the efficiency of hybridization. To maintain efficient hybridization, one strategy is to attach the probe by one point attachment at the 5' or the 3' end of the probe strands (52).

1.3 Nucleic Acids Theory

1.3.1 DNA Structure

Nucleic acid polymers consist of nucleotide residues covalently linked by phosphodiester bonds. Nucleotides consist of a pentose sugar, a heterocyclic nitrogenous base, and at least one phosphate group (refer to Figure 1.1).

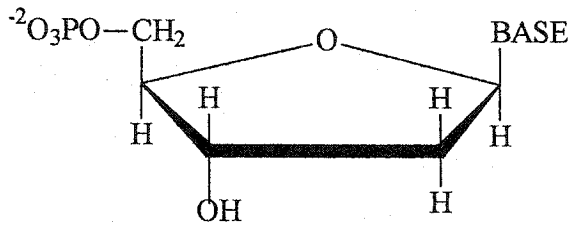

Figure 1.1 The chemical structure of deoxyribonucleotides.

The pentose is usually either ribose (D-ribofuranose) or 2-deoxyribose (2-deoxy-D-ribofuranose). Nucleotides containing ribose are called ribonucleotides, and nucleotides containing deoxyribose are called deoxyribonucleotides. There are two classes of nitrogenous bases: pyrimidines and purines (refer to Figure 1.2).

The sugar is connected to the base by a β-N-glycosidic bond between the anomeric carbon of the sugar and the N-1 of the pyrimidine or N-9 of the purine base. The amino group of a base is joined to C-1' of the pentose sugar, and the phosphate group is attached to the C-5' of the sugar. The bases lie nearly perpendicular to the sugar-phosphate backbone of nucleic acid polymers.

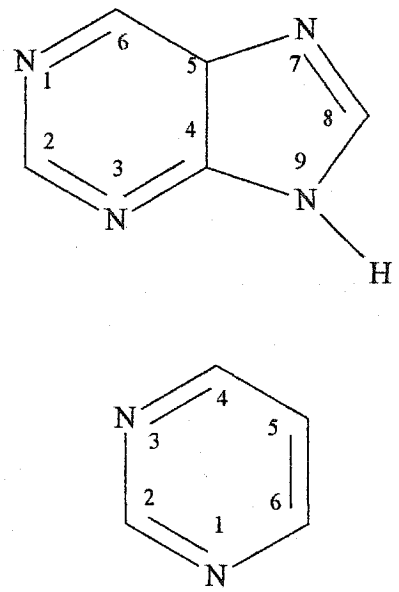

Figure 1.2 Basic structure of purine and pyrimidine bases.

1.3.2 Pyrimidines and Purines

The major pyrimidines are uracil (U), thymine (T) and cytosine (C). The major purines are adenine (A) and guanine (G). Adenine, guanine, and cytosine are found in both ribonucleotides and deoxyribonucleotides. In contrast, uracil is found mainly in ribonucleotides and thymine in deoxyribonucleotides. Pyrimidine is a heterocyclic structure composed of four carbons and two nitrogen atoms. Purine is a bicyclic structure composed of pyrimidine fused to an imidazole ring. The ring structures of both types of bases consist of conjugated double bonds and are planar.

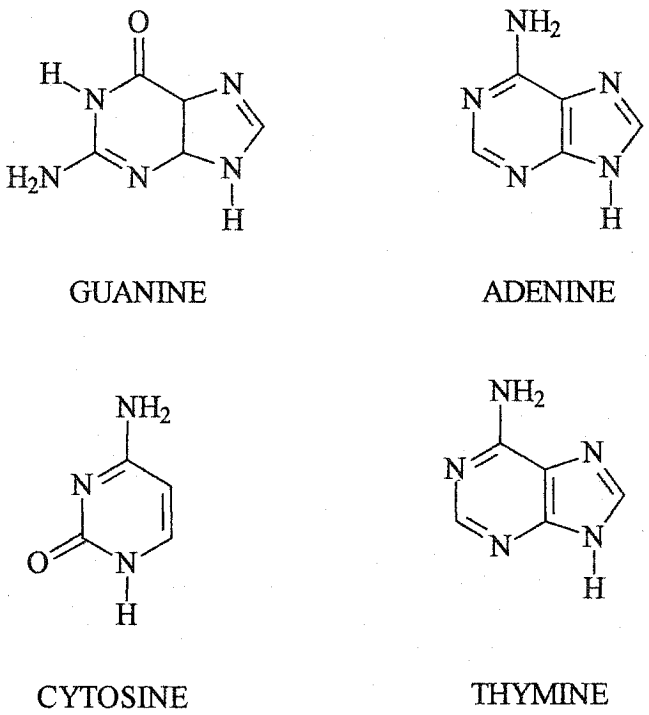

Figure 1.3 Structure of guanine and adenine; cytosine and thymine bases.

These bases exist in different tautomeric forms. Adenine and cytosine (cyclic imidines) can exist in either amino or imino forms, and guanine, thymine, and uracil (cyclic amides) can exist in either lactam (keto) or lactim (enol) forms.

The bases can rotate about the β-N- glycosidic bond to adopt different conformations. In purine nucleosides, the syn and anti conformations are in rapid equilibrium. The anti conformation predominates in the common pyrimidine nucleosides. The anti conformations of purines and pyrimidines, predominate in nucleic acids.

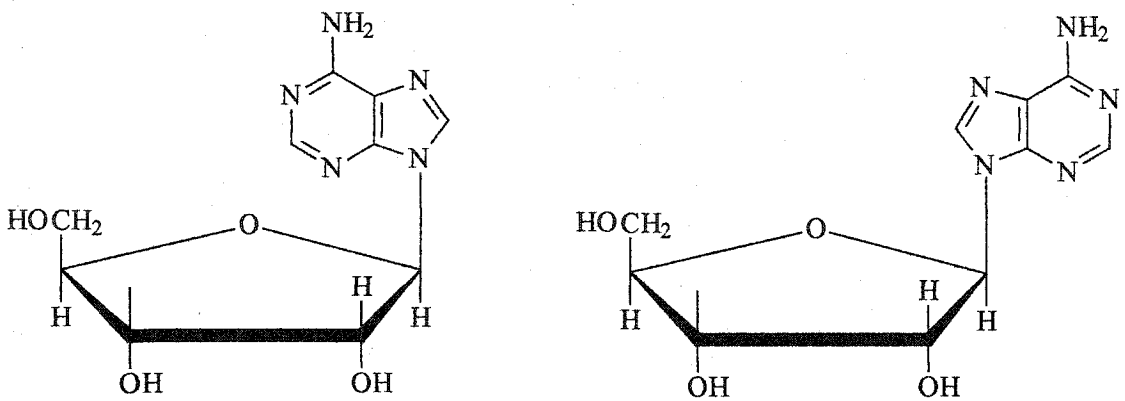

Figure 1.4 Syn and anti conformations of adenosine.

Polynucleotide chains have directionality. The polynucleotide chain has a 5' end (no residue attached to its 5'-carbon atom) and a 3' end (no residue attached to its 3'-carbon atom). The forward direction is 5'-3' as shown in Figure 1.5 (53).

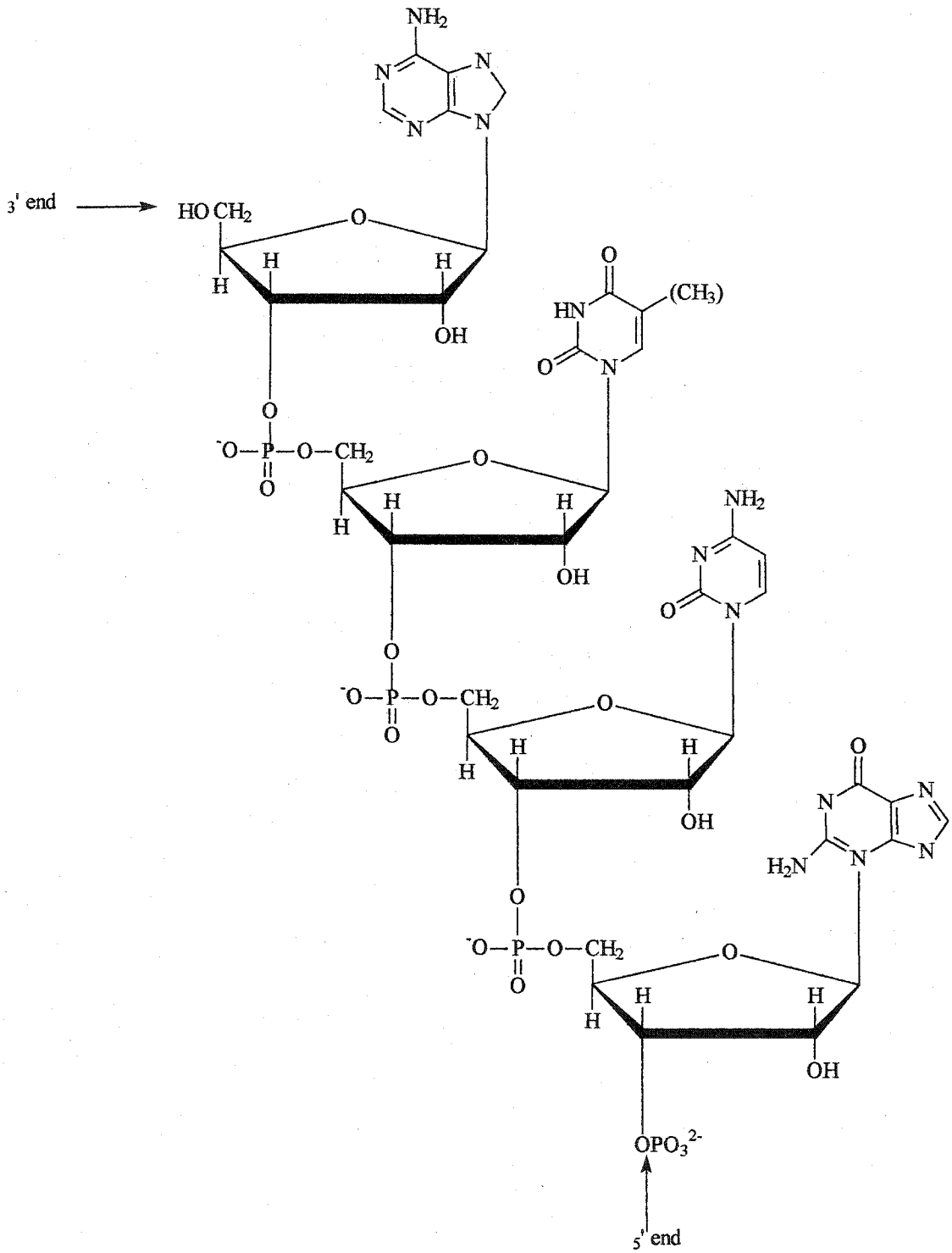

Figure 1.5 Stucture of a tetranucleotide. This tetranucleotide can be abbreviated as ATCG.

1.3.3 Double-stranded DNA

Double-stranded DNA consists of Watson-Crick base pairs. Guanine base pairs with cytosine, and adenine base pairs with thymine. The G/C base pairs have three hydrogen bonds, and A/T base pairs have two. The strands are antiparallel (refer to Figure 1.6) (53).

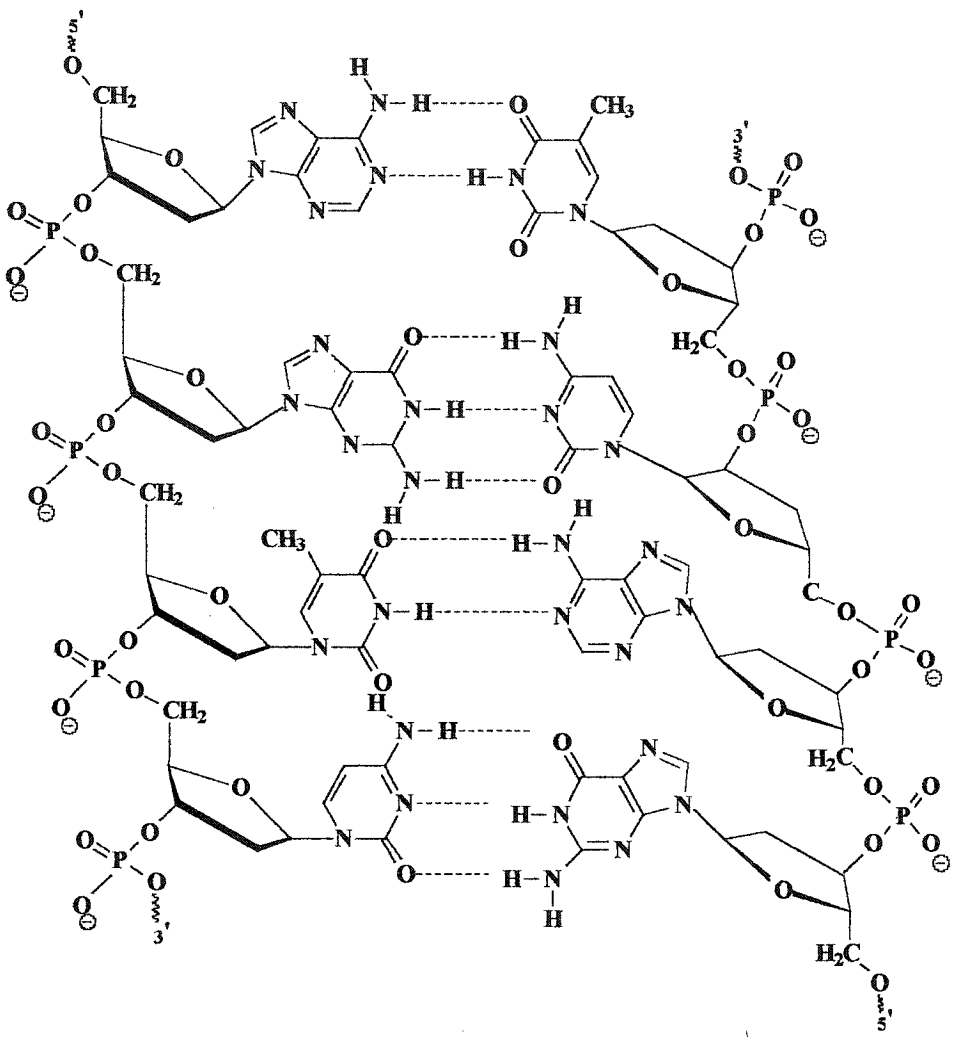

Figure 1.6 Diagram of double-stranded DNA.

The two complementary strands are wound around one another creating a helix. The hydrophobic base pairs are buried in the interior of the helix and the sugar-phosphate backbones are wound around the outside of the helix. The base pairs are stacked on top of one another, forming van der Waals contacts in the interior of the helix. Different conformations of double stranded DNA can exist.

B-DNA is the most common form of DNA. The two strands are antiparallel forming a right-handed helix with a diameter of 2.37nm. The distance between base pairs along the helical axis (rise) is 0.33nm, and the distance to complete one turn (pitch) is 3.40nm. There are about 10.4 base pairs per turn of the helix. The angle of rotation between adjacent nucleotides within each strand (twist) is 34.6°. B-DNA has a major and minor groove in the sugar-phosphate backbone. The major forces that affect the stability of double-stranded DNA are hydrophobic interactions, base stacking, hydrogen-bonding, and electrostatic repulsion. The strength of these forces is additive. The G/C base pairs are stronger than those involving A/T base pairs. The C-2' endo form of deoxyribose residues predominates and the distance between adjacent phosphorus atoms is 0.7nm. Nucleotides adopt an anti conformation.

Another form of DNA is A-DNA. Like B-DNA, it is a right-handed helix with Watson-Crick base pairs. The helix is wider than in B-DNA because bases are tilted approximately 20° relative to the helix axis resulting in 11 base pairs per turn rather than the 10.4 found in B-DNA and a different sugar pucker. Furthermore, A-DNA has a deeper major groove because the base pairs wind around the center of the helix. The base pairs are not stacked on top of each other, resulting in a solvent-accessible core. In contrast to DNA, the sugar in A-DNA has a C-3' endo conformation and the adjacent phosphorus atoms are closer together.

The third form of DNA is Z-DNA. Z-DNA is a left-handed helix with about 12 base pairs per turn. The distance between base pairs is greater than in other forms of DNA. The base pairs are only slightly tilted relative to the helix axis and are centered on the

axis. Z-DNA is longer and thinner than B- and A-DNA helices. The repeating unit is 2 base pairs. Furthermore, there is variation in the conformation of the nucleotides.

1.3.4 Denaturation of DNA

Denaturation is defined as complete unwinding of a double helix and the separation of the complementary single strands. Denaturation is initiated by slowly raising the temperature of a solution of duplex DNA. At a characteristic temperature, the strands separate.

The transition from the double-stranded to the single-stranded state can be examined by monitoring the change in absorbance of ultraviolet light at 260nm while increasing the temperature. As the temperature is increased, the bases progressively become unstacked and this is signified by an increase in UV absorbance, by approximately 12-40% at all wavelengths (53).

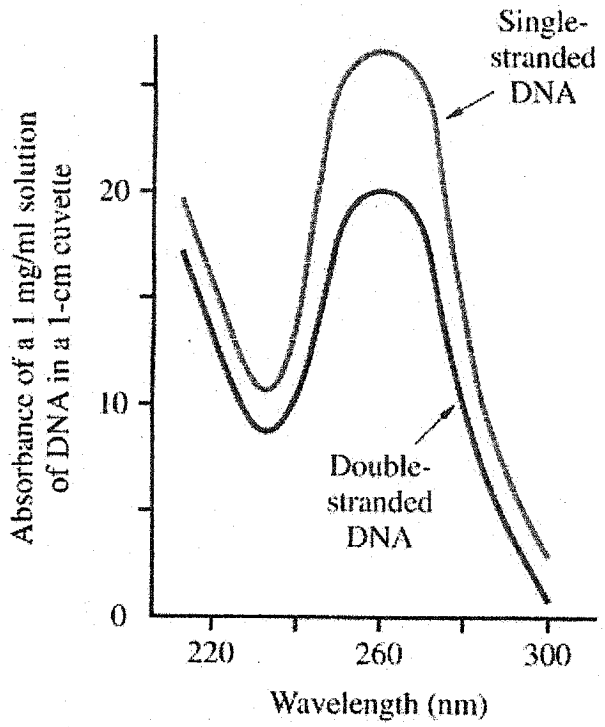

Figure 1.7 Absorbance spectra of double-stranded and single-stranded DNA.

A plot of the change in absorbance versus temperature of a DNA solution is called a melting curve (refer to Figure 1.8). "The sharp transition from the double-helical state to the single-stranded state reflects disruption of the interactions between the stacked, hydrogen-bonded base pairs in double-helical DNA" (53). The melting temperature, T_m, is defined as the temperature at which half of the DNA is single-stranded. This is the midpoint of the melting curve. The T_m is a measure of the stability of the DNA double helix. Chaotropic agents, such as urea, guanidinium chloride, and formamide, also destabilize double-stranded DNA (53).

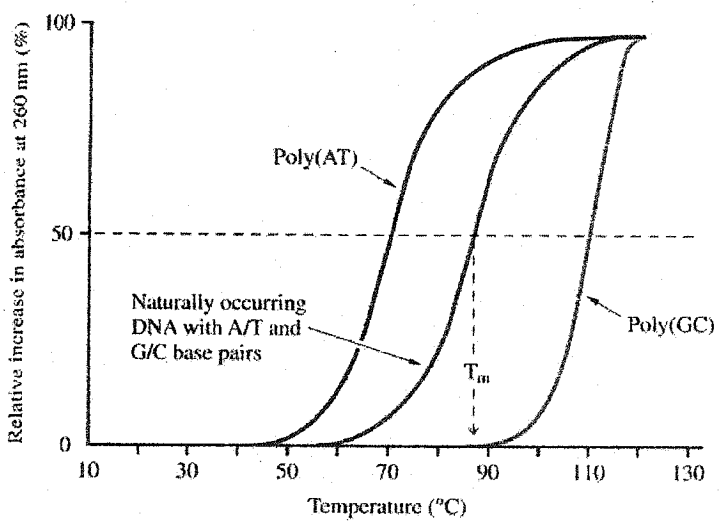

Figure 1.8 Melting curve of DNA.

1.4 Physical Properties of PNAs

1.4.1 PNA structure

Peptide nucleic acid (PNA) is a DNA mimic that consists of N- (2-aminoethyl)glycine units linked by amide bonds. Hence, the PNA backbone is charge neutral. The standard nucleotide bases (i.e., adenine, cytosine, guanine, and thymine) are attached to the backbone via methylene carbonyl linkages to the central amide of the backbone. PNA oligomers have the same bonds between the attached bases and the backbone as DNA. Finally, proteases and nucleases do not recognize the hybrid chemistry of PNA, therefore, PNAs are not susceptible to digestion and have a long half-life in serum (54).

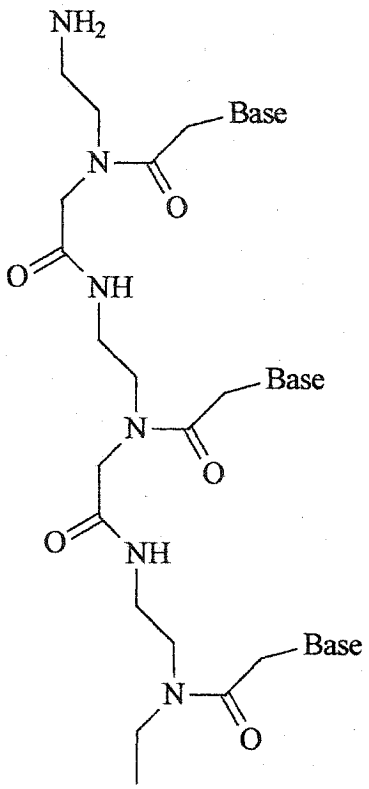

Figure 1.9 Structure of peptide nucleic acid (PNA).

1.4.2 PNA-nucleic acid complexes

PNA forms duplexes with any Watson-Crick complementary sequences of DNA and RNA oligonucleotides. In addition, PNA can form triplexes (PNA•DNA-PNA) where a homopurine DNA strand is required to bind matching homopyrimidine PNA strands. This forms T•A-T and C^+•G-C base triplets. Thirdly, PNA can form duplexes with other Watson-Crick complementary sequences of PNA (55).

1.4.3 PNA hybridization properties

The hybridization of PNA oligomers with their complementary DNA sequences obeys Watson-Crick base-pairing rules with the PNA and DNA strands joined via hydrogen bonding. As a consequence of its neutral backbone and proper interbase spacing, PNA binds to its complementary nucleic acid sequence with higher affinity and specificity compared to traditional oligonucleotides. In addition, as a consequence of its charge neutral backbone, PNA-DNA duplexes lack the interstrand repulsion between the PNA and DNA strands as seen for the corresponding DNA strands. Hence, PNA-DNA duplexes possess a higher thermal stability independent of salt concentration in the hybridization solution (47). On average, the melting temperature, T_m, of a PNA-DNA duplex is 1°C higher per base pair compared to that of the corresponding DNA-DNA duplex (54).

PNAs are achiral. They lack 3' to 5' polarity and can bind complementary DNA in the antiparallel (amino-terminal of the PNA facing the 3'-end of the oligonucleotide) and the parallel orientation. However, the antiparallel orientation is preferred because it is more thermally stable (~1°C T_m per base pair) than the parallel orientation (54,56).

Circular dichroism studies indicate that the PNA-DNA duplexes are helical. Nuclear magnetic resonance studies demonstrate that PNA-DNA duplexes exhibit characteristics of both A- and B-type helices(47).

The rate of hybridization of PNA to its complementary single-stranded DNA sequence is rapid ($K_a^{PNA} \cong 10^6 M^{-1}s^{-1}$) (47). The rate of association is equivalent to that observed for the hybridization of complementary DNA sequences due to the lack of interstrand

repulsion (57), indicating that PNA can hybridize properly to its complementary DNA sequence.

1.4.4 PNA-DNA duplex

The solution structure for an antiparallel PNA-DNA duplex was determined by NMR techniques. The structure is a right-handed Watson-Crick base paired helix with a wide and deep major groove and a narrow and shallow minor groove. The helical rise is approximately 42Å, with close to 13 base pairs per turn and the helix diameter is about 23Å. The base pairs are stacked in a varied manner, but are all displaced towards the minor goove. The major groove extends to near the center of the helix. The carbonyl groups on the backbone-base linkers are oriented along the backbone, pointing in the C-terminal direction. The primary amide bonds are in the trans conformation. Like B-DNA, the sugar rings of the DNA strand are predominantly in the C2'-endo conformation and the glycosidic torsion angles are all anti. However, the α, β, γ, ε, and δ backbone torsion angles are close to those in A-form DNA (refer to Figure 1.10) (57).

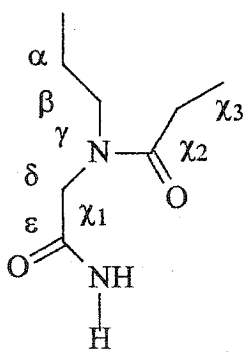

Figure 1.10 Backbone torsion angles for PNA.

CD measurements indicate that the structures of DNA-DNA and antiparallel PNA-DNA duplexes are similar, suggesting that these PNA-DNA are right-handed helices with a base-pair geometry similar to B- or A-form DNA helices. Furthermore, the structures of antiparallel and parallel PNA-DNA duplexes are distinctly different as given by CD spectra (47).

1.4.5 Sequence specificity

As mentioned earlier, PNA-DNA duplexes possess higher thermal stability than their DNA-DNA counterparts. Therefore, it is affected by the presence of imperfect matches, and thus PNA oligomers are capable of high sequence specificity. The imperfect matches have a more destabilizing effect on the PNA-DNA duplex than their DNA-DNA counterparts. Specifically, single base mismatch results in 15°C lowering of the T_m of PNA-DNA duplexes compared to the corresponding DNA-DNA duplex in which the T_m is only lowered 11°C. Hence, PNA is far superior to DNA in discrimination between perfect matches and mismatches (57).

1.4.6 PNA Biosensors

The specificity of DNA biosensors depends primarily on the selection of the probe and secondarily upon the hybridization conditions. However, most DNA biosensors are not capable of selectively discriminating against single-base mismatches, as desired, for example, for the detection of disease-related point mutations. The field of DNA diagnostics has been revolutionized with the discovery of peptide nucleic acid (PNA). PNA has unique structural and hybridization features in solution that afford it a

higher sensitivity and specificity than DNA. PNA retains these features as probes attached to transducer surfaces. Wang and coworkers first showed that PNA immobilized onto a carbon-paste electrode transducer (via adsorption) could be used to detect the specific mutation of the p53 gene that is related to various types of cancer (54,58).

1.5 Definition of the EIS structure

The EIS structure (electrolyte/ insulator (dielectric)/ semiconductor) consists of a doped semiconductor (Si) with an oxide layer immersed in an electrolytic solution. The oxide layer acts as an insulator preventing the transfer of electrons between the electrolyte and the semiconductor and prohibits all faradaic phenomena (59).

1.6 Semiconductors

Semiconductors are network solids. Strong covalent bonds between individual atoms with filled and vacant orbitals link the atoms together throughout the network as shown in Figure 1.11 (60).

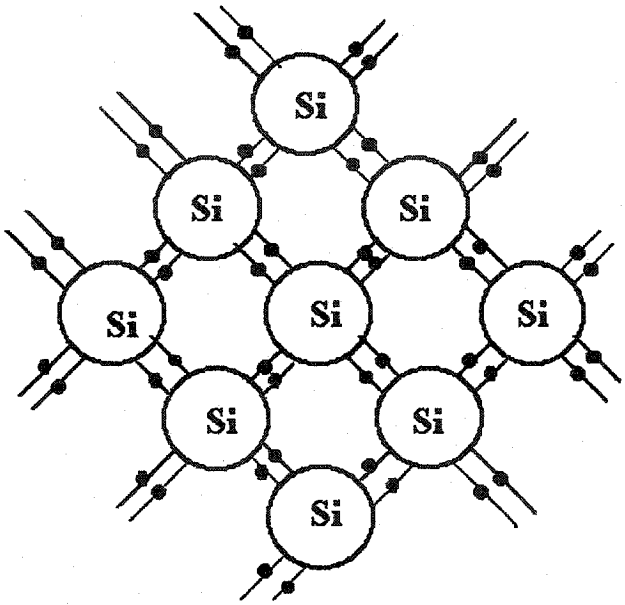

Figure 1.11 Two-dimensional representationof an intrinsic semiconductor lattice at absolute zero.

The atoms assemble into a lattice forming new molecular orbitals of different energies. These energy levels are closely spaced forming a continuum of energy levels called a band of molecular orbitals. The energy level diagram of a network solid consists of a stacked series of energy bands, some of which may overlap. The lower and higher energy molecular orbitals are formed by the overlap of filled valence orbitals (bonding molecular orbitals) and partially filled or empty higher orbitals (antibonding molecular orbitals). Thus, the lower energy molecular orbitals are occupied by valence electrons forming the valence band; the highest filled band. The empty molecular orbitals, that are higher in energy, form the lowest unfilled energy band, the conduction band (61).

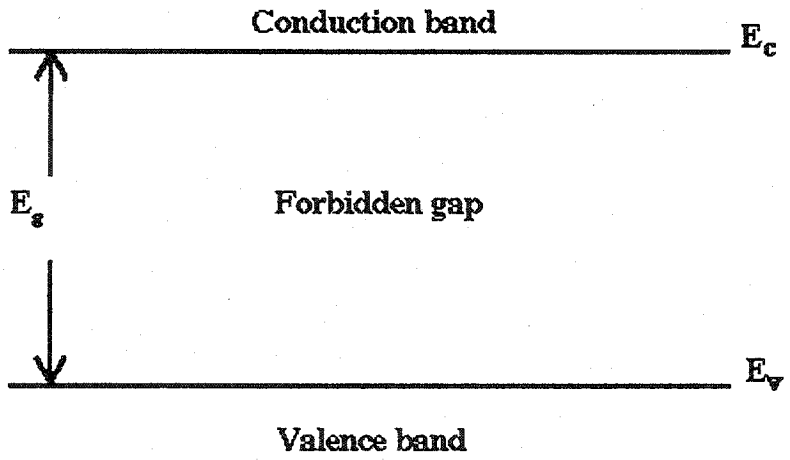

Figure 1.12 Energy bands of an intrinsic semiconductor lattice at absolute zero. E_C= lower edge of conduction band; E_V= upper edge of the valence band; E_g= band.

1.6.1 Conductors, Insulators, Semiconductors

In a semiconductor or insulator, the valence and conduction bands are separated by an energy gap (Eg). Eg is defined as the difference in energy between the conduction and valence bands (refer to Figure 1.12) (61). For electrical conductivity, solids require the movement of electrons.

Metals are good conductors because there is no energy gap between the conduction and valence bands; they overlap. Thus, very little energy is required for electrons in metals to go from the filled valence band into the empty conduction band where they become mobile. The conductivity depends upon the concentration of mobile charge carriers. The concentration of mobile charge carriers in a metal (electrons) is high and, therefore, so is the conductivity.

If, on the other hand, there is an energy gap between the valence and conduction bands which is very large compared to the thermal energy, kT, of the electrons (E_g>>kT),

very few electrons can reach the conduction band and produce electrical current. Such a material (e.g. diamond with $E_g = 5.4$ eV) (62) will behave like an insulator.

In the case of a semiconductor, like Si, there is a relatively small gap (E_g= 1.17eV) (62) allowing the thermal excitation of the electrons to the conduction band, giving a conductivity which lies somewhere between that of a metal and an insulator. At absolute zero, semiconductors are non-conducting. The valence band is completely filled and the conduction band totally empty.

1.7 Intrinsic and Extrinsic Semiconductors

When electrons are promoted to the conduction band, they leave behind holes in the valence band (refer to Figure 1.13). Both charge carriers (holes and electrons) are mobile within their respective energy bands. Electrons are promoted to the conduction band, leaving behind holes in the valence band. Electrons can move along the empty energy levels and the valence band electrons can rearrange themselves by occupying a vacancy (60).

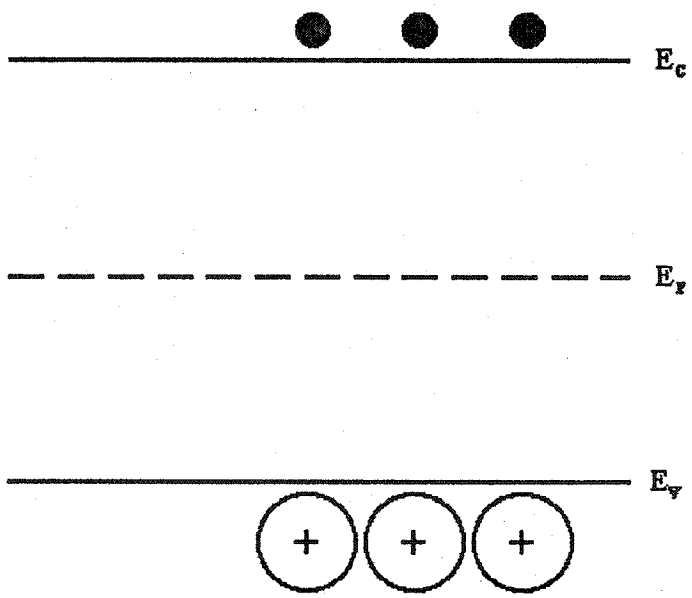

Figure 1.13 Energy bands of an intrinsic semiconductor where there are electrons in the conduction band and holes in the valence band. E_F represents the Fermi level in this intrinsic semiconductor.

In an intrinsic semiconductor, the electron and hole densities are equal and are given approximately by the expression:

$$[n][p]=N_cN_v \exp(-E_g/kT) \qquad (1.1)$$

N_C and N_V are the "effective" density of energy levels at the conduction band edge and valence band edge. The Boltzmann factor dictates that the densities of electrons[n] and holes[p] depends on the absolute temperature and the bandgap energy. Charge carriers generated by thermal excitation in an intrinsic semiconductor results in [n] = [p]. For example, for silicon, $n=p\approx1.4x10^{10}cm^{-3}$ (60). In the conduction band, the electrons are mobile. Hence, the conduction band electrons can conduct electricity.

For a semiconductor to conduct electricity, mobile charge carriers can be generated by one of three possible mechanisms: thermal generation (mentioned earlier), doping, and photo-excitation.

1.7.1 Extrinsic Semiconductors

By means of doping, useful conductivity can be imparted to semiconductors with E_g as large as 3.5eV (61). Doping involves replacing atoms of the host crystal lattice with atoms having a different valence. There are two types of extrinsic semiconductors: n-type and p-type.

1.7.1.1 N-type Semiconductors

N-type semiconductors are materials doped with donor atoms. N-type semiconductors are so called because of the presence of an extra negative charge (electron) (60).

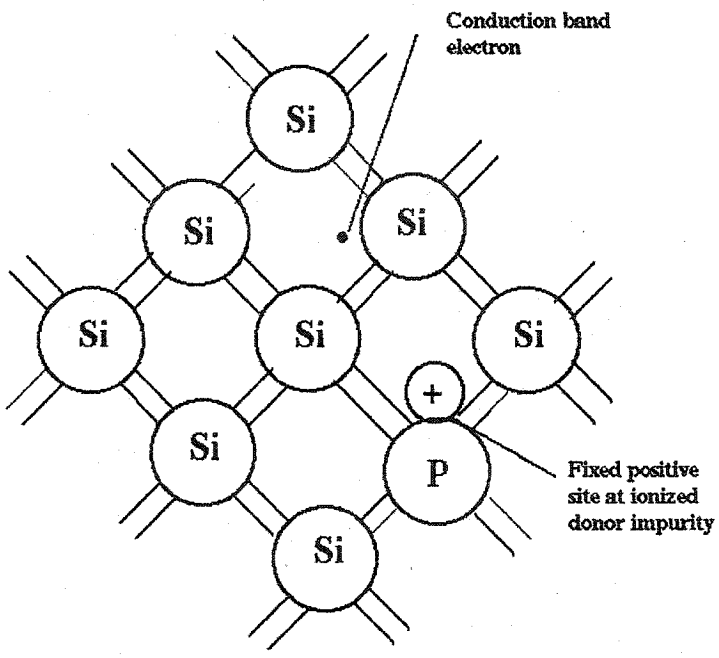

Figure 1.14 Two-dimensional representation of extrinsic n-type semiconductor.

The electrons are the majority charge carriers. If Si (valence 4) is doped with phosphorus atoms (valence 5), it has a loosely bound electron. These phosphorous atoms act as electron donors by introducing an energy level in the band gap, at E_D, a few kT (within ~0.045eV) (62) below the conduction band edge (refer to Figure 1.15). At room temperature, the donor atoms are ionized, yielding an electron in the conduction band and leaving behind an isolated positive site at the donor atom (60).

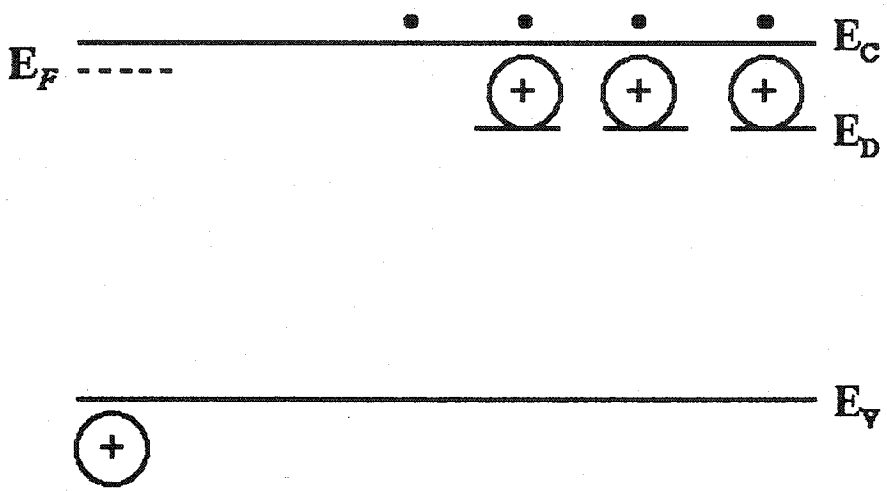

Figure 1.15 Energy bands of extrinsic n-type semiconductor.

In this type of material, the negative charge carriers in the conduction band are responsible for conducting the electrical current, hence the term n-type. For standard dopant densities (donor density, N_D) of ~5 × 10^{15} cm^{-3} (60) which is essentially the conduction band electron density, n, the hole density, p, is much smaller and is given by the electron hole equilibrium relationship,

$$p = n_i^2/N_D \qquad (1.2)$$

1.7.1.2 P-type Semiconductors

P-type semiconductors are materials doped with acceptor atoms (refer to Figure 1.16) (60).

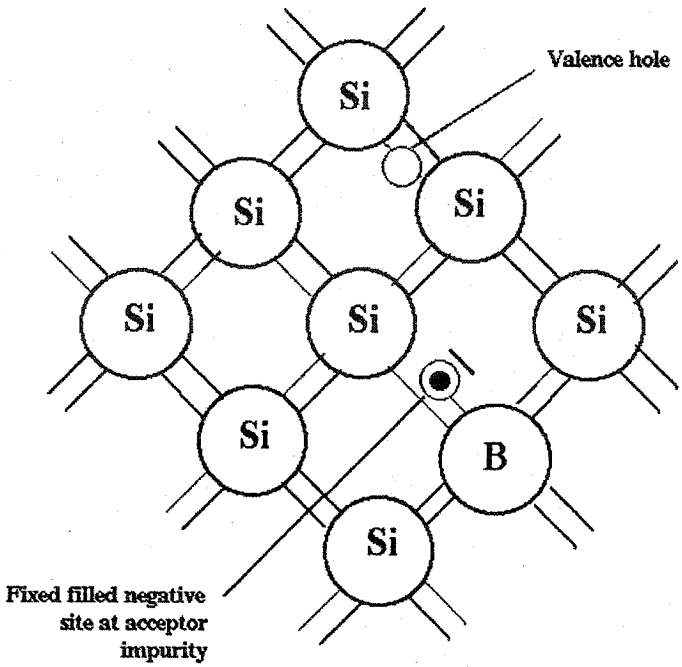

Figure 1.16 Two-dimensional representation of extrinsic p-type semiconductor.

The holes are the majority charge carriers. If Si is doped with Boron atoms, these Boron atoms act as electron acceptors by introducing an energy level in the band gap, at E_A a few kT (within 0.045ev) (62) above the valence band edge. At room temperature, the acceptor atoms are ionized, yielding holes in the valence band which act as positive charge carriers (60).

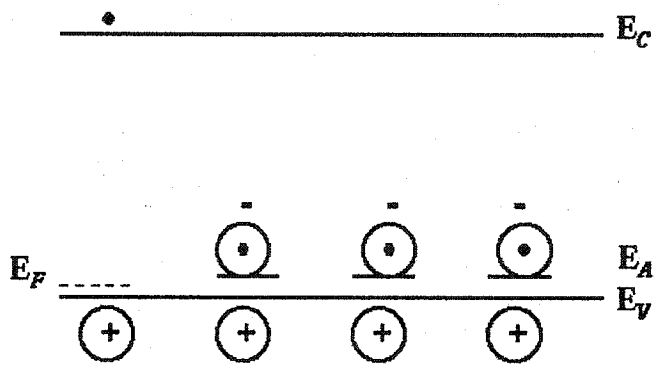

Figure 1.17 Energy bands of extrinsic p-type semiconductor.

In this type of material the positive charge carriers are responsible for conducting the electrical current, hence the term p-type. For standard dopant densities, acceptor density, N_A is essentially the hole density, p, and the conduction band electron density, n is given by

$$n = n_i^2/N_A \qquad (1.3)$$

1.8 Fermi level

The Fermi level (E_F appearing in Figure 1.13) is the energy at which the probability of occupation by an electron is exactly 1/2. The probability of occupancy above and below the E_f is determined by the Fermi-Dirac distribution function:

$$f(E) = (1 + \exp [(E-E_f)/kT])^{-1} \qquad (1.4)$$

For an intrinsic semiconductor, the E_F lies midway between the conduction band and valence band edges in the band gap. For n-type semiconductors, the E_f lies slightly below the conduction band edge. For p-type semiconductors, the E_f lies slightly above the valence band edge.

1.9 The Interphasal Structure

Interphase is defined as the region near a surface in contact with a solution in which the properties of the region are not those of the bulk of either phase.

1.9.1 Helmholtz-Perrin Model

Helmholtz was the first to propose the idea of "the electrical double layer" in the 1850's. Several assumptions with this model are made. There are no electron transfer reactions at the electrode and the solution is composed only of electrolyte. The electrode surface has an excess or deficiency of charge. Counter-charge ions from the solution are electrostatically attracted to the electrode surface forming a layer. Hence, there are two layers of counter-charge at the electrode/solution interface (termed the double layer) thereby generating a neutral interface. There is a linear potential drop in this region (termed the outer Helmholtz plane, OHP) in solution.

The limitations associated with the Helmholtz model are that it does not take into account other factors such as diffusion/mixing in solution, adsorption onto the surface electrode and the interaction between solvent dipole moments and the electrode.

1.9.2 The Gouy-Chapman Model

An alternative model to the Helmholtz model was proposed in 1910. This new model is referred to as the "diffuse-layer model". Gouy showed that there was no Helmholtz layer of ions or water molecules at the electrode-solution interface. Gouy model proposes that there is a diffuse layer of charge in solution. The concentration of charge decreases the further the distance away from the electrode with the greatest concentration of excess charge at the electrode-solution interface because the electrostatic attractive force is greater at the interface. This distance is affected by potential and electrolyte concentrations.

1.9.3 The Stern Model

In 1924, Stern combined the theories of Helmholtz and Gouy and made two innovations to create the most accepted model for the electrical double layer.

In this model, the interface is still considered electrically neutral. He proposed that there are two layers of charge separation; the Helmholtz layer and a diffuse layer of charge. The inner Helmholtz plane (IHP) is the layer of solvent ions specifically adsorbed to the electrode interface by electrostatic interactions. This is known as the

Helmholtz layer. This region of charge extends from the electrode to the locus of the centers of the adsorbed ions. The outer Helmholtz plane (OHP) is the layer of nonspecifically adsorbed solvated ions. This region of charge extends from the electrode to the locus of the centers of the nearest solvated ions. The solvated ions are distributed in the diffuse layer that extends from the OHP into the bulk of the solution.

1.10 Semiconductor/Solution Interface

When an n-type semiconductor is brought into contact with an electrolytic solution containing a redox couple (O/R), the two phases adjust their thermodynamic potential. That is, the Fermi level of the semiconductor and the electrolyte must become equal via the transfer of charge between the phases. If the E_f of the semiconductor lies above the E_f of the solution, electrons will flow from the semiconductor to the solution phase leaving behind immobile positive charge in the semiconductor near the interface. This region of positive charge is referred to as the space charge region or layer and corresponds to a potential difference between the semiconductor (positively charged) and the solution (negatively charged).

A bending of the bands represents an excess of positive charge in the space charge region. In going from the interface to the bulk, the bands are bent downward. Because of the electric field, an excess electron in the space-charge layer is directed toward the bulk semiconductor, whereas, an excess hole in the space-charge layer is directed toward the surface.

The potential at which no electric field and no space charge layer exist in the semiconductor (the bands are not bent) is called the flat band potential, V_{fb}.

This space-charge layer is analogous to an electrical parallel-plate capacitor. The capacitance is given by

$$C = A\varepsilon\varepsilon_{\circ}/d \qquad (1.5)$$

where ε is the dielectric constant of the medium, $\varepsilon_{\circ}$ is the permittivity of free space, d is the distance between the plates, and A is the surface area.

CHAPTER 2

ELECTROCHEMICAL IMPEDANCE THEORY

2.1 Principle of AC Impedance

AC impedance can be used to measure the capacitance of the EIS structure. An AC potential of small amplitude and fixed frequency is superimposed on the applied DC potential, and the combined potential is applied to the semiconductor electrode. The current flowing through the electrode is detected and analyzed by a lock-in analyzer. The parameters obtained are the magnitude and the phase difference (the in-phase and out-of-phase components) of the current relative to the ac potential. The phase difference is the angle by which the current leads the voltage. This phase angle can be 0° (current and voltage in phase) or 90° (current and voltage out of phase).

Impedance has two components: the impedance component in phase with the potential and the impedance component out of phase with the potential (referred to as the imaginary component).

The current (i) and the voltage (v) are sinusoidal signals. Each is shown as a separate phasor (I or V). Each rotates at the same frequency. The rotate out of phase with respect to one another and are separated by a phase angle, ϕ. The current lags the voltage. This is expressed as,

$$i = I \sin(\omega t + \phi) \qquad (2.1)$$

For a sinusoidal voltage, v, applied across a pure resistance, R, the phase angle is zero. The sinusoidal voltage applied across a resistance is given by,

$$v = V \sin\omega t \qquad (2.2)$$

Where ω is the angular frequency, which is 2π times the frequency in Hz.(60).

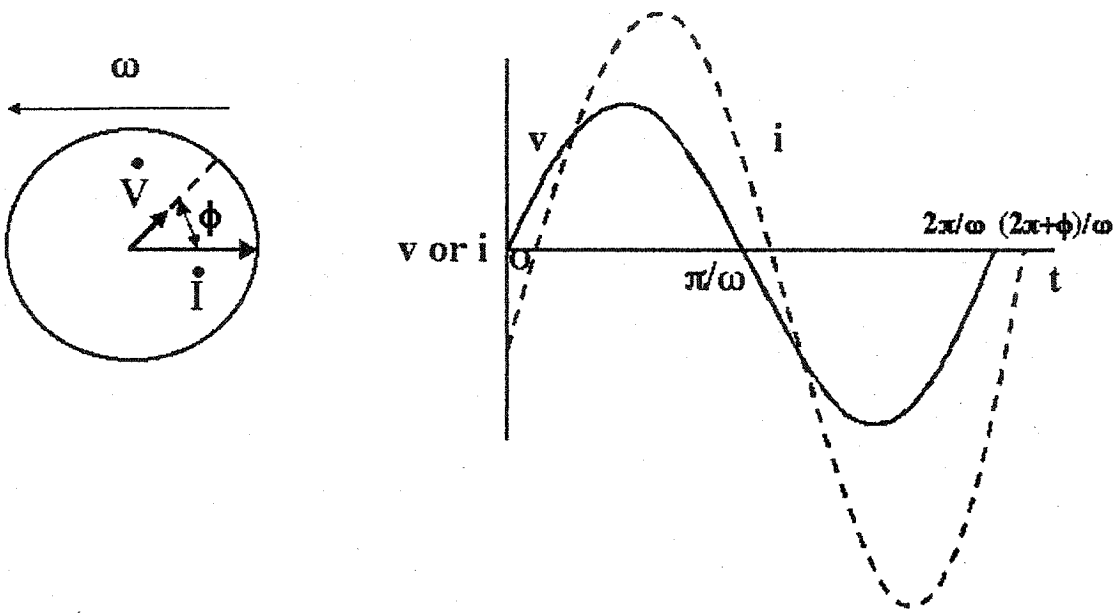

Figure 2.1 Phasor diagram showing the relationship between alternating current and voltage signals at frequency ω.

Its length is the amplitude V, and its frequency of rotation is ω. Given Ohm's law, the current, in phasor notation, is

$$I = V/R \qquad (2.3)$$

The vector diagram is shown in Figure 2.2 below (60).

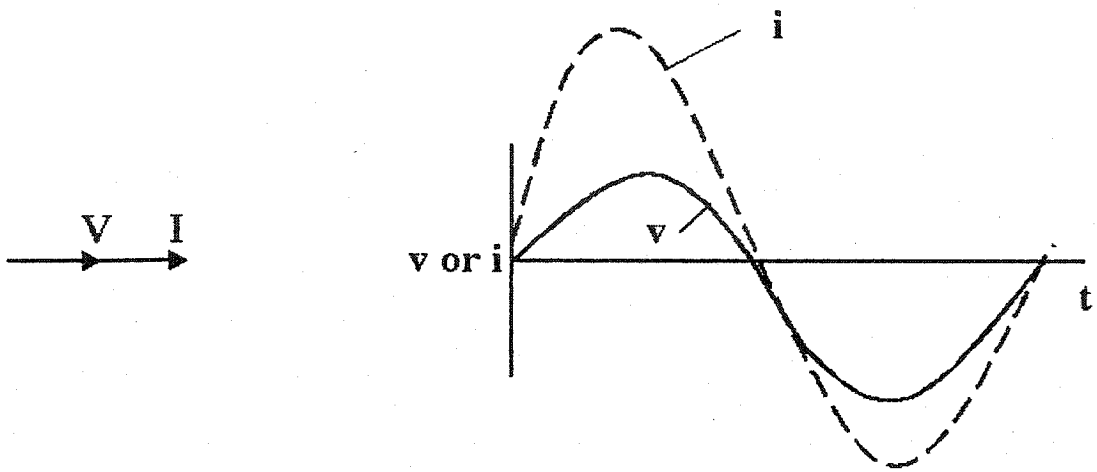

Figure 2.2 Relationship between the voltage across a resistor and current through the resistor.

For a pure capacitance, C, to which a sinusoidal voltage is applied,

$$i = \omega CV \cos\omega t \qquad (2.4)$$

$$I = V/X_C \sin(\omega t + \pi/2) \qquad (2.5)$$

where X_C is the capacitive reactance

$$1/\omega C \qquad (2.6)$$

The phase angle is $\pi/2$ and the current leads the voltage.The vector diagram shown in Figure 2.3 (60).

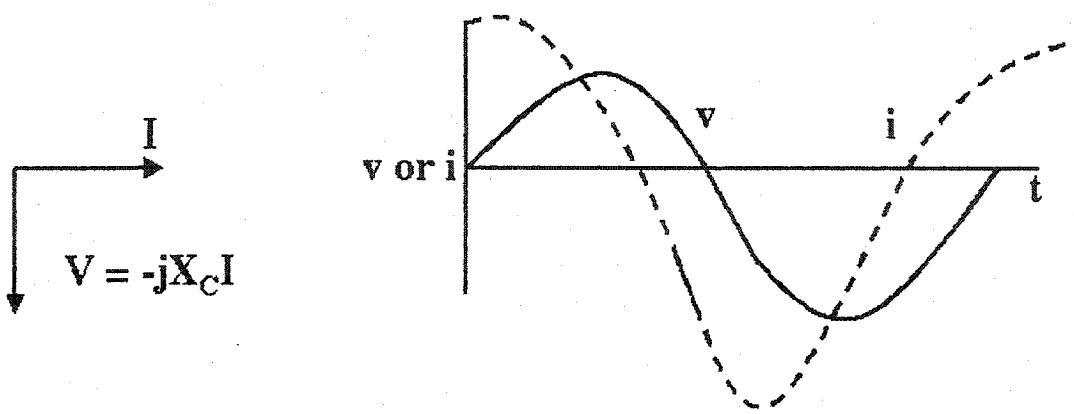

Figure 2.3 Relationship between an alternating voltage across a capacitor and the alternating current through the capacitor.

The phasors can be represented in terms of complex notation. Components along the ordinate are assigned as imaginary and are multiplied by j = square root of -1.

A voltage, V, applied across a resistance, R, and a capacitance, C, in series, is given by

$$V = V_R + V_C \qquad (2.7)$$

$$V = I\,(R - j\,X_C) \qquad (2.8)$$

$$V = IZ \qquad (2.9)$$

The voltage is related to the current through the vector called impedance

$$Z = R = -j\,X_C \qquad (2.10)$$

The information is converted into capacitance using an equivalent circuit model of the cell impedance as shown in Figure 2.4. Thus, the cell impedance is given by the space charge capacitance in series with the electrode and solution resistance.

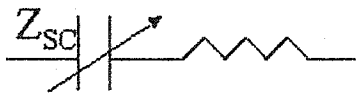

Figure 2.4 Equivalent circuit model of the cell impedance.

In general, the impedance can be represented as

$$Z(\omega) = Z_R - jZ_I \qquad (2.11)$$

Where Z_R and Z_I are the real and imaginary parts of the impedance.

$$Z_R = R \qquad (2.12)$$

$$Z_I = X_C = 1/\omega C \qquad (2.13)$$

The magnitude of Z, written $|Z|$ or Z, given by

$$|Z|^2 = R^2 + X^2_C = (Z_R)^2 + (Z_I)^2 \qquad (2.14)$$

and the phase angle, ϕ, is given by

$$\tan\phi = Z_I / Z_R = X_C / R = 1/\omega RC \qquad (2.15)$$

The impedance is a kind of generalized resistance and equation V = IZ is a generalized version of Ohm's law:

$$V = IZ \qquad (2.16)$$

$$V = (Z_R - jZ_I)I \qquad (2.17)$$

$$V = V_R - jV_I \qquad (2.18)$$

$$I = I_R - jI_I \qquad (2.19)$$

For each continuous polarization value, and for a given modulation frequency, in-phase (Z_R) and out-of-phase (Z_I) impedance can be expressed as

$$Z_R = (V_R I_R + V_I I_I)/ (I_R^2 + I_I^2) \qquad (2.20)$$

$$Z_I = (V_I I_R - V_R I_I)/ (I_R^2 + I_I^2) \qquad (2.21)$$

2.2 The Differential Capacity Due to the Space Charge

The space-charge region inside the semiconductor has the ability to store charge. To calculate the differential capacity (q_{sc}) of the semiconductor/electrolyte interface, the expression for q_{sc} is differentiated by the potential drop (ψ_S) inside the semiconductor. Thus,

$$C_{SC} = dq_{sc}/d\psi_S \qquad (2.22)$$

The overall capacitance (C) consists of two capacitors in series, the space-charge capacitance (C_{SC}) and Helmholtz-Perrin C_{HP} capacitors. Thus,

$$1/C = 1/C_{SC} + 1/C_{HP} \text{ but } C_{HP} >> C_{SC} \qquad (2.23)$$

and hence,

$$1/C \cong 1/ C_{SC}$$

For dilute electrolytic solutions, a diffuse-charge region in solution exists. The diffuse layer, the Helmholtz layer, and the space charge layer are planes of charge separated by distance with associated capacitances. These three capacitors are in series at the semiconductor-electrolyte interface and the total differential capacity for the Si/SiO_2 substrates for the depletion regime is given by

$$1/C = 1/C_{SC} + 1/C_{HP} + 1/C_{GC} \qquad (2.24)$$

Because the three capacitances are in series, the smallest one dominates the total capacitance.

The observed capacitance depends upon the electron concentration in the semiconductor and the ionic concentration in solution. In concentrated electrolytes the diffuse capacitance is so large that it can be completely ignored. The Helmholtz capacitance is small relative to this number, thus, the overall capacitance can be assigned to the space charge capacitance ($1/C_{SC}$). The value of capacitance due to the space charge of a semiconductor is usually smaller than the capacitance of the double layer (Helmholtz and Gouy layers) thus the space-charge capacitance will dominate.

2.3 Effect of polarization on the EIS structure

By varying the DC applied potential, the polarization affects the charge distribution in the space charge layer, and, as a result, three polarization ranges can be distinguished in the out-of-phase impedance (Z_I) versus V curve corresponding to inversion, depletion, and accumulation of majority charge carriers in the silicon valence band (refer to Figure 2.5).

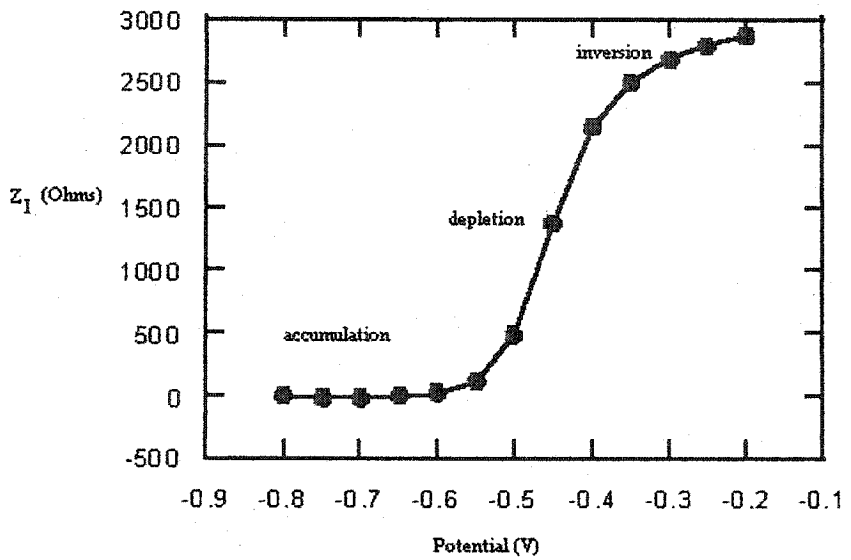

Figure 2.5 Regimes of impedance versus DC potential.

2.3.1 Accumulation Regime

When a potential negative of that of the flatband potential is applied, the electrons in the conduction band flow from the bulk towards the semiconductor surface resulting in band-bending downwards and the formation of an accumulation layer (refer to Figure 2.6) (61). The Fermi level is raised, moving into the conduction band at the surface and remains constant throughout the bulk of the semiconductor (refer to Figure 2.6). The semiconductor capacitance is determined by the majority charge carriers,electrons. Redox couples readily exchange elecrons in both directions.

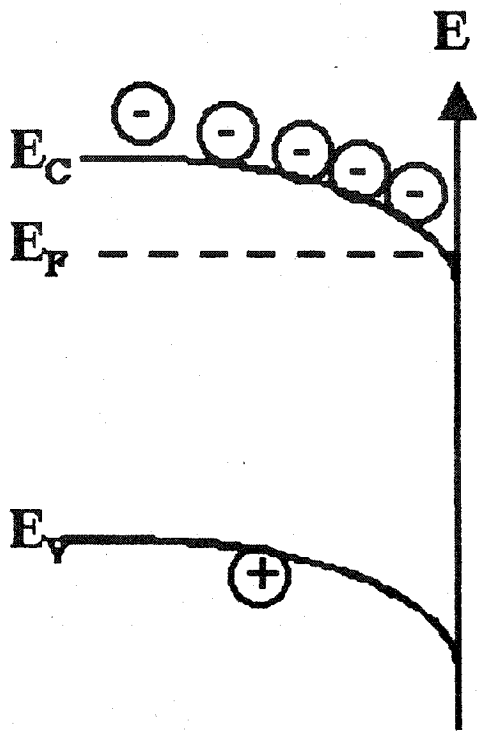

Figure 2.6 Accumulation layer in a n-type semiconductor.

2.3.2 Depletion Regime

When an intermediate potential, positive of flatband potential, is applied to the semiconductor, the minority charge carriers (holes) accumulate at the surface, resulting in removal of majority charge carriers (electrons). The bands are bent upward. Thus the space charge layer is called a depletion layer (refer to Figure 2.7) (61). The depletion layer is positively charged due to the immobile ionized donor species in the crystal lattice. The surface concentration of minority carriers remains low. Electron exchange between the semiconductor and electrolyte is kinetically hindered by the absence of holes or electrons at the surface. The electrode is said to be blocking.

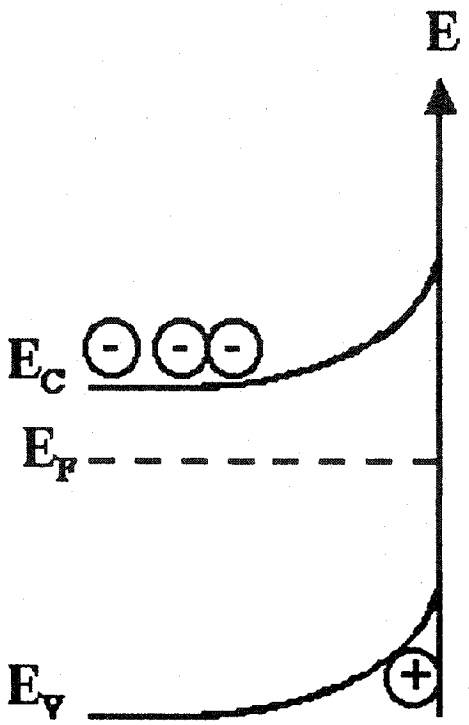

Figure 2.7 Depletion layer in a n-type semiconductor.

2.3.3 Inversion Regime

For potentials much more positive than that of the flatband potential, an inversion layer develops. The concentration of holes is in excess to that of electrons (refer to Figure 2.8)(61).

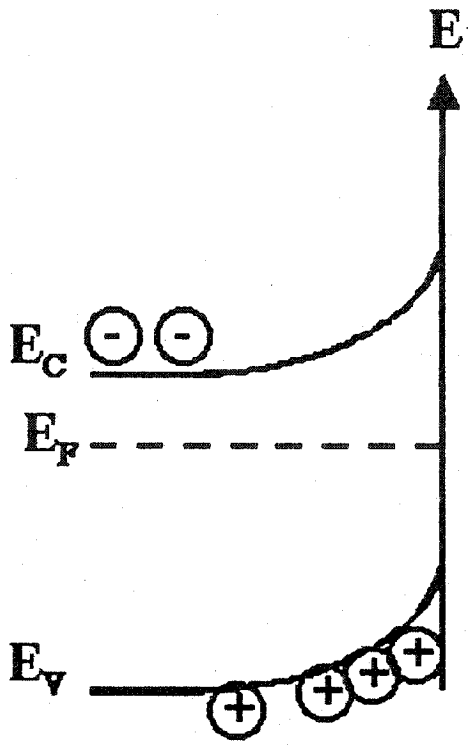

Figure 2.8 Inversion layer in a n-type semiconductor.

2.4 Determination of Flat-band Potential

Treating the entire heterostructure (electolyte/dielectric/semiconductor) as an ideal blocked interface made of several capacitors in series, one can relate the out-of-phase impedance, Z_I, to the total capacitance, C, using the following equation

$$Z_I = 1/C\omega \qquad (2.25)$$

Where ω is the ac signal frequency ($2\pi f$). Therefore, the out-of-phase impedance of the device is inversely related to the capacitance of the heterostructure and consequently to the thickness of the dielectric.

A plot of the reciprocal square of the capacitance per unit area versus the potential is linear with an intercept at the V_{fb}. A straight line is obtained in the depletion region whose potential intercept is V_{fb}. The magnitude of the flat-band potential is affected by the degree of band-bending.The charges present on the dielectric surface influence the band bending of the semiconductor. The Mott-Schottky plot is the most common method for determining flat band potential. In the depletion region, the space charge capacitance varies with the width of the space charge layer, which in turn is a function of the potential relative to V_{fb}. The Mott-Schottky equation is based on the capacitance associated with the space charge layer. The semiconductor/electrolyte capacitance is related to the applied DC potential (V) through the Mott-Schottky equation.

$$C^{-2} = (2/(qN_D \varepsilon \varepsilon^{\circ}))(|V-V_{fb}|-kT/q) \qquad (2.26)$$

Where $\varepsilon_{\circ}$ and ε are the permittivity of free space and the relative permittivity of the semiconductor, N_D, is the dopant density, A is the area of the working electrode, q is the electronic charge, V is the applied potential, V_{fb} is the flatband potential, k is the Boltzmann constant and T is the absolute temperature.

Modification of the oxide surface through immobilization and hybridization causes a change in the charge distribution within the space-charge layer of the semiconductor, resulting in a change of flat-band potential. The change in V_{fb} is reflected by a displacement of the out-of-phase impedance curves along the DC potential axis, toward more negative or more positive potentials depending on the effect the surface transformations have on the aforementioned charge distribution. The values of the V_{fb}

are directly obtained by extrapolating the steeply rising portion of the Z_I versus applied DC potential curves.

CHAPTER 3

MATERIALS AND METHODS

3.1 Materials and Reactants

3.1.1 Chemicals

The source and purity of all the chemicals and reactants are specified in the following tables. All chemicals were used as received. Whenever applicable, the source of materials obtained from other companies and their purity, are specified. Water used in preparing solutions was distilled and deionized.

3.1.2 Nucleic Acids

Table 3.1 Nucleic Acids

Name	**Nucleotide Sequence**	**Supplier**
PNA Sequence	N-O-AGTCCATTGCAGTCCATTGC-C	Applied Biosystems
DNA Sequence	5'-GCAATGGACTGCAATGGACT-3'	BioCorp Inc.
PNA Sequence	N-O-AGTCCATTGC-C	Applied Biosystems
DNA Sequence	5'-GCAATGGACT-3'	BioCorp Inc.
PNA Sequence	Flu-OO-AGTCCATTGCAGTCCATTGC-O-Lys	Applied Biosystems
DNA Sequence	GCAATGCACTGCAATGGACT-Flu	BioCorp Inc.

All PNA sequences are written from N (amino) to C (carboxy) terminal.

All DNA sequences are written from 5' to 3'.

PNA and DNA are fluorescein-labelled (Flu).

PNA has an amino linker (O-linker).

All PNA and DNA samples have been obtain lypholilyzed, and the nucleic acids are quantified spectrophotometrically.

All nucleic acids were stored at -20C.

3.2 Reagents

Table 3.2 Reagents Used

Name	**Purity**	**Supplier**
Distilled-deionized water	Milli-RX 20 device	Millipore
Hydrochloric acid	Reagent grade	Fisher
Sodium chloride	Reagent grade	Fisher

Table 3.3 Reagents used in the GPTS functionalization method

Name	**Purity**	**Supplier**
3-glycidoxypropyltrimethoxysilane	98%	Sigma-Aldrich
N-N diisopropylethylamine	99.5%	Sigma-Aldrich
N_2	High purity grade	Pradair
Acetone	HPLC grade	Fisher Scientific
Ethanol	98%	Commercial SAQ
Propane-2-ol	Reagent grade	Analar

3.3 Silicon/Silicon Dioxide Semiconductor Electrodes (Substrates)

The Si/SiO_2 substrates (TRONICS Microsystems, France) are $1x1cm^2$ with a 300μm thick silicon layer. The Si (100) was phosphorus doped (n-type) to a density of 10^{15} cm^{-3}. There is a silicon dioxide layer of 150Å on the front. This layer is sufficiently blocking preventing all faradaic processes. The back of the chip has a gold/chromium ohmic contact of 2000/500Å.

3.4 Preparation of the Electrolyte

All the impedance results obtained during this investigation were acquired by using a 0.1M NaCl solution.

3.5 Preparation of Synthetic Peptide Nucleic Acid

PNA sample was prepared as instructed by the manufacturer.

PNA sample was dissolved in d-d H_2O to make a 100μM stock solution.

During solubilizing, the PNA solution is allowed to sit at RT for at least 10 minutes with intermittent vortexing. PNA solution is warmed to 50°C for 10 minutes then vortexed.

PNA solution is centrifuged briefly. PNA is quantified spectrophotometrically.

3.5.1 Quantification of PNA

Add 10μl of PNA to 990μl d-d H_2O.

Determine the A_{260} using a standard quartz cuvette (1cm path length)

Calculate and record the PNA concentration using a specified formula unique to each PNA sample.

3.6 Preparation of Synthetic Deoxyribonucleotide Acid Solutions

The synthetic complementary single stranded deoxyribonucleic acids were used as received and dissolved in d-d water. Samples were stored in eppendorf tubes at -10°C.

3.6.1 Quantification of DNA

The concentration in picomoles/μl can be determined by diluting an aliquot of the resuspended oligonucleotide 100 fold and measuring the A_{260}. The concentration is calculated according to the following formula:

$$[A_{260}/\text{length of oligo}]\text{x } 100 \text{ x Dilution factor } (100) \qquad (3.1)$$

3.7 Preparation of Functionalized Electrodes:General Scheme

In our approach, the PNA is covalently linked to the surface of Si/SiO_2 chips that have been functionalized with a silane, 3-glycidoxypropyltrimethoxysilane (GPTS). The functionalization procedure has been optimized to ensure maximum available sites for probe attachment. The immobilization of nucleic acids to the silicon surface consists of 4 steps: cleaning, hydroxylation, silanization, and coupling of the nucleic acids to the surface via their linkers.

3.7.1 Cleaning of the Substrate

It is necessary to have a clean surface to which the probe molecules are attached. The substrates were cleaned to remove all of the organic molecules, especially the oils and any dust that could have become deposited during the storage of the samples thereby hindering the functionalization. The chips are cleaned to remove any of these pollutants.

The cleaning procedure consisted of immersing the substrates in acetone for 5 minutes, boiling d-d water for 10 minutes, thorough rinsing with d-d water, and drying under nitrogen.

3.7.2 Hydroxylation of the Silica Layer

The surface of the silicon (silicon dioxide) is composed of siloxane (Si-O-Si) bonds and hydroxyl groups (Si-OH). The siloxane linkages are unreactive. The hydroxyl sites are very reactive, allowing for silanization of the surface. The hydroxylation process transforms the siloxane bonds to hydroxyl groups. The surface treated in this way is covered uniformly with OH sites.

The siloxane bond in amorphous and crystalline silicon is cleaved by placing the chip in sufficiently electrophilic conditions (hydrochloric acid for a couple of minutes). Water completes the reaction creating OH groups (63, 64). The reaction scheme is shown in Scheme 3.1.

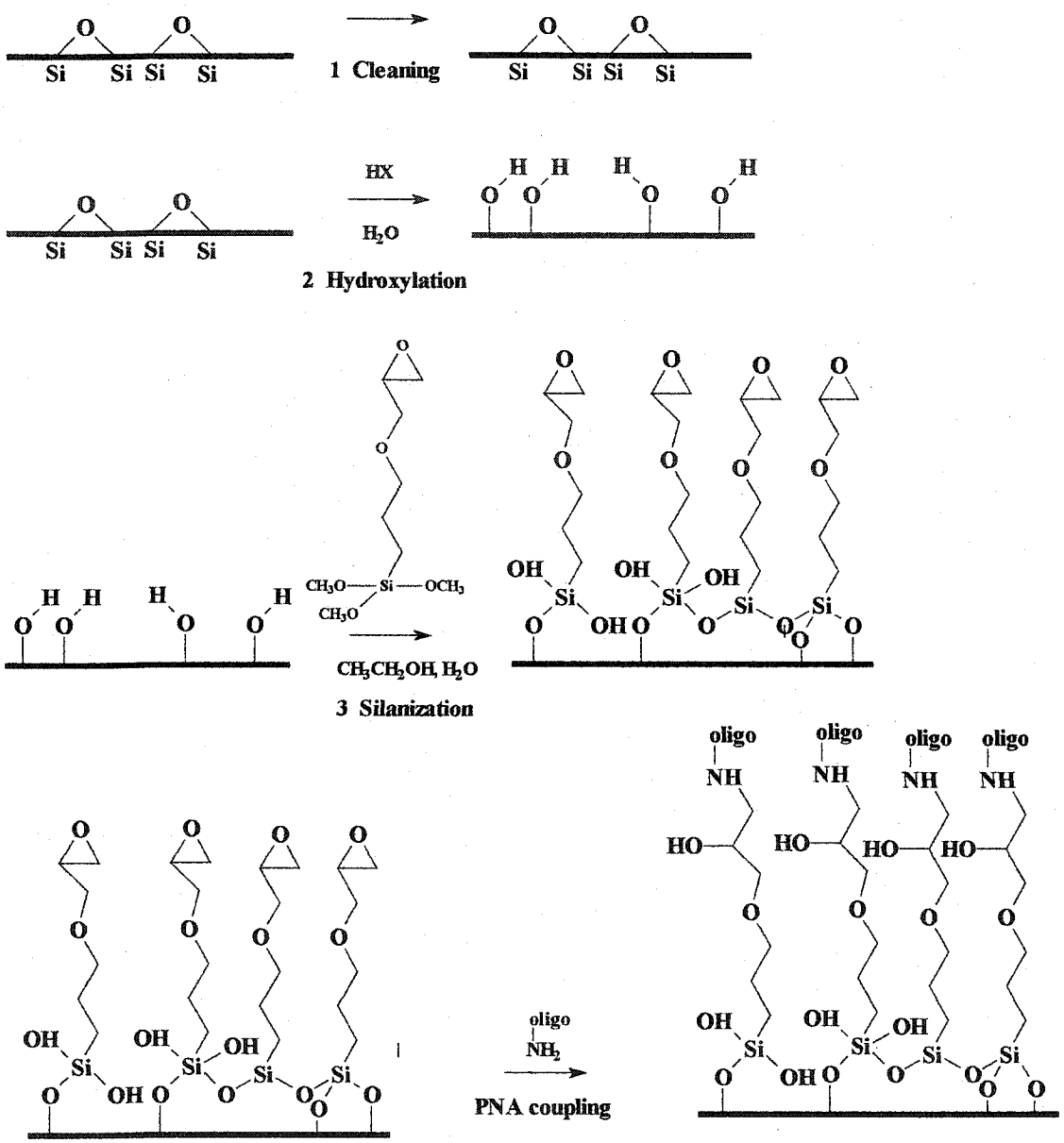

Scheme 3.1 Functionalization scheme.

The formation of silanol groups (referred to as hydroxylation) was performed by acid treatment of the oxide. The substrates were immersed in concentrated hydrochloric acid solution for 2 minutes. Following acid treatment, the chips were, once again, placed in boiling d-d water for 10 minutes, rinsed thoroughly with d-d water and dried under N_2.

3.8 Electrode Functionalization with GPTS (Silanization)

3.8.1 Chemical Structure of Silane Coupling Agent

The general structure for commercial silane coupling agents is $X_3Si\ (CH_2)_nY$, where n=0-3, X is a hydrolyzable group on silicon, and Y is an organofunctional group (61,62). The "coupling" mechanism of organofunctional silanes depends on a stable link between the organofunctional group (Y) and the PNA amino linker. Neutral organofunctional silane coupling agents have a methacryloxy, glycidoxy, vinyl, chloro, etc. Y group (65, 66). Refer to Table 3.4 for some common silane coupling agents.

Table 3.4 Representative Commercial Coupling Agents

Organofunctional Group	**Chemical Structure**
Vinyl	CH_2=CHSi$(OCH_3)_3$
Chloropropyl	$ClCH_2\ CH_2\ CH_2Si(OCH_3)_3$
Epoxy	$CH_2OCH_2O\ CH_2\ CH_2\ CH_2Si(OCH_3)_3$
Methacrylate	CH_2=C-$(CH_3)COO\ CH_2$ $CH_2CH_2Si(OCH_3)_3$
Diamine	$H_2N\ CH_2CH_2NH\ CH_2\ CH_2CH_2Si(OCH_3)_3$
Primary Amine	$H_2N\ CH_2CH_2CH_2Si(OC_2H_5)_3$
Methyl	$CH_3Si(OCH_3)_3$
Cationic Styryl	CH_2=$CHC_6H_4\ CH_2NH\ CH_2CH_2$ $NH(CH_2)_3Si(OCH_3)_3$•HCl
Phenyl	$C_6H_5Si(OCH_3)_3$

3.8.2 Silanization Procedure

Prior to silanization, the silane mixture was stirred for 5 min and the chips were immersed in a thin film of ethanol for 5 min to remove any adsorbed particles. The silane mixture consisted of a 1% GPTS solution [mixture of ethanol, water, diisopropylethylamine (DPEA) and GPTS (23.5:1.25:0.25:0.25 v/v/v/v)]. The chips were left to react with the silane mixture under medium agitation for ~4h in a sealed

polystyrene container. Following silanization, the subtrates were immersed in propane-2-ol for 5 min (to remove excess GPTS or any contaminants), rinsed with d-d water for 30s, and dried under N_2. The substrates were stored in closed welled plates under ambient temperature.

3.8.3 Chemisorption of Silanes to Silicon Chips

The chemical reaction in the silanization is not a trivial one. Reproducibility problems often arise due to the high number of variables that need to be controlled. The surface coverage resulting from the silanization reactions depends on reaction time, temperature, silane concentration, degree of hydration of the substrates, the cleaning procedure utilized prior to the silanization of substrates. (67). To obtain robust films, the silane must be securely anchored to the surface through Si-O-Si linkage. There is one common mechanism for the coupling of the silane to the silica surface. It is a three-step process: hydrolysis, physisorption, and condensation.

3.8.3.1 Hydrolysis

Organofunctional trialkoxysilanes, $RSi(OR)_3$, hydrolyze relatively fast (minutes) and stepwise in the presence of water to give the intermediate silanetriol. The silanols can undergo condensation which is much slower (several hours) compared to hydrolysis (65).

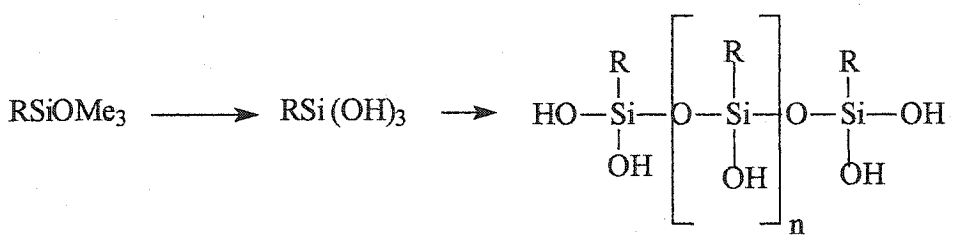

Scheme 3.2 Hydrolysis mechanism.

There is disagreement as to whether the hydrolysis occurs in the bulk solution phase or at the substrate surface (68-74). For our substrates, water was added to the solvent/GPTS/diisopropylethylamine mixture.

3.8.3.2 Physisorption

The silanetriol then physisorbs onto the substrate via hydrogen bonding. Siberzan et al. have demonstrated that close to ambient temperatures produce the most robust monolayers (74).

3.8.3.3 Condensation

The adsorbed silanetriol condenses with the surface SiOH groups to form a surface Si-O-Si bond. The tendency of silanols to condensation increases with the number of hydroxyl groups attached to the silicon atom. The order is:

$$RSi(OH)_3 > R_2Si(OH)_2 > R_3SiOH$$

A trisilanol that is bound to the surface through condensation forms a lateral, polymerized network to adjacent molecules. (73, 75).

There is a competition between direct condensation of silane with surface silanols and self-condensation of individual silane molecules with one another. The tendency of self-condensation decreases with the number of hydroxyl groups attached to the silicon atom, opposite to that of direct condensation. The condensation of the first hydroxyl group of a

trisilanol readily occurs, the condensation of the second and third hydroxyl groups attached to the same silicon atom becomes increasingly more difficult (73,76,77). The reaction mechanism for solution self-condensation is similar to that of direct condensation. Both reactions proceed via a pentacoordinate transition state. In self-condensation, the nucleophilic oxygen atom attached to silicon of one silane molecule attacks the silicon atom containing more hydroxyl groups of another silane molecule at 180 or 90 degrees to the leaving group, thereby forming a pentacoordinate transition state (73).

Direct condensation is an acid-base mechanism. In direct condensation, the oxygen atom of the surface nucleophilic SiOH group attacks the silicon atom of the alkylsilanol, forming a pentacoordinate intermediate. The surface silanol groups are more acidic than the SiOH of the silane, thus the leaving group water is formed by the OH group of the silane abstracting a proton from the surface SiOH group (73).

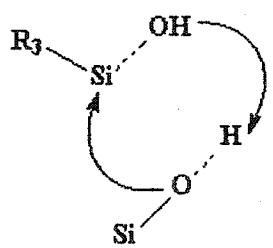

Figure 3.1 Pentacoordinate transition state.

3.8.4 Possible Attachment Structures of Silane

The structure of the silanized surface can have different forms. The silane can be attached to the surface via one bond for each silane molecule (refer to (1) in Figure 3.2). Each silane molecule can form multiple bonds with the surface (refer to (2) in Figure 3.2). The silane can undergo hydrolysis and no subsequent condensation (Refer to Figure (3) in Figure 3.2). In addition, siloxane bonds may be formed between adjacent silanes to form "horizontal" (refer to (4) in Figure 3.2) or "vertical" polymers (refer to (5) in Figure 3.2) (78).

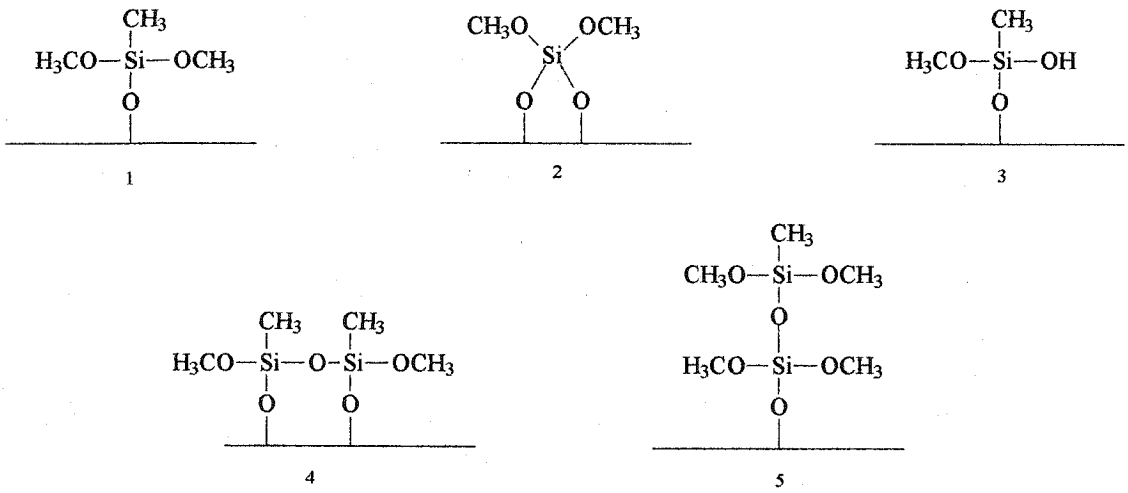

Figure 3.2 Structures of silane covalently bound to silicon surface

3.8.5 Use of Catalyst and Water

To promote direct condensation, a catalyst is used. It has been shown in previous studies that amines with exchangeable protons can promote direct condensation between the silane and the surface silanols. In a study by Blitz and Leyden, results indicated that ethylamine, diethylamine, and ammonia are more effective catalysts than triethylamine and pyridine (78).

These amine catalysts can be used in hydrolysis and condensation reactions. Amines can catalyze the hydrolysis of alkoxy groups on the silane. Secondly, amines can catalyze the condensation between the hydrolyzed silane and surface hydroxyls. Thirdly, amines can catalyze the direct condensation of unhydrolyzed silane with surface hydroxyls. For condensation between the hydrolyzed silane and surface hydroxyls, the amine forms strong hydrogen bonds with surface silanols rendering them highly nucleophilic favoring attack of the silane by surface silanol.

3.9 Immobilization of Peptide Nucleic Acid to Functionalized Silicon Chip

3.9.1 Immobilization Methods

Various methods have been reported for the immobilization of PNA onto a transducer. Burgener and co-workers have examined the hybridization characteristics of PNA, as covalently coupled onto a sensor surface (79). This method consists of a coupling between the maleimide group attached to the N-terminal of the PNA and the sulfhydryl groups of an activated dextran matrix on the sensor surface. Another approach was used by Wang and co-workers in which the PNA, derivatized with a thiolate anchor group, was immobilized as a self-assembled monolayer onto a gold-plated QCM (80).

In our approach, the PNA is covalently linked to the surface of Si/SiO_2 chips that have been functionalized. GPTS has an epoxide functional group that enables binding of the

PNA. Using a procedure derived from work by Lamture and co-workers (81), the covalent binding in this case is achieved through an epoxide-amine coupling reaction between the epoxide group of the GPTS and the aminolinker of the PNA oligomer

(referred to as PNA coupling in Scheme 3.1).

3.9.2 *Immobilization Procedure*

Immobilization of the probe layer was performed by placing 100µl of a 0.02µg/µl (in 0.1M NaCl) aqueous solution onto the modified Si/SiO_2 chip forming the working electrode of a specially designed three-electrode cell. Impedance measurements were taken while the reaction took place. The substrates were thoroughly rinsed with d-d water to remove any non-specifically adsorbed PNA from the surface. In order to confirm the presence of the immobilized PNA and the hybridized DNA, the oligonucleotides were labelled with a fluorescent probe, fluorescein.

3.10 Hybridization of Single-Stranded PNA with Complementary DNA

The hybridization was performed using fluorescein-labelled DNA. The concentration of DNA is equal to the concentration of the PNA used for the immobilization. The hybridization consisted of placing 100µl of a 0.02µg/µl DNA in 0.1M NaCl aqeous solution in the specially designed cell and leaving the chips to react while taking impedance measurements. The substrates were thoroughly rinsed with d-d water to remove any unhybridized DNA from the surface.

3.10.1 Fluorescence measurements

The chips with the immobilized fluorescein-labelled PNA strands and the fluorescein-labelled DNA strands were prepared using the procedure described in the previous section. The immobilization and hybridization steps were done in the dark. Following immobilization and hybridization, the chips were mounted on a standard microscope slide. The fluorescence measurements were taken using a Genepix 4000B fluorescence microarray scanner. The image of the chip showed the circular region where immobilization of labelled PNA had been done. The Genepix scanner aligns user-constructed blocks with features on an array. The blocks were constructed with features to our specifications. The pixel size was set at 20μm. The diameter of the feature indicator was set to the diameter of the spot. The features were aligned on the spots. The photomultiplier tube (PMT) voltage, focus and feature diameter were set each time a new slide was scanned. The PMT voltage and focus were adjusted to ~1000V and 200μm, respectively. A median intensity was taken at a wavelength of 532 nm.

3.11 Electrochemical Methods

3.11.1 Electrochemical Cell

The electrochemical cell used in this study was a specially designed classical three - electrode set-up. The design of the electrochemical cell is shown in Figure 3.2 below. The volume of electrolytic solution used in the electrochemical cell was 100μl.

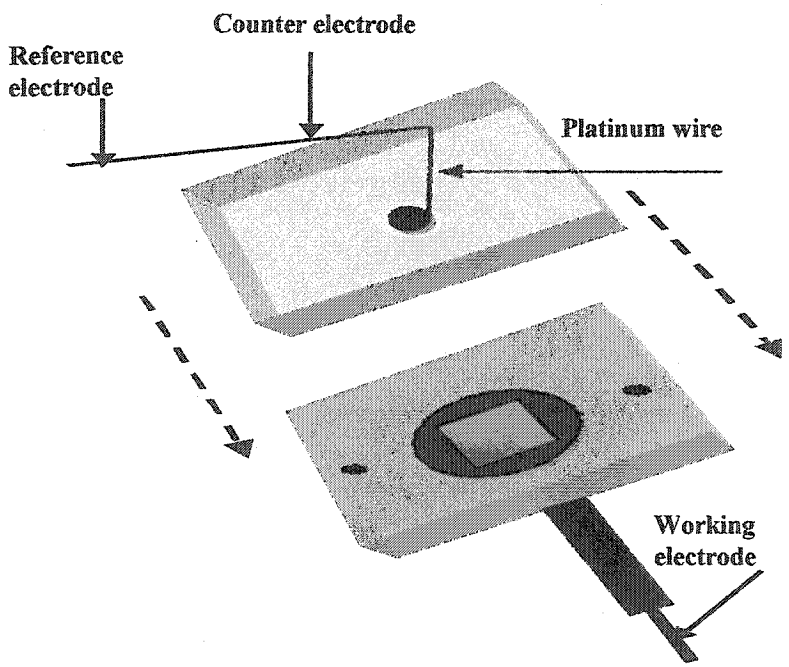

Figure 3.3 Schematic representation of working cell.

3.11.2 Impedance measurements

A DC potential of -0.5 to 2V was applied to the chips using the three-electrode potentiostatic set-up as described in the previous section. An AC voltage of 100kHz frequency and 10mV amplitude was superimposed onto the DC potential. Impedance measurements were taken using a computer controlled Voltalab electrochemical

workstation (model PGZ 301 by Radiometer, Copenhagen), and the accompanying Voltamaster computer program was used to calculate the out-of-phase impedance (Z_I) and generate the plots. All measurements were done at room temperature and conducted in the dark to avoid photogeneration of charge carriers in the semiconducting electrode.

3.12 Procedure for T_m Determination

A typical T_m determination is performed by measuring the impedance of the system while increasing the medium temperature with a setup composed of a three-electrode potentiostatic setup connected to a temperature regulation system (±0.2°C). Both temperature and impedance values are recorded simultaneously. The impedance versus temperature data obtained will yield a melting curve.

3.13 X-Ray Photoelectron Spectroscopy Measurements

X-ray photoelectron spectroscopy (XPS) is a qualitative method providing information about the elemental compositions on the surface of solids. XPS indicates which atoms are present in a sample, structure and oxidation state of a compound being examined.

Figure x is a schematic representation of the physical process involved in XPS. The three lower lines labeled, E_b, E'_b, and E''_b represent energies of the inner shell K and L electrons of an atom. The upper three lines labeled, E_v, E'_v, and E''_v represent some of the energy levels of the outer shell or valence electrons (82).

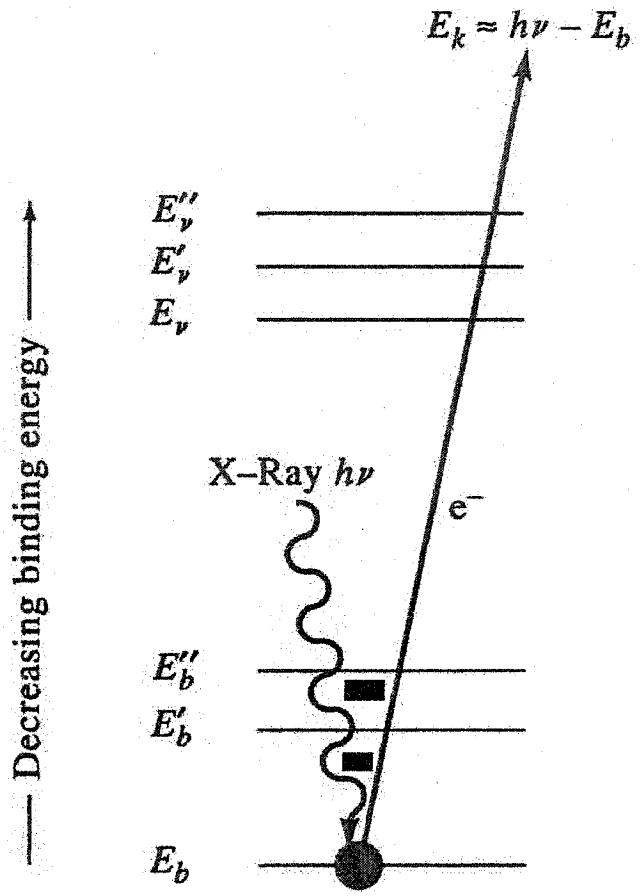

Figure 3.4 Schematic of XPS.

A photon of monochromatic X-ray beam of energy hν is absorbed by the sample resulting in displacement of an electron e^- from a K orbital E_b. The reaction is

$$A + h\nu \rightarrow A^{+*} + e^- \text{ (x-x)}$$

where A can be an atom, molecule, or an ion and A^{+*} is an electronically excited ion with a positive charge one greater than that of A.

The emission process has three steps. The electron is promoted from its ground state to the final state above the Fermi level. The electron is then transported to the surface where it escapes into the vacuum. In XPS the kinetic energies of the emitted electrons

form the spectral peaks. The kinetic energy of the emitted electron E_k is measured in an electron spectrometer. The binding energies of these electrons can be calculated from the following equation:

$$E_b = h\nu - E_k - w \quad (x\text{-}x)$$

where E_b is the electron binding energy in the solid, $h\nu$ is the energy of the incident photon, E_k is the electron kinetic energy and w is the difference in work functions between the sample and the detector material. A low resolution XPS survey spectrum consists of a plot of electron counting rate as a function of binding energy E_b. Photoelectrons produced in XPS are incapable of passing through more than 1- 4 nm of a solid (83).

3.13.1 XPS Measurement Procedure

The X-ray photoelectron spectroscopy measurements were carried out at the INRS Energie and Materiaux laboratores Montreal, Canada , using a VG 220iXL spectrometer with monochromatic Al Kα radiation. The X-ray source was 1486.6 eV Al. The pressure used was 10^{-10} torr under vacuum.

CHAPTER 4

RESULTS AND DISCUSSION

4.1 Functionalization method

The first step involves the formation of silanol groups by acid treatment of the oxide. GPTS consists of hydrolyzable methoxy groups that allow for the covalent binding of the silane to the oxide surface through siloxane bonds.

4.1.1 Optimization of Silanization

To determine the optimal silanization time (the best GPTS coverage), a preliminary experiment was performed using fluorescein-labelled bovine serum albumin protein (BSA). Chips were prepared by varying the silanization times (30,60,90,120,360,and 480 minutes). The chips were placed in propane-2-ol for 2 minutes, rinsed with d-d water for thirty seconds and dried under nitrogen. Each chip was coated with 10μL of a BSA aqueous solution and the immobilization was carried out at room temperature in water-saturated atmosphere for two hours. The washing procedure described above was performed. Fluorescence measurements were taken immediately after silanization.

Prior to silanization, the silane mixture was stirred for 5 minutes and the chips were immersed in a thin film of ethanol for 5 minutes to remove any adsorbed particles. The silane mixture consisted of a 1% GPTS solution (mixture of ethanol, water, DPEA, and GPTS (23.5:1.25:0.25:0.25 v/v/v/v)). The chips were left to react with the silane mixture under medium agitation for approximately 4 hours in a sealed polystyrene container. Following silanization, the substrates were immersed in propane-2-ol for five minutes (to

remove excess GPTS or any contaminants), rinsed with d-d water for 30 seconds, and dried under N_2. The substrates were stored in closed welled plates under ambient atmosphere.

Figure 4.1 shows the observed fluorescence intensities and the optimal silanization time was found to be 4 hours, which corresponds to the highest median intensity of $5.4x10^3$ a.u.

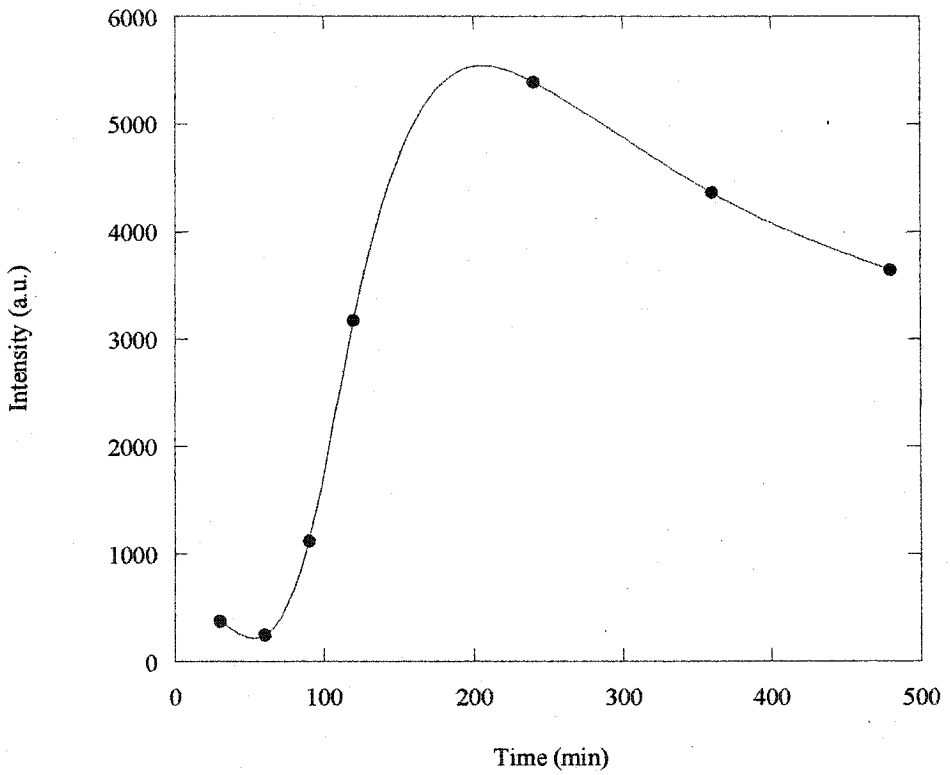

Figure 4.1 Fluorescence intensity as a function of the silanization time.

X-ray photoelectron spectroscopy was used to confirm the adequate functionalization of the surface. A survey spectrum (low-resolution, wide-scan XPS spectrum) of the

sample was taken. The survey spectrum allows one to determine which elements are present at the surface of the sample (refer to Figure 4.2).

Figure 4.2 and 4.3 have the main peaks due to Si (2p and 2s), C (1s) and O (1s). At low resolution, the XPS pattern of a GPTS modified Si/SiO_2 substrate (Figure 4.3) shows no significant differences to that shown in Figure 4.2 for unmodified Si/SiO_2 substrate.

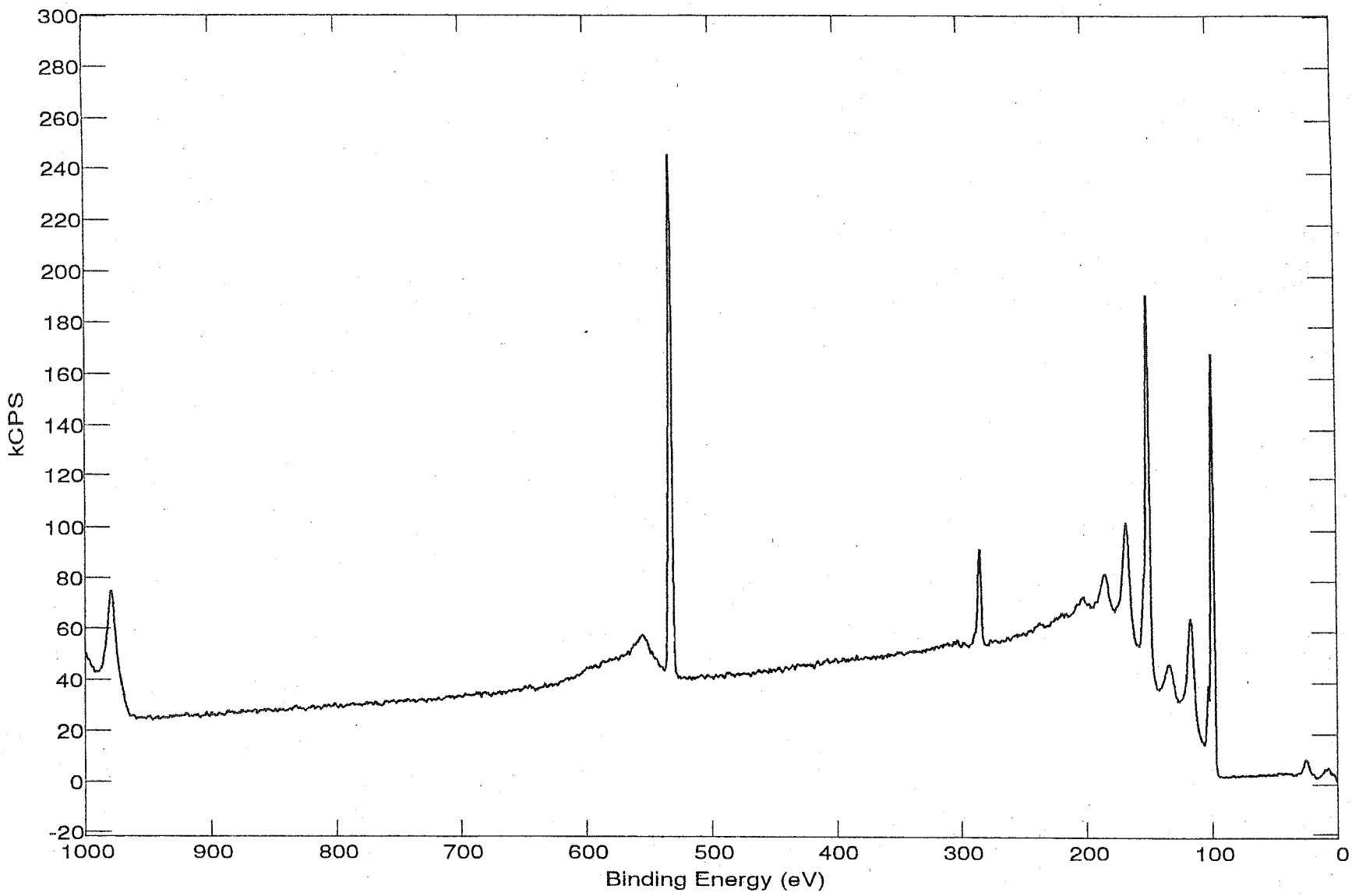

Figure 4.2 Survey spectrum of the Si/SiO_2 substrates.

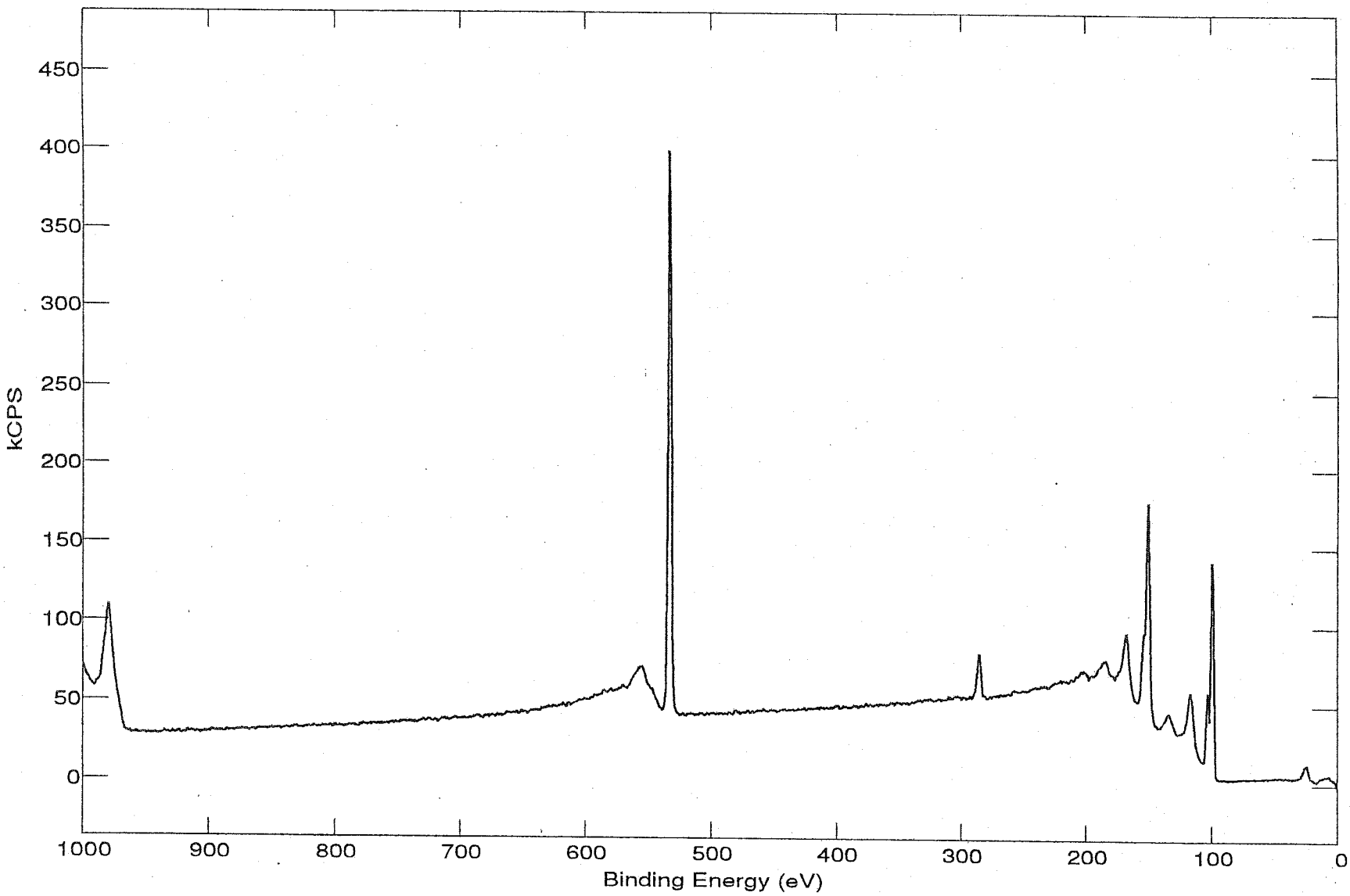

Figure 4.3 Survey spectrum of the GPTS-modified substrates.

At higher resolution, however, the peak for the carbon 1s binding energy in the 280-290 eV region shows an important change following modification of the oxide layer with GPTS. Pure saturated aliphatic hydrocarbons give peaks in the range 285.1-285.3eV (83). For the unmodified oxide, the carbon peak is at 285.45 ev (expected for any carbonaceous compound) (Figure 4.4). The energy of the C 1s peak due to carbon contamination on the sample can be assigned to the internationally accepted value of 284.6 eV (83). In the ideal case this carbon consists only of hydrocarbons in electrical contact with all surface species. Oxygen-bonded carbon gives distinct chemical shifts in the carbon 1s line.

For the GPTS-modified substrate (Figure 4.5), there are two distinct peaks at 285.8 eV (characteristic of aliphatic carbons) and 287.6 eV (characteristic of ethers) (84,85). The XPS measurements for another sample were performed to further confirm the reproducibility of the functionalization procedure. There were two distinct peaks at 285.5 eV and 287.4 eV. This provides good qualitative evidence that modification of these substrates with GPTS was successful. Scanning various regions of the substrates also showed the coverage to be quite uniform.

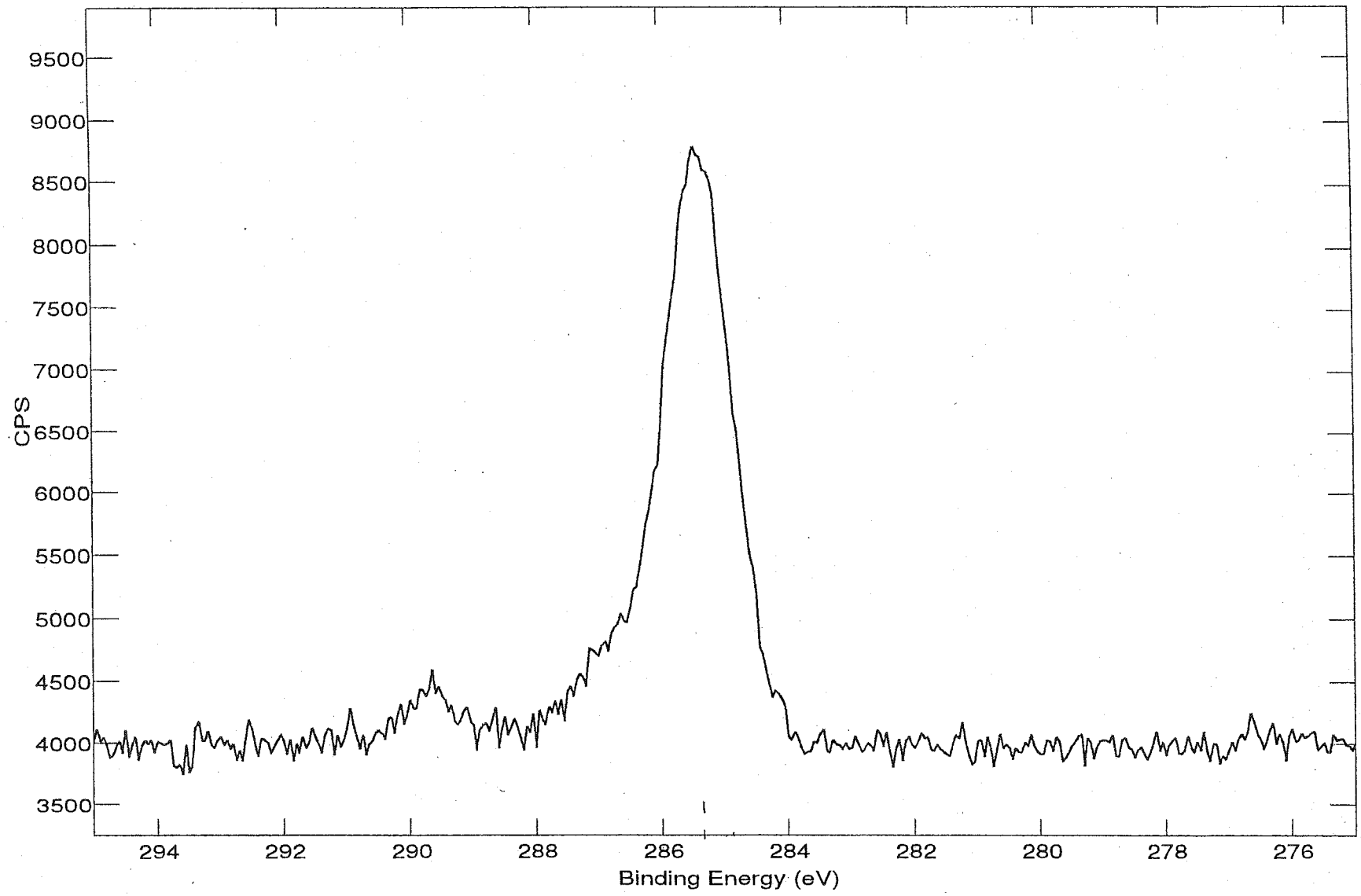

Figure 4.4 Carbon 1s peak for unmodified Si/SiO_2 substrates.

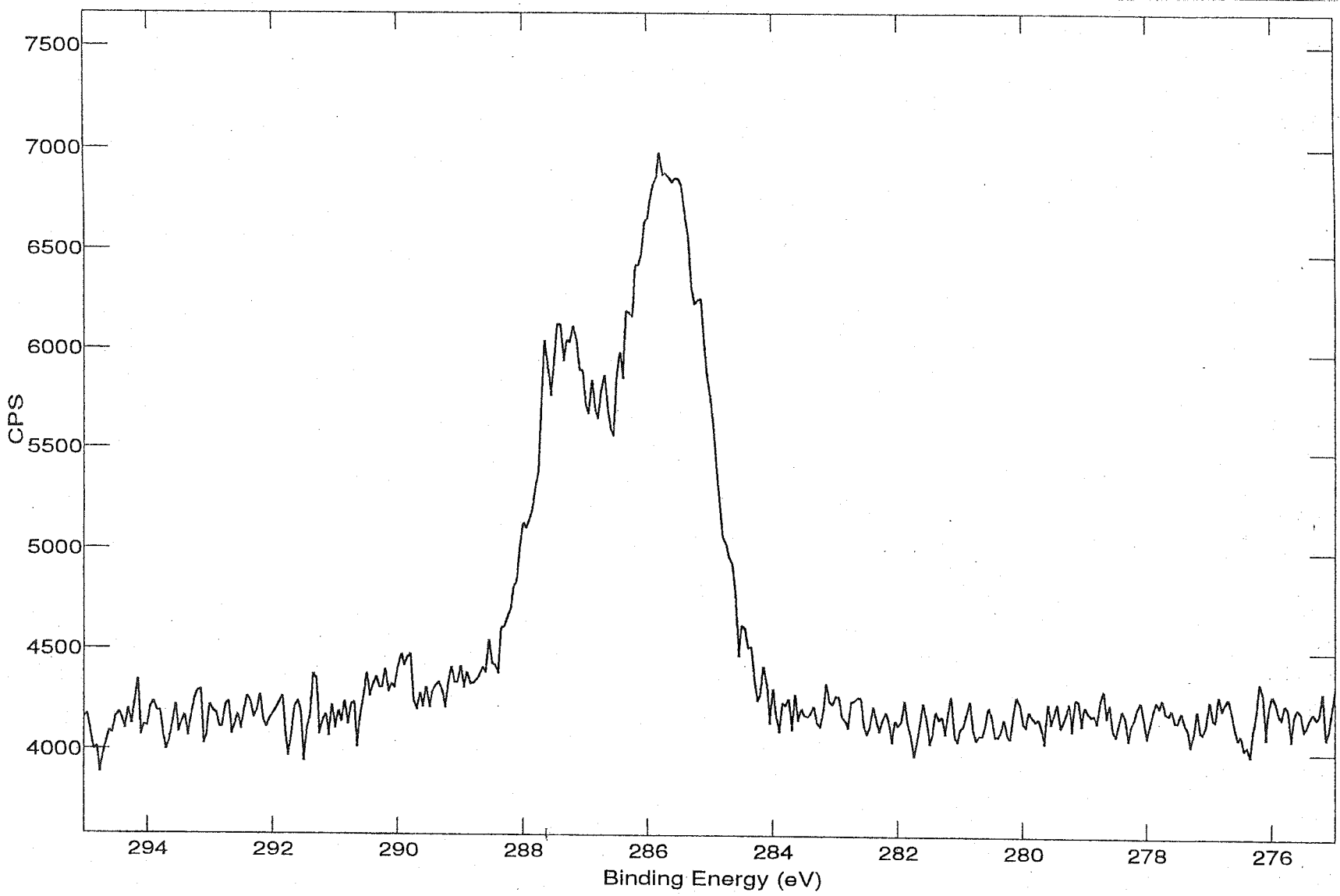

Figure 4.5 Carbon 1s peaks for GPTS-modified Si/SiO_2 substrates.

When assigning chemical states it is important to ensure consistency between the different elements present. In the example of oxygen-containing polymers, evidence for ester bonding in the C1s line, then the O 1s line should be checked for the presence of the equivalent state. The oxygen 1s line gives a broad spectral feature in the range 531-533 eV for a range of organic bonding configurations, hence it is difficult to assign the curves as to whether there are siloxane oxygens versus silanols. Figures 4.6 and 4.7 show the peaks for Si/SiO_2 and for hydroxylated Si/SiO_2.

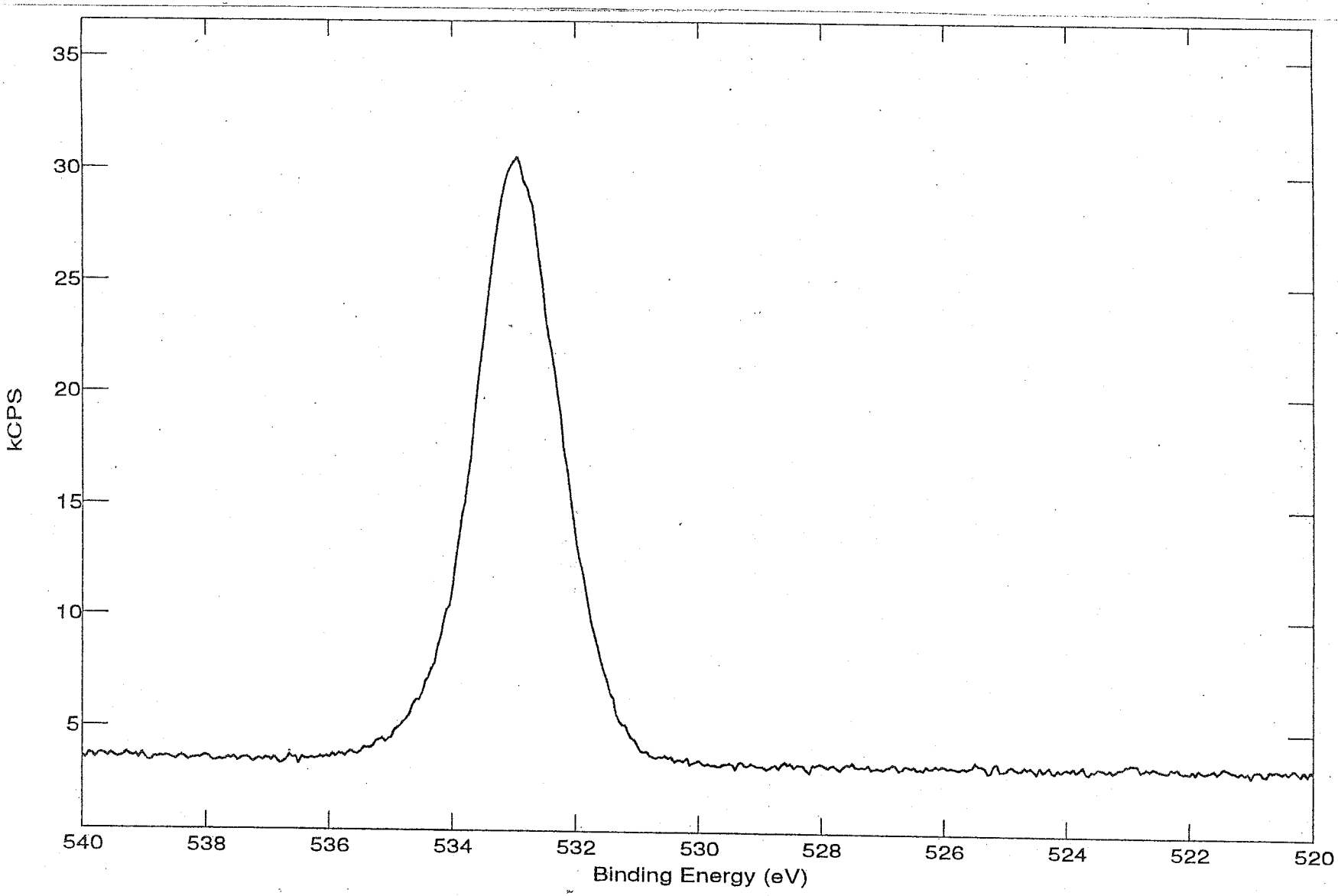

Figure 4.6 Oxygen 1s peak for unmodified Si/SiO_2 substrates.

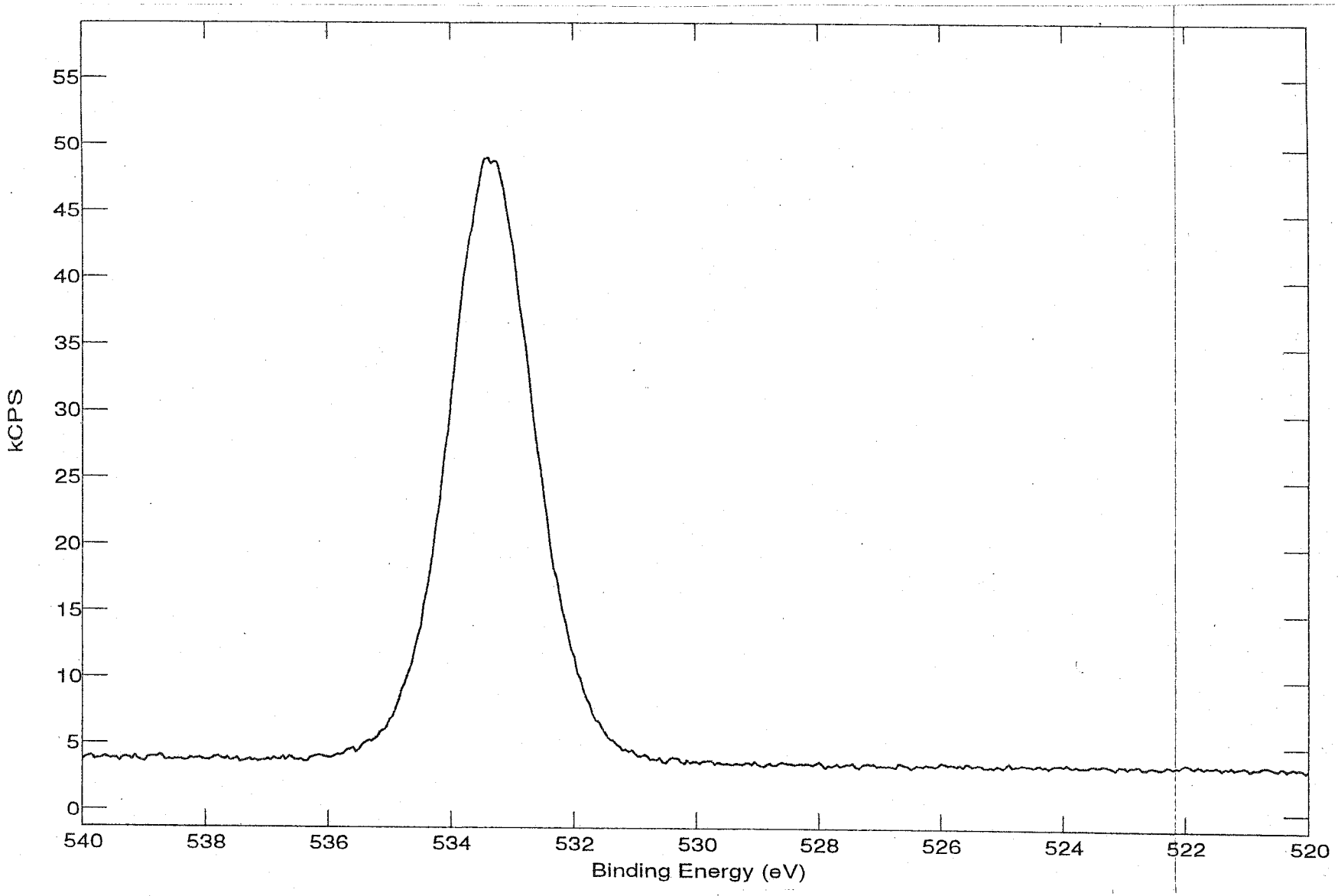

Figure 4.7 Oxygen 1s peak for GPTS-modified Si/SiO_2 substrates.

More conclusive information can be obtained from the XPS spectra for Si 2p. Firstly, by examining the XPS spectra for unmodified substrates (refer to Figure 4.8) versus GPTS-modified substrates (refer to Figure 4.9), there is an evident decrease in intensity of the Si 2p peak (~ 33%). This is due to an increase in the surface thickness. Electrons are only able to penetrate 1-4 nm of the substrate surface (83). Thus, by increasing the surface thickness, the distance of penetration of the electrons is decreased. Furthermore, the GPTS-modified substrates exhibit peaks at 103.8 eV, 101 eV, and 99.55 eV. These peaks are characteristic of Si/SiO_2 (siloxane linkages between adjacent GPTS molecules), Si of the surface GPTS, and elemental Si respectively (86, 87, 88).

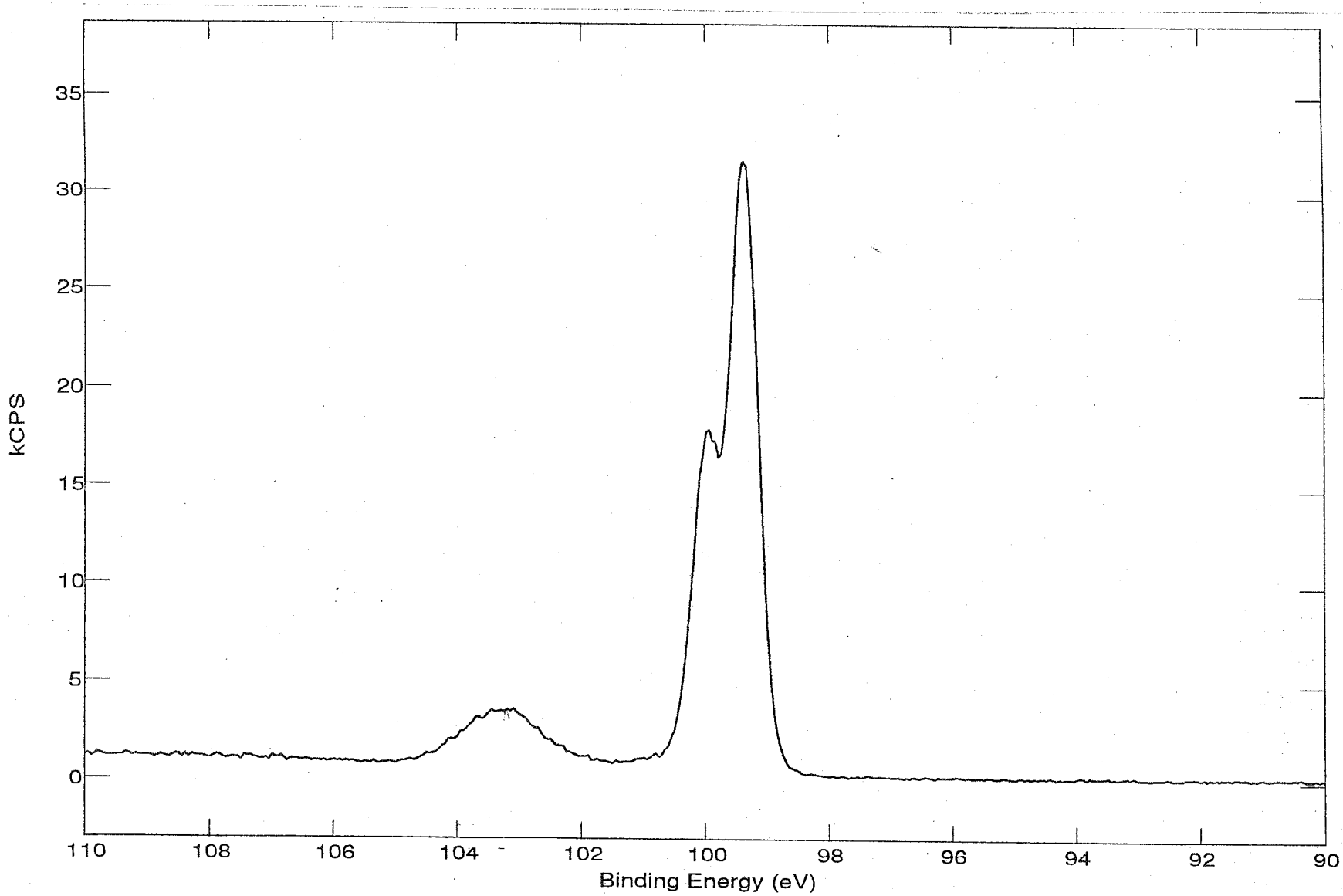

Figure 4.8 Silicon 2p peaks for unmodified Si/SiO_2 substrates.

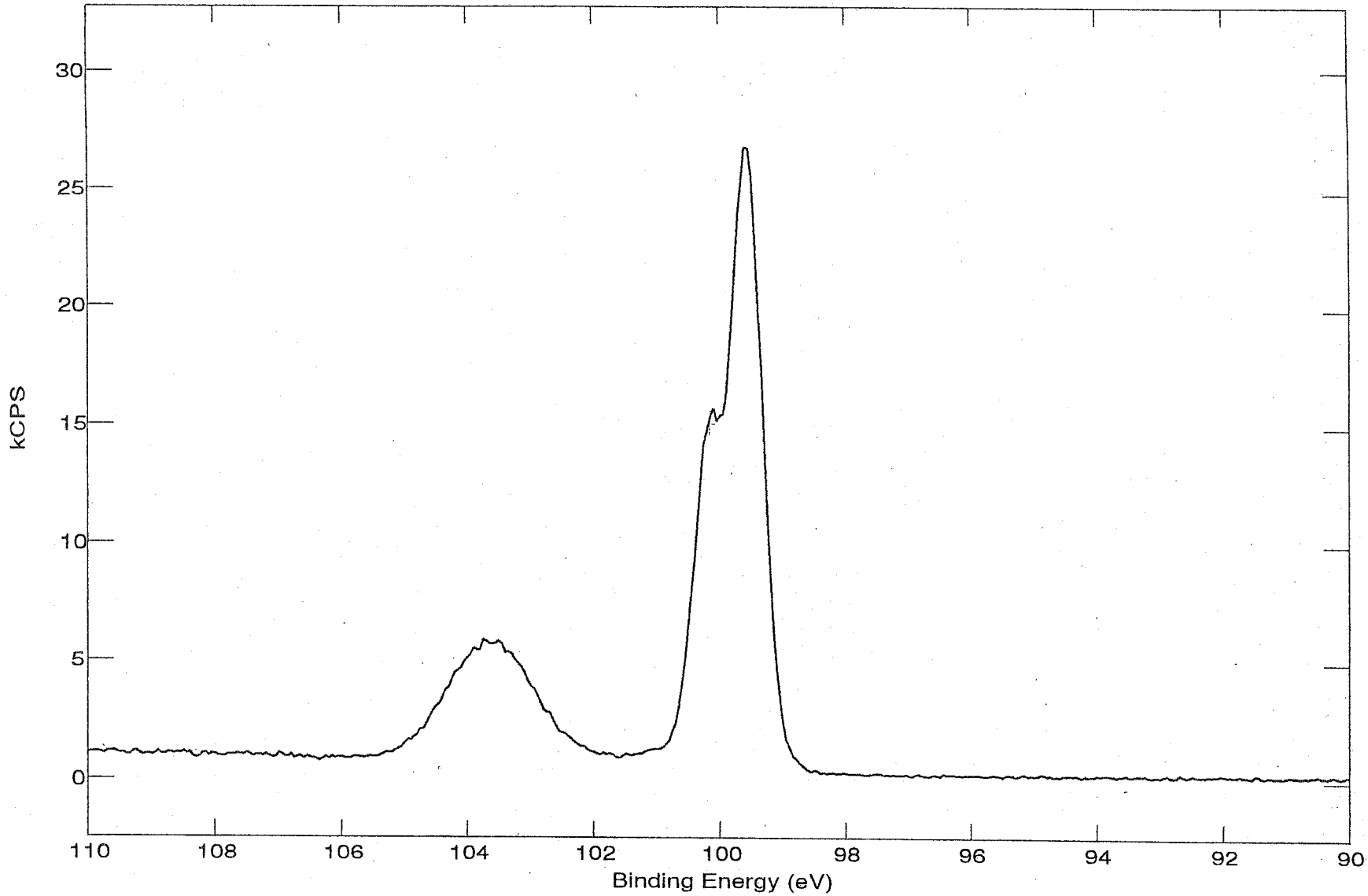

Figure 4.9 Silicon 2p peaks for GPTS-modified Si/SiO_2 substrates.

4.2 PNA Immobilization Results

Figure 4.10 shows the shift in Z_I values due to the immobilization of the PNA probe layer on GPTS modified Si/SiO_2 chips. Fluorescein-labeled 20-mer PNA (refer to Table 3.1) was used in these measurements to further confirm the presence of the probe layer following the immobilization. The actual time used to immobilize the PNA probe layers was 1 hour, to ensure that the probe layer was not too dense, in order not to inhibit the subsequent hybridization process. The impedance measurements were taken during the immobilization to monitor the change over time. Five successive impedance curve measurements were taken, each measurement lasting 12 minutes. Curve 1 (closed circle) in Figure 4.5 shows the initial measurement taken at the start of the immobilization. Curve 2 (open circle) is the final measurement taken at the end of the immobilization. The curves taken in between kept their general shape and progressively shifted to more negative potentials (not shown for clarity). The overall shift in V_{fb} was found to be -202 mV. The overall change in impedance at a fixed DC potential of 1.1 V, was 196 Ω.

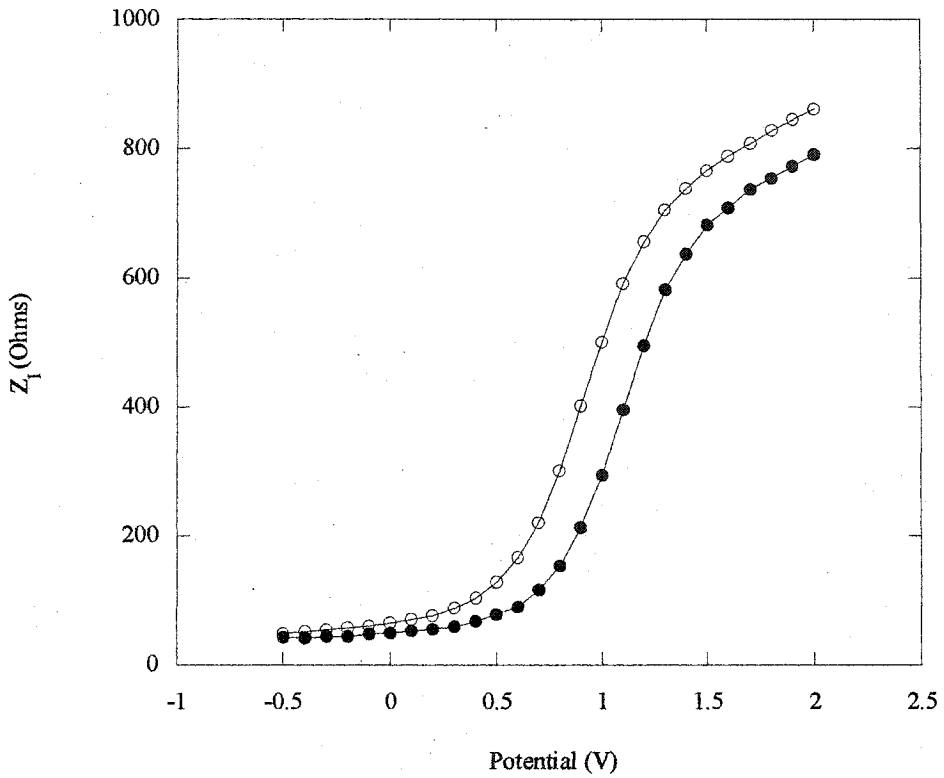

Figure 4.10 Imaginary impedance as a function of the DC applied potential, (closed circle) after 12 min, and (open circle) after 60 min, immobilization of PNA.

A blank run (Figure 4.11) was performed to assess the shift due to the electrolyte alone (without PNA) and the effect of the electrolyte is minimal, causing a change in V_{fb} of only -8 mV (not shown) and a change in Z_I of only 46 Ω at a fixed DC potential of 1 V.

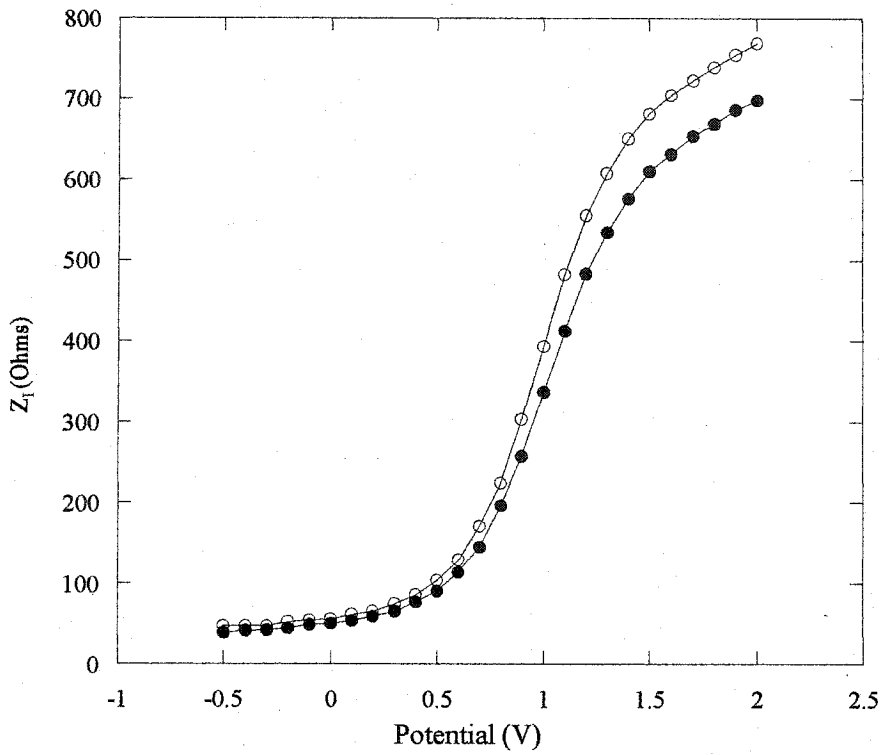

Figure 4.11 Imaginary impedance as a function of the DC applied potential, (closed circle) after 12 min, and (open circle) after 60 min, in contact with electrolyte (no PNA).

Therefore the overall shift in V_{fb} attributed to immobilized PNA is of -194 mV and the overall change in Z_I can be attributed to immobilized PNA is of 150 Ω.

Fluorescence measurements were taken after the immobilization (following the impedance curves). The median intensity of the PNA probe layer was determined to be 2.3×10^4 a.u. From the standard curve shown in Figure 4.12, which was generated by depositing known amounts of fluorescein-labeled PNA on Si/SiO_2 chips (allowing the solvent to evaporate, but not removing any of the PNA by rinsing in this case, to preserve the known amount) the median intensity is found to correspond to a surface density of the order of $1x10^{13}$ strands of PNA oligomer per cm^2. Typical surface coverage of probe DNA is in the order of 10^{11} - 10^{13} molecules per cm^2 (89).

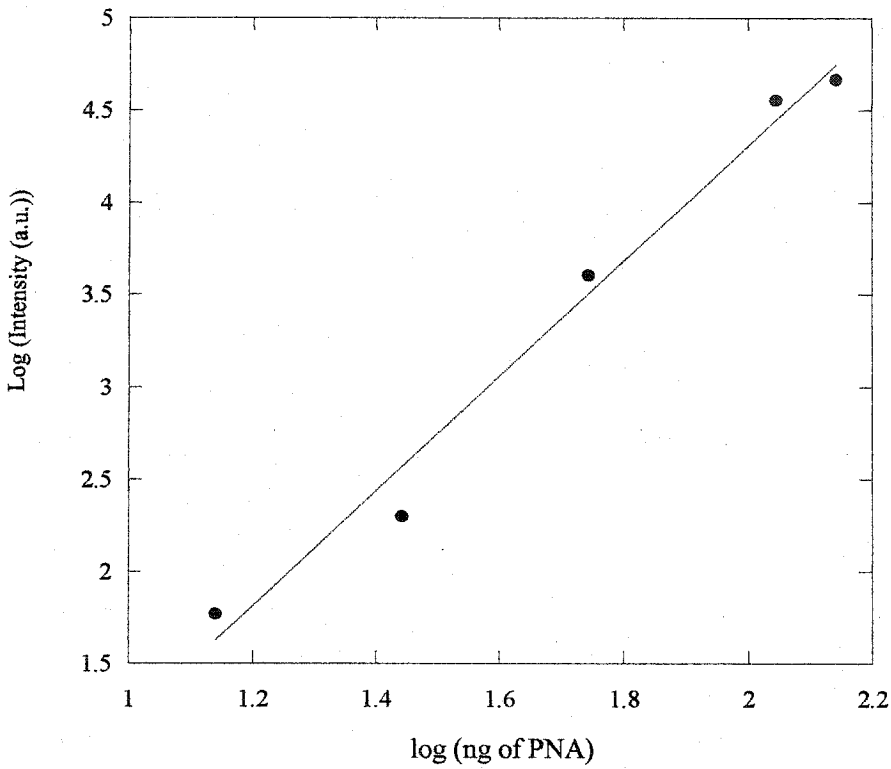

Figure 4.12 Standard curve of fluorescence intensity for the immobilization of PNA.

4.3 DNA Hybridization Results

Figure 4.13 shows the impedance results obtained for PNA/DNA hybridization, using fluorescein-labeled DNA, performed at room temperature for 1 hour. Unlabeled PNA was used as the probe layer and the chips were vigorously washed with distilled water to remove any unbound PNA prior to hybridization. The impedance measurements were taken using 0.1M NaCl as electrolyte. As in the case of the PNA immobilization, impedance measurements were taken as the hybridization took place (Figure 4.8).

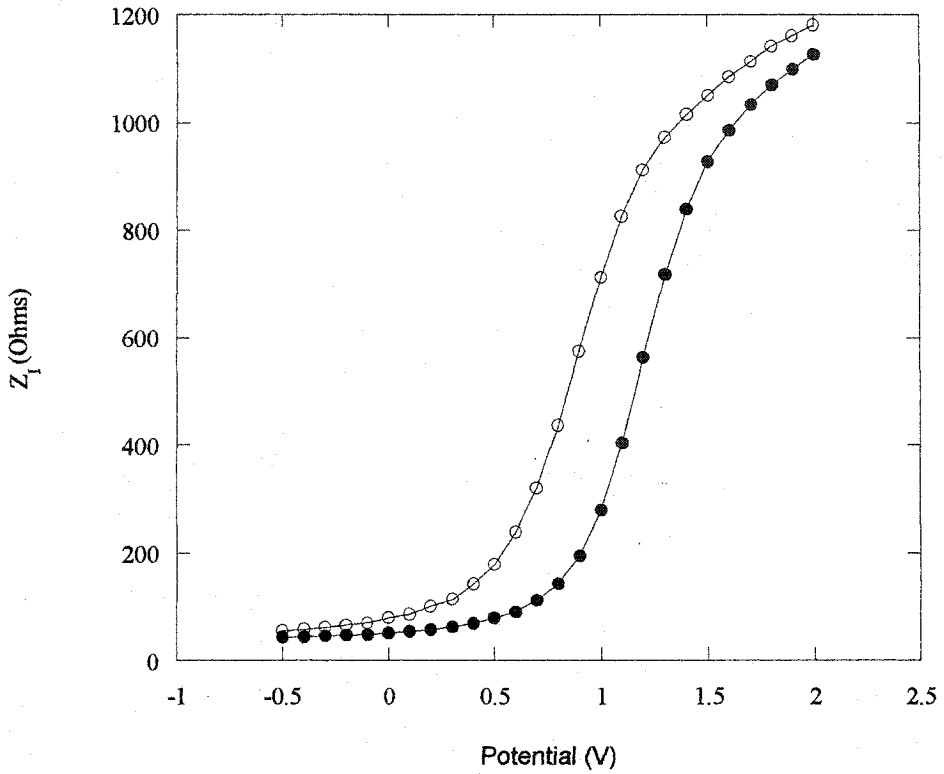

Figure 4.13 Imaginary component of impedance as a function of the DC applied potential, (closed circle) after 12 min, and (open circle) after 60 min, hybridization with complementary DNA.

A blank run was performed to determine if any V_{fb} shift was caused by the electrolyte. The effect of the electrolyte was negligible (approximately 0mV) (Figure 4.14)

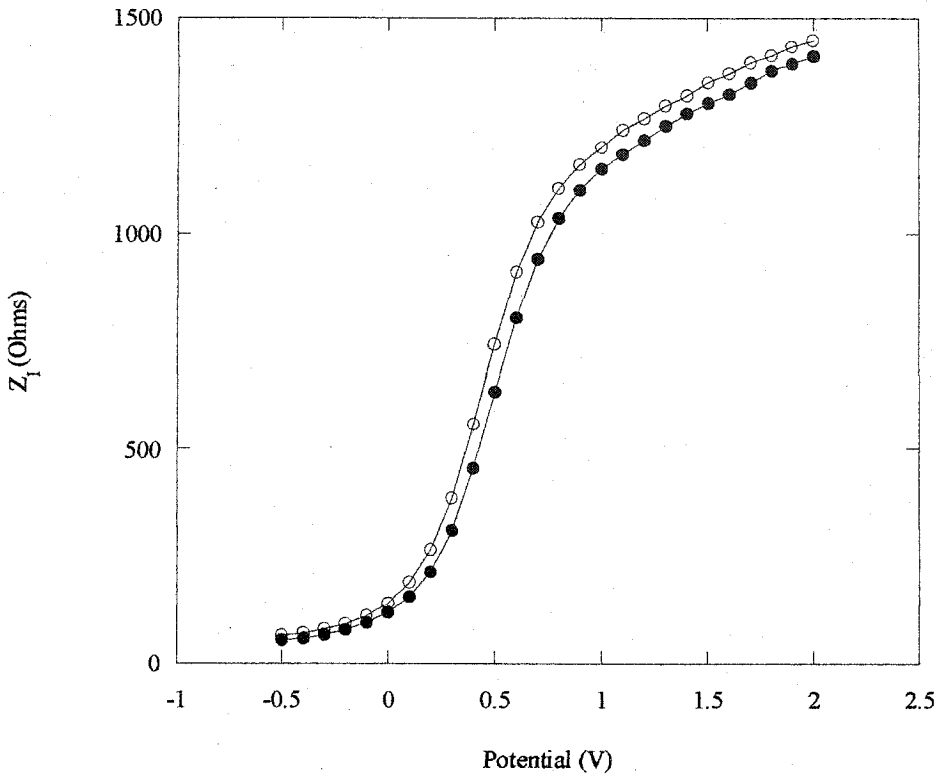

Figure 4.14 Imaginary impedance as a function of the DC applied potential, (closed circle) after 12 min, and (open circle) after 60 min, in contact with electrolyte (no DNA).

Therefore, the change in V_{fb} due to hybridization of DNA was found to be -375 mV. The change in Z_I due to hybridization of DNA was found to be 363 Ω at 1.0V. Following hybridization, the chips were washed with distilled water (room temperature) to remove any unhybridized-labeled DNA. Fluorescence measurements taken immediately after the washing gave an intensity of 1.1×10^4 a.u. confirming the presence of the complementary DNA, and indicating that approximately 80% of the surface immobilized PNA have been hybridized.

Figure 4.15 serves to compare the electrochemical impedance responses for the immobilization and hybridization steps observed during the series of five measurements

taken over 1 hour (taken from experiments shown in Figures 4.10 and 4.13). The data is presented in the form of Z_I values taken at fixed applied dc potentials of 1.1V for the immobilization, and 1.0V for the hybridization, as a function of time. The overall variations in Z_I were found to be of approximately 200 Ω and 450 Ω for the immobilization and hybridization steps, respectively. This is in accordance with the fact that the impedance-based approach to detection is sensitive to charge variations at the semiconductor/electrolyte interface, and is therefore expected to be more sensitive to the hybridization event involving charged DNA, as opposed to the immobilization of PNA. These results also show that hybridized DNA surface densities of the order of 10^{12} to 10^{13} molecules/cm^2, which yield Z_I variations of ~400Ω, can be readily measured.

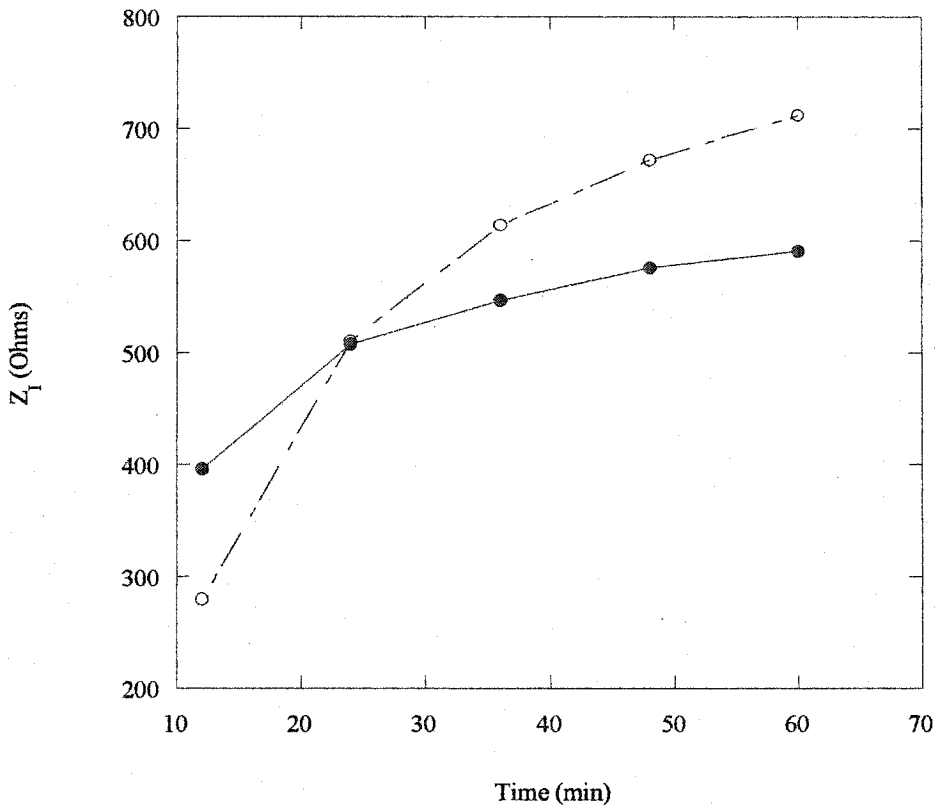

Figure 4.15 Imaginary component of impedance variations at 1.1 V for immobilization (closed circle), and 1.0 V for hybridization (open circle) as a function of time.

The sensor sensitivity to concentration variations in that range was also tested, and the results are shown in figure 4.16. Individual chips were each exposed to a 100uL amount of DNA solutions of four different concentrations (0.1, 0.2, 1, 2 ng/μL), and left to hybridize for 1 hour. The results show a linear relationship for Z_I versus DNA concentrations in this range.

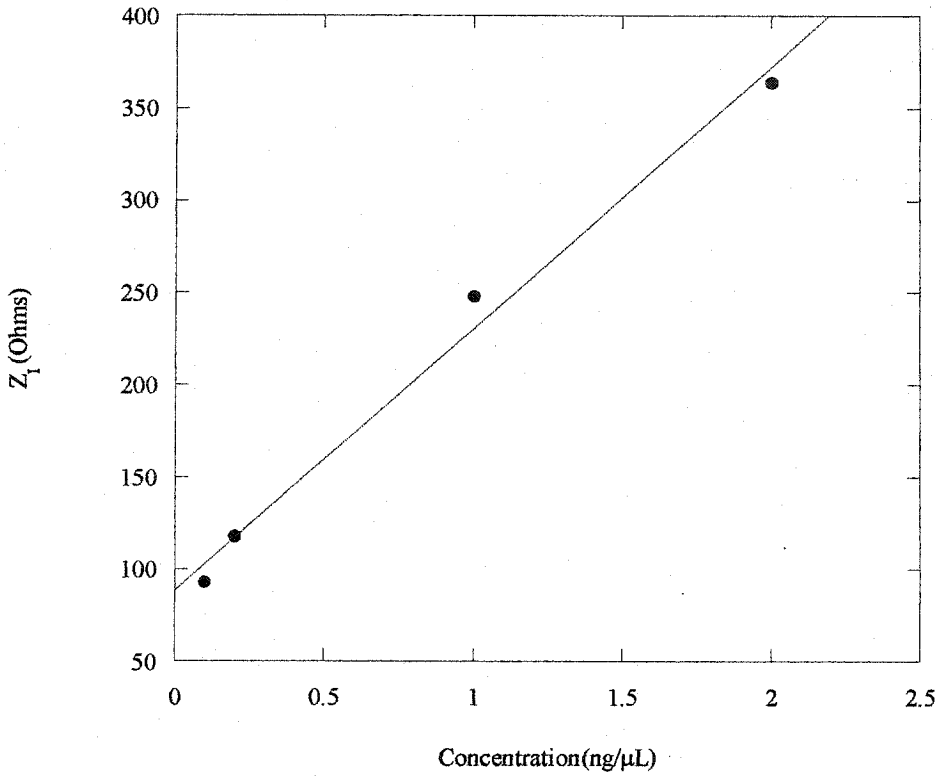

Figure 4.16 Imaginary impedance as a function of DNA concentrations varying from 0.1ng/μL to 2ng/μL.

In a study by Jensen et al., they investigated the kinetics for hybridization of PNA with DNA and RNA using the BIAcore technique by measuring the amount of DNA that hybridized to the surface-bound PNA as a function of time. For the analysis of the hybridization kinetics, a two-state model, A+B↔AB, is assumed. The association kinetics was analyzed with respect to the concentration dependence of the association rate by varying the concentration of the complementary DNA, agent A, in the mobile phase. In this study they found that by increasing the concentration of the complementary DNA, the rate of hybridization increases (90). Our findings are in accordance with results of Jensen et al. The k_a values were obtained by using the Zi values used in Figure 4.16. By plotting k_a versus concentration, we see that the association rate increases with the

concentration of the complementary DNA (refer to Figure 4.17). There is a linear correlation of the observed rate constant with concentration of associating strand.

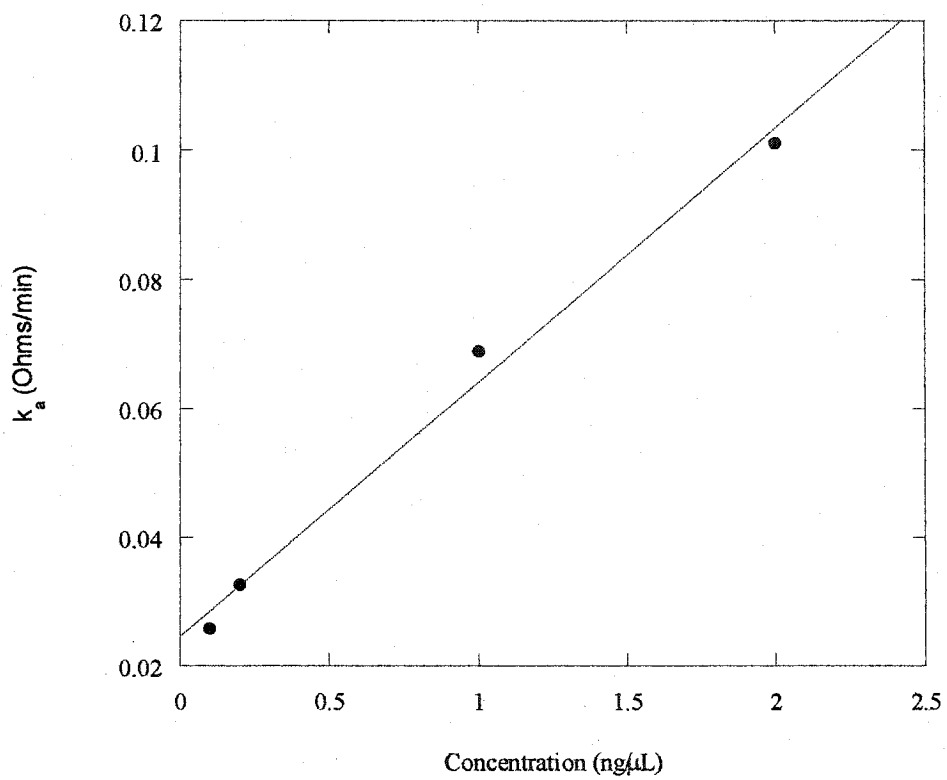

Figure 4.17 Plot of association rate constant (k_a) versus concentration (μg/ μL).

4.4 Probe density as a function of immobilization time

The rate and extent of hybridization strongly depends on surface probe density. Controlling the reaction time of PNA with the solid support (91-94) can control the probe density. Immobilized oligomers at a solid surface can experience significantly different environments from those experienced in bulk solution, which will affect the selectivity of the probe (95, 96). In addition, it is the orientation of the immobilized probe that is affected by the probe density and this may affect the kinetics of hybridization. If the

density is too low, the strands may be collapsed flat on the surface. At a higher density, the strands will lie proper to the surface, however, the density cannot be too high, preventing efficient hybridization. By controlling the probe density, we ensure that the probe layer is not too tightly packed allowing for efficient hybridization. If the density is too high, there is not enough space between probe molecules, thus the complementary DNA strands cannot insert between the probe molecules to hybridize properly because this close packing is much more likely to facilitate interactions between neighboring strands. Consequently, the hybridization efficiency is decreased at high probe density. In the lowest probe density regimes, the majority of probes should be hybridized because there is enough space between probe molecules to allow for complementary DNA to hybridize. There should be little or no interactions between neighboring strands that may affect hybridization (96).

The chips were prepared by varying the immobilization times (15, 30, 45, 60 minutes). The same concentration of PNA (0.02μg/μL) and ionic strength (0.1M NaCl), as in previous experiments, was used. For each immobilization time, the target/probe hybridization was performed for one hour under the same conditions of solution concentration and ionic strength (0.02μg/μL DNA and 0.1M NaCl). Impedance measurements were taken while the reaction took place for the immobilization and hybridization. Figure 4.18 serves to show that as the immobilization time increases, the impedance value increases corresponding to an increase in the amount of PNA oligomers covalently bound to the GPTS-functionalized silicon chip. The data is presented in the form of the overall change in Z_I taken at a fixed applied dc potential for each

immobilization time (different for each immobilization time). The effect of the electrolyte is subtracted from the overall change in Z_I.

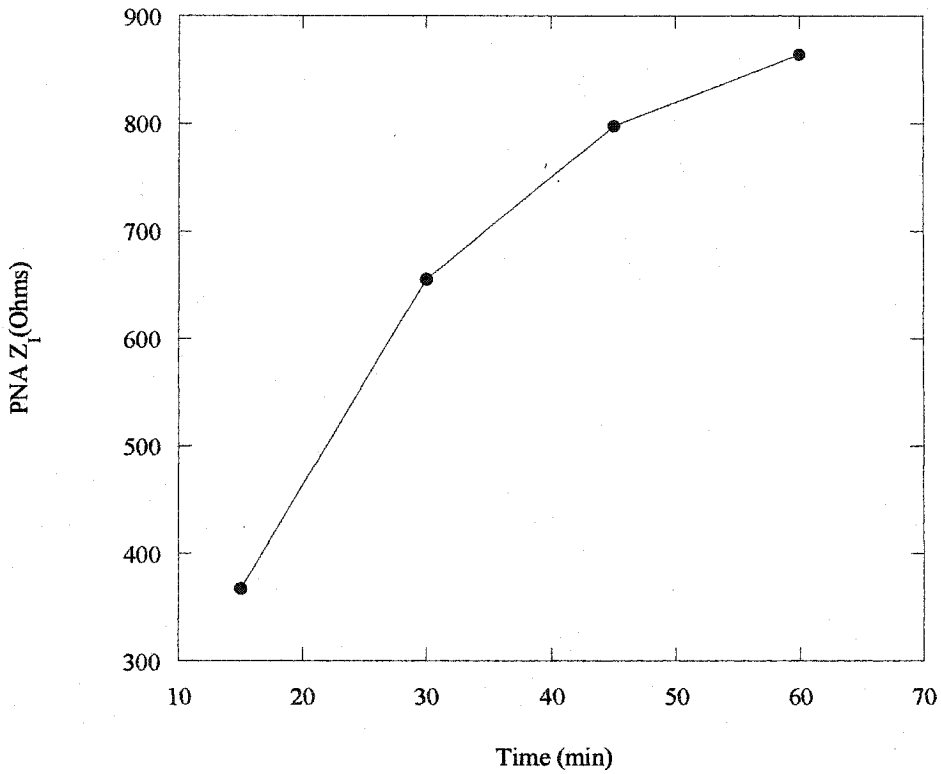

Figure 4.18 Varied PNA immobilization time.

The magnitude of the change in impedance for hybridization decreases as the density of the probe increases (as shown in Figure 4.19). That is, the efficiency of the hybridization decreases with increasing probe density. The data is presented in the form of the overall change in Z_I for the DNA hybridization taken at a fixed applied dc potential for each overall change in PNA Z_I. The effect of the electrolyte is subtracted from the overall change in Z_I.

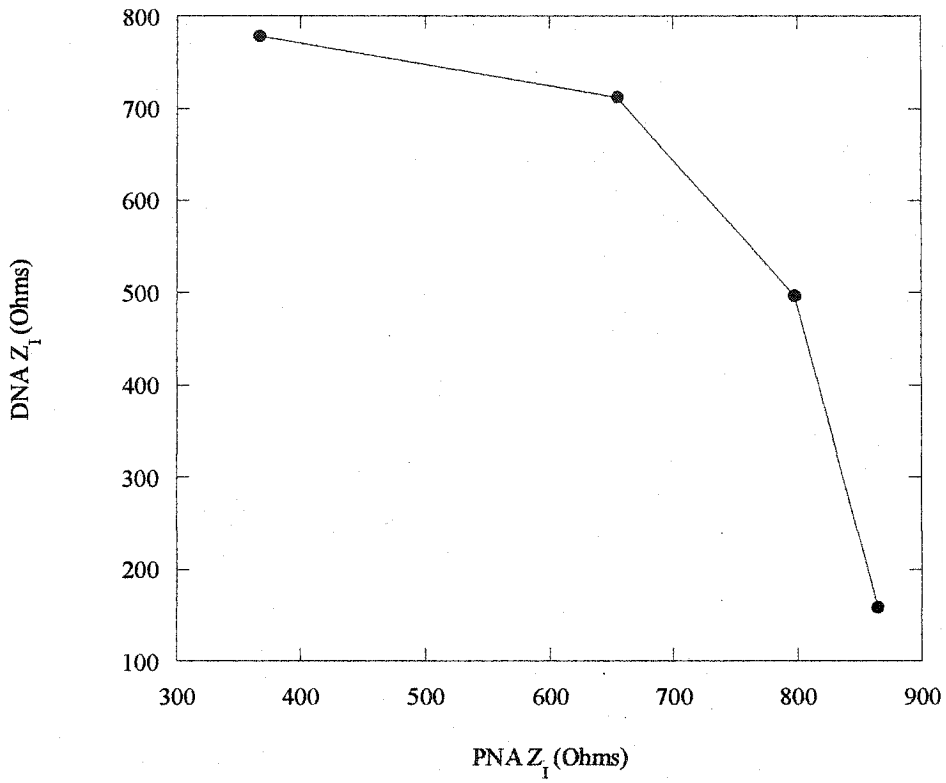

Figure 4.19 Change in impedance for DNA hybridization versus change in impedance for varied PNA immobilization times.

A long immobilization time of 60 minutes yields a large immobilization change in impedance while the corresponding hybridization change in impedance is small, demonstrating the presence of a high density of single strands at the surface (approximately 10^{13} probe molecules/cm^2) to which few complementary strands can bind. Conversely a large change in impedance is observed for hybridization following the low immobilization reaction time of 15 minutes. The results suggest that an immobilization of fifteen minutes is sufficient enough to obtain a single strand layer with a good balance between density and steric hindrance.

By examining the Z_I values taken at fixed applied dc potential (-0.45 V) for one hour of immobilization (taken every five minutes), we can see that the amount of probe bound reaches saturation (Figure 4.20). The greatest amount of strands that can bind to the functionalized surface is reached after ~25 minutes (approximately 10^{13} strands/cm^2).

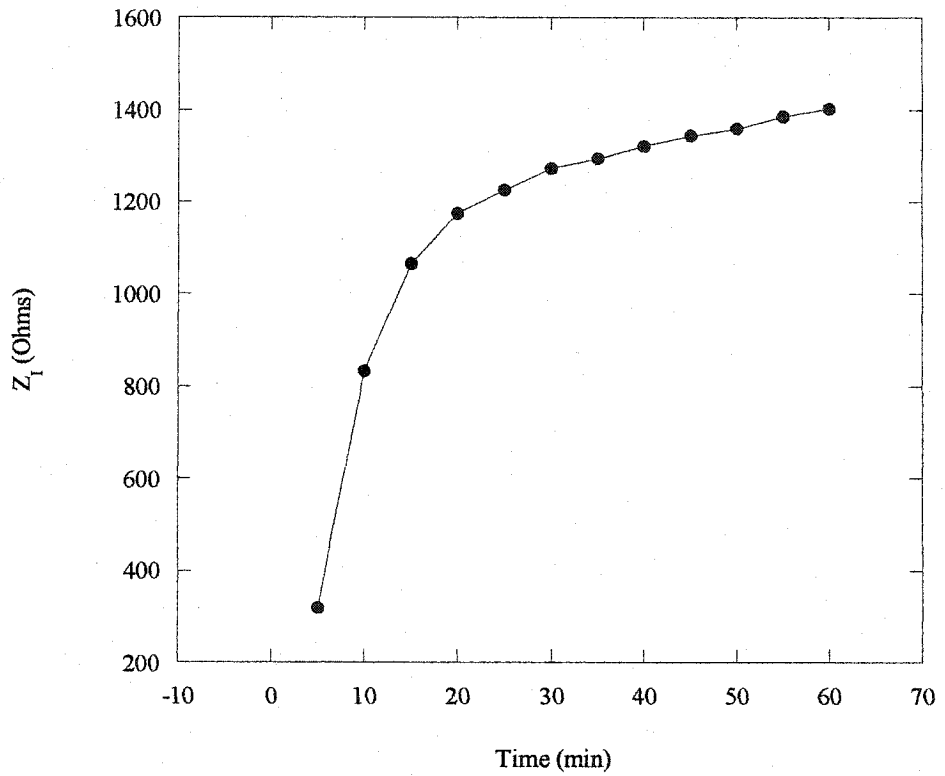

Figure 4.20 Imaginary component of impedance variation at -0.45V for immobilization as a function of time.

The data presented in Figure 4.21 is presented in the form of Z_I values taken at fixed applied dc potential (-0.6 V) for the hybridization as a function of time. One hour of immobilization allows for maximum immobilization efficiency (maximum amount of probe bound).

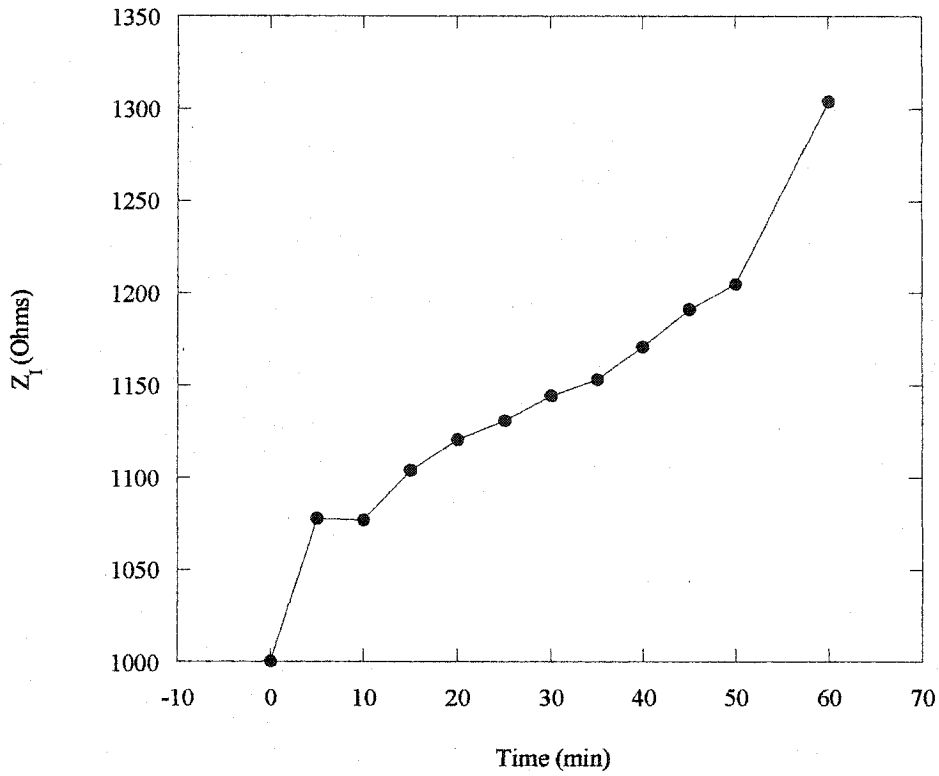

Figure 4.21 Imaginary component of impedance variations at -0.6V for hybridization as a function of time.

However, this affects the hybridization efficiency. The rate of hybridization is slow and does not reach saturation. In addition, the hybridization process does not follow Langmuir-like kinetics. Consequently, we can see that the kinetics of hybridization has a distinct dependence on probe density. This effect is possibly due to the steric constraints at this higher probe density. Steric interactions increase with increasing probe density, therefore, as we increase the immobilization time from 15 minutes to 1 hour, we see that hybridization efficiency decreases and the rate of hybridization decreases.

If we examine the Z_I values taken at fixed applied dc potential for the 15-minute-immobilization reaction as a function of time we see that the immobilization reaction

does not reach saturation (not shown). The hybridization examined at fixed dc potential (-0.45 V) demonstrates that the hybridization does reach saturation (Figure 4.22).

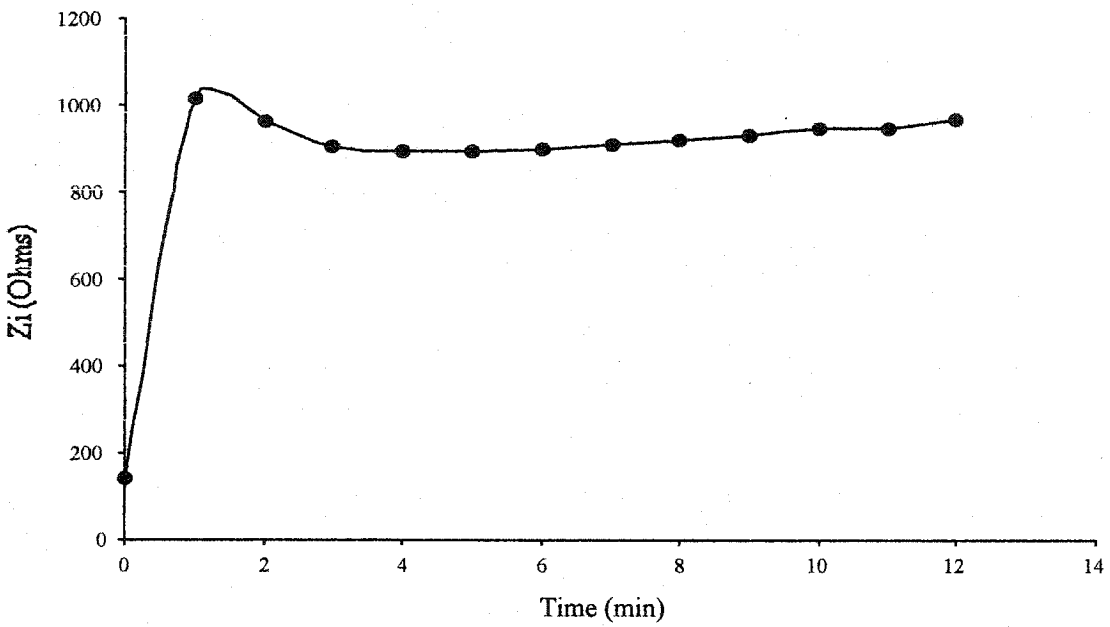

Figure 4.22 Imaginary component of impedance variations at -0.55 V for hybridization of low density probe layer as a function of time.

Upon examination of the kinetic profiles for high density and low-density substrates, we see that the kinetics of hybridization is dependent on probe density. For probe densities below 10^{13} molecules/cm^2, the initial hybridization rate (initial five minutes) was rapid (faster than for hybridization of chips immobilized for 1 hour).

From these results, we confirmed that for perfectly matched DNA, in which the probe density was varied by an order of magnitude, both the rate and the extent of hybridization depend strongly on surface probe density. In the lowest probe density regimes, the majority of probes (~ 100%) should be hybridized, whereas at high probe density, the efficiencies drop to 80% and the kinetics are slower. It is worth noting that the general

trends are reproducible from one batch of chips to the next. That is, that 15-minute immobilization time will allow for the most efficient hybridization and 1-hour immobilization time results in the most inefficient hybridization. However, the actual Z_I values for each immobilization times are different from batch to batch.

4.5 Probe density as a function of PNA concentration

As mentioned earlier, controlling the probe solution concentration allows control of the immobilized probe density. Individual chips were each exposed to 100μL amount of PNA solution at a concentration of 0.00002, 0.0001, 0.0002, 0.001, 0.002μg/μL, and left to immobilize for one hour (refer to Figure 4.23).

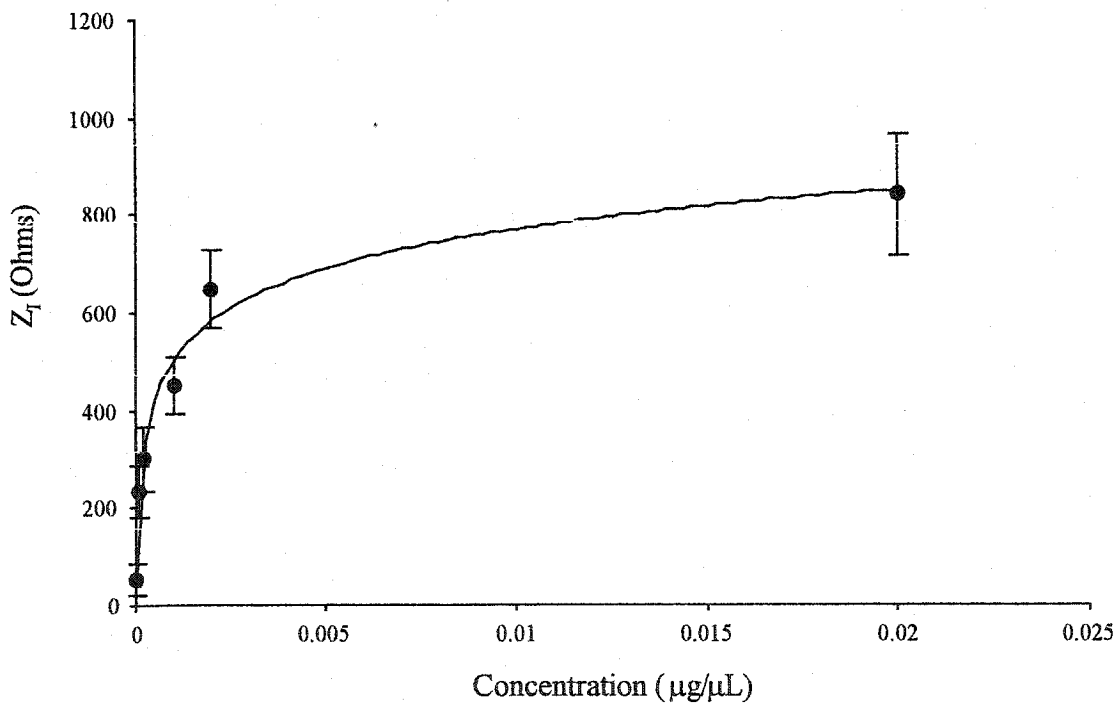

Figure 4.23 Change in impedance as a function of PNA concentration.

The results show that at lower oligonucleotide concentrations, the efficiency of probe immobilization is directly proportional to the concentration of the PNA oligomer. The probe density reaches a plateau with a PNA concentration of approximately 0.002μg/μL.

Following immobilization, each chip was hybridized with 0.02μg/μL target DNA for 1 hour. Examining the change in impedance at a fixed dc potential (-250 mV) for the immobilization as a function of time, we see that at a concentration of 0.0001μg/μL, the immobilization reaches saturation after 40 minutes (Figure 4.24). There is no change in Z_I after this point.

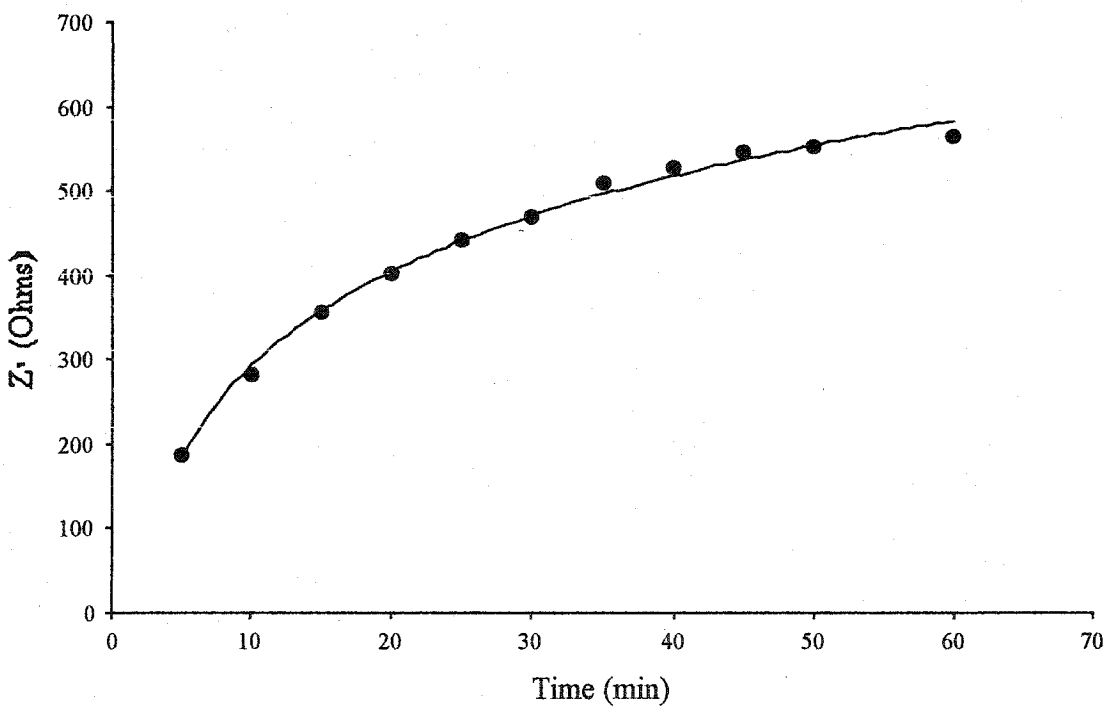

Figure 4.24 The change in impedance at -250mV as a function of time for 0.0001 μg/μL.

The subsequent hybridization also reaches saturation after 25 minutes (refer to Figure 4.25).

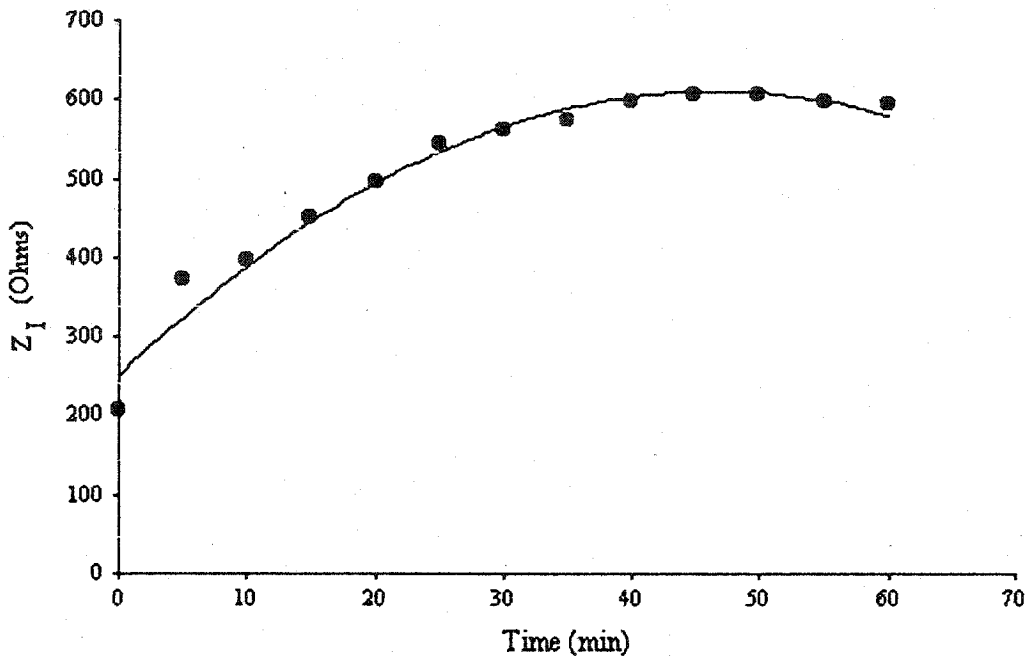

Figure 4.25 The change in impedance at -250mV for hybridization as a function of time for 0.0001 μg/μL PNA immobilization.

We can conclude that at a concentration of 0.0001μg/μL PNA, it is assumed that the greatest amount of strands of PNA that can bind to the chip are covalently bound to the surface is achieved after one hour of reaction. This probe layer is not too dense because the probe strands are efficiently hybridized as shown in Figure 4.26.

4.6 Melting temperature determination

An accurate determination of melting temperatures for PNA-DNA duplexes will allow for the accurate detection of single base mismatches. The stability of the double helix state is often measured by means of the thermal denaturation temperature, T_m, which is

defined as the temperature at which half of all duplexes originally formed are denatured into the single-stranded state. The stability of double-stranded DNA (dsDNA) is dependent on base composition, strand concentration, and ionic strength. Base pair mismatches can reduce the observed T_m by reducing the thermal stability of the double helix; the magnitude of which is dependent on the number of mismatches and length of the duplex. In duplexes that are 14-20 nucleotides in length the T_m is reduced by up to 5-10°C depending on the G + C content of the sequence. At higher salt concentrations, duplexes may be more stabilized, thus decreasing the sensitivity of the probe to mismatches. This is less of a consideration for PNA-DNA duplexes. The effect to the T_m at higher strand concentrations (above 75μM) is due to strand aggregation, which is thought to preferentially stabilize dsDNA relative to ssDNA (96-98).

The present work uses as a model the determination of the T_m of a complex sequence PNA 10-mer by impedance measurements. All thermal denaturation profiles for hybridization occurring at the surface of the sensor were acquired by measuring the change in impedance at a fixed potential as a function of temperature, recording the Zi at a fixed potential from room temperature (~24°C) to 60°C. The temperature ramp rate was 1.5°C/min to ensure that equilibrium conditions were satisfied.

The melting curves represent at all temperatures the equilibrium between the duplex and the two single strands. Combining the relation

$$\Delta G^\circ = \Delta H^\circ - T\Delta S^\circ = -RT\ln K_D \qquad (4.1)$$

with the expression for K_D

$$K_D = [C_T/2]\,[(1-\alpha^2)/\alpha] \qquad (4.2)$$

Gives at $T = T_m$ ($\alpha = 1/2$);

$$1/T_m = [(\Delta S^\circ + R\ln 4)/\Delta H^\circ] - [(R/\Delta H^\circ) \ln C_T \qquad (4.3)$$

Where R is the ideal gas constant, C_T is the total strand concentration, and α is the fraction of the duplex (91, 99).

4.6.1 Procedure for Tm determination

A typical Tm determination is performed by measuring the impedance of the system while increasing the temperature with a setup composed of a three-electrode potentiostatic set-up connected to a temperature regulation system (±0.2°C). The regulation system consisted of a heater equipped with a PID controller and a motor-driven, variable speed, water pump that controls the temperature of the circulating electrolyte. Both temperature and impedance values are recorded simultaneously. The impedance curves obtained generate a melting curve. As in previous work from this group, the T_m is considered the point on the melting curve at which the impedance approaches a minimum. The point at which there is a break in the linearity of the curve is considered the minimum. This higher temperature value corresponds to the maximum matching of the probe to the complementary DNA. This is the most reliable T_m value (46). All of the measurements were done in triplicate.

4.6.2 Tm determination of simple oligo-20-mer DNA

In previous work from this research group, using this method, we have shown that we can accurately detect the T_m for simple oligonucleotide sequences, however, the ability of this method to detect single-base mismatches needed to be explored. Oligo

d(T)20 were immobilized on chips with a 15-min incubation time and hybridized with oligo d(A)20 for 1 hour at room temperature. A linear temperature ramp, from room temperature to 55°C, was then applied to the d (T)20/d(A)20 chip, while measuring the imaginary component of impedance variation at a fixed DC potential (-0.2V). The impedance versus temperature curve (melting curve) obtained is presented in Figure 4.26.

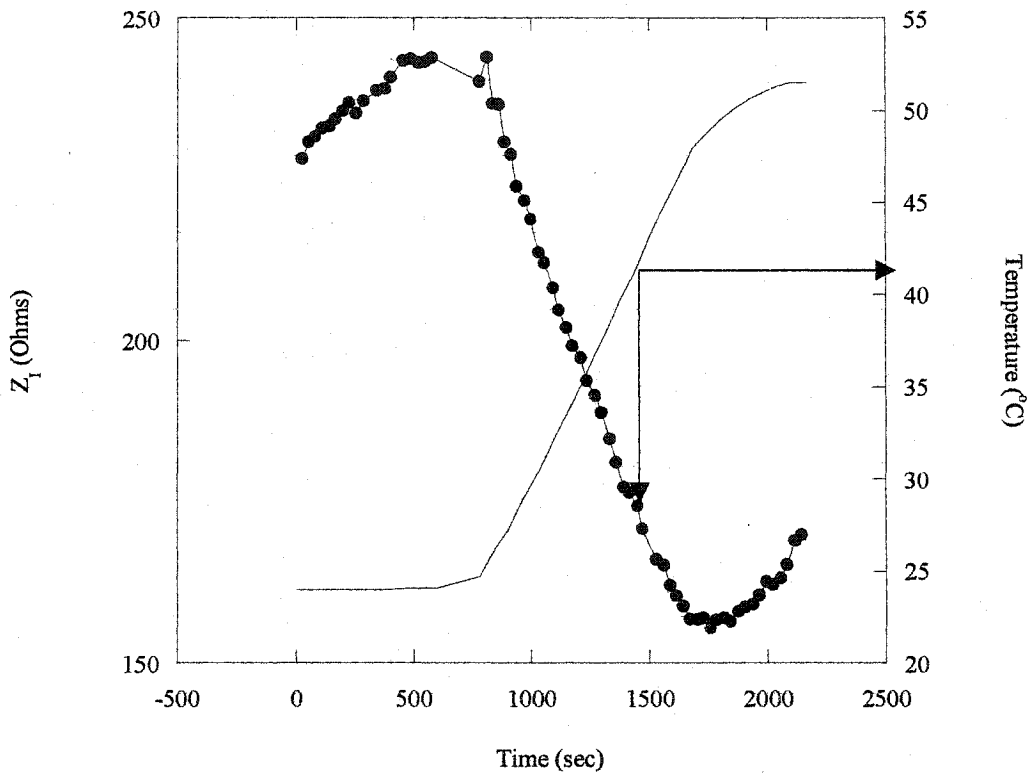

Figure 4.26 Imaginary impedance at -200 mV (closed circle) and temperature variation (plain line) for dT/dA denaturation curves.

A reproducible 100Ω Z_I drop is clearly observed. The T_m is estimated at 42°C. This experimental value compared reasonably well to the theoretical one of 43°C as calculated using equation (100,101):

$$T_m = 100.5 + (41 * (yG+zC)/(wA+xT+yG+zC)) - (820/(wA+xT+yG+zC)) + 16.6 * \log_{10}([Na+]) \quad (4.4)$$

Where w,x,y,z are the number of the bases A,T,G,C in the sequence, respectively. The term 16.6*log10([Na+]) adjusts the T_m for changes in the salt concentration, and the term log10(0.100) adjusts for the salt adjustment at 100 mM Na^+. This equation is used for sequences in the 18-25mer range. This experiment was repeated for a single-base mismatch. The Tm is affected by the position of the base-pair mismatches within the duplex (96, 102, 103). An adenine base was replaced with a cytosine in the tenth position of the dA oligomer. Figure 4.27 presents the denaturation curve obtained under the same conditions as those for the single-base mismatch chip. The T_m was estimated to be 35°C. This 7°C lowering of the T_m indicates that there was a significant lowering of the thermal stability as a direct result of a base-pair mismatch.

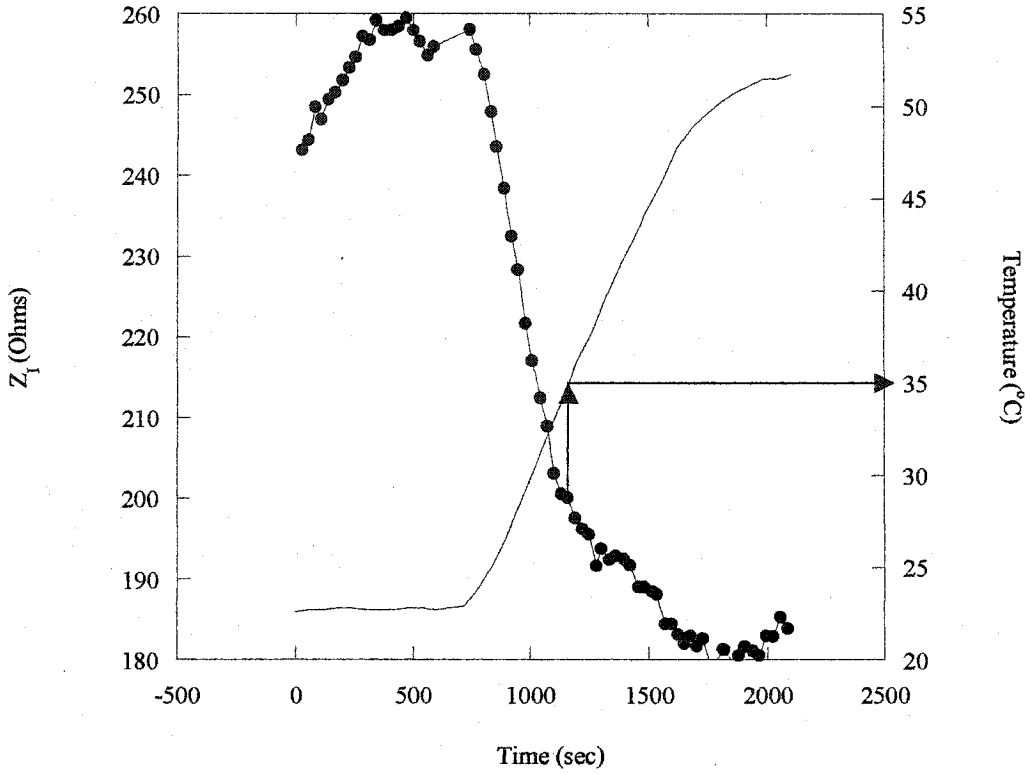

Figure 4.27 Imaginary impedance at -250mV and temperature variation (plain line) for dT/dA mismatch denaturation curves.

4.6.3 PNA-DNA Tm determination

The chips were prepared under the same conditions, as previously described for low-density chips (15-minute probe immobilization), for perfectly matched and single base-pair mismatched PNA/DNA duplexes. A linear temperature ramp, starting at room temperature and ending at 60°C was applied to the chips (reaching 60°C in 30 minutes), while measuring the imaginary component of the impedance at a fixed potential. The melting temperature was determined as previously mentioned. Figure 4.28 presents the denaturation curve for the perfect matched chip. For the sample shown,the Tm is 52°C.

The standard error is 52.2°C ± 0.3°C. This experimental value compared reasonably well to the theoretical one of 50°C.

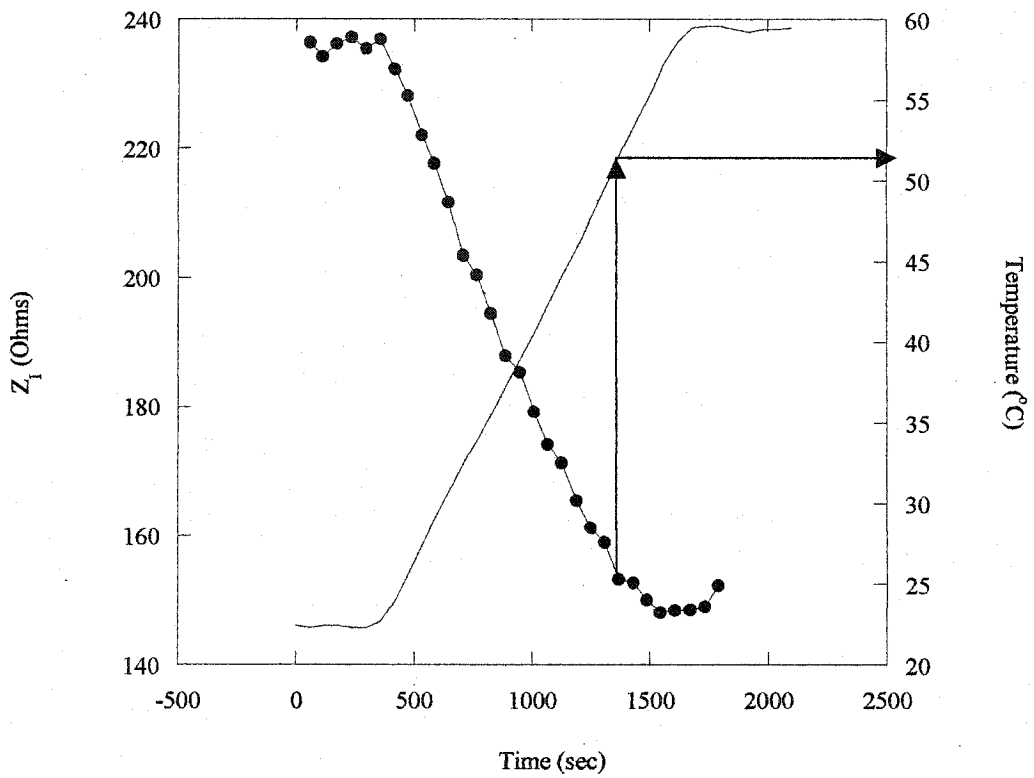

Figure 4.28 Imaginary impedance at -250mV and temperature variation(plain line) for PNA-DNA measurement.

Figure 4.29 presents the denaturation curve for the mismatched chip. A thymidine base was replaced with a cytosine in the fifth position of the complementary DNA oligomer. For the sample shown, the Tm is 40°C. The standard error is 39.7 ± 0.7°C.

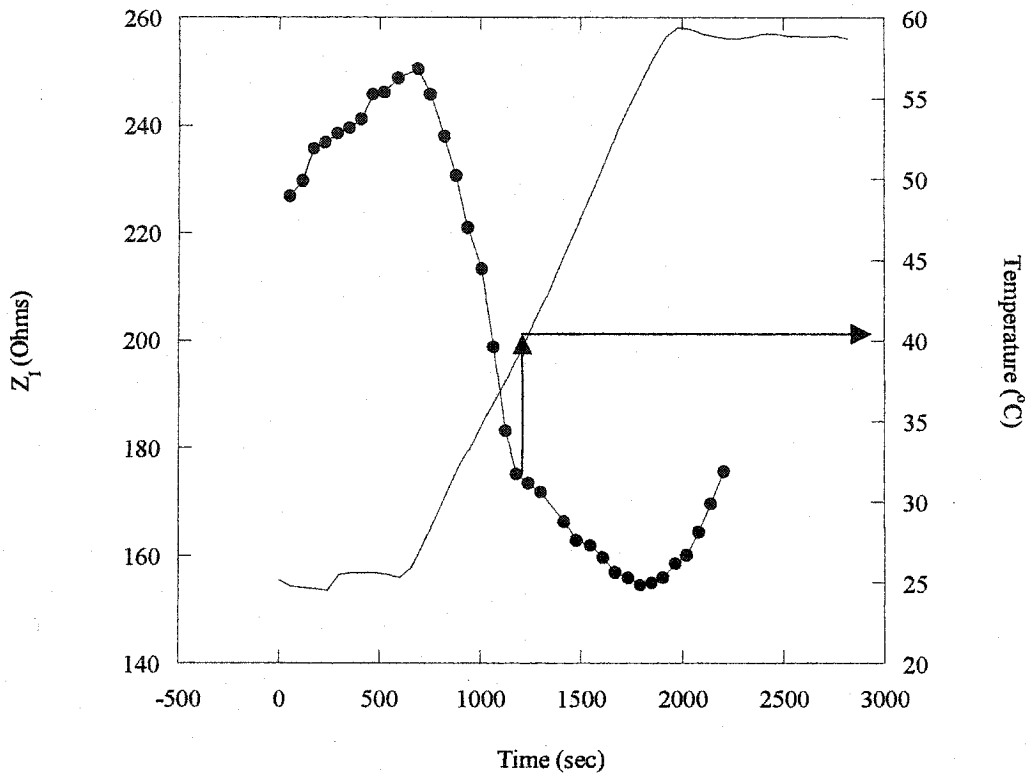

Figure 4.29 Imaginary impedance at -200mV and temperature variation (plain line) for a PNA-DNA mismatch T_m measurement.

Figure 4.30 shows that for a chip prepared just with single-stranded PNA does not generate an impedance drop with increasing temperature. This result suggests that the Z_I drop observed for the denaturation curves is due to the "release of DNA" from the chip. This initial rise and dip may be due to release of adsorbed PNA probe.

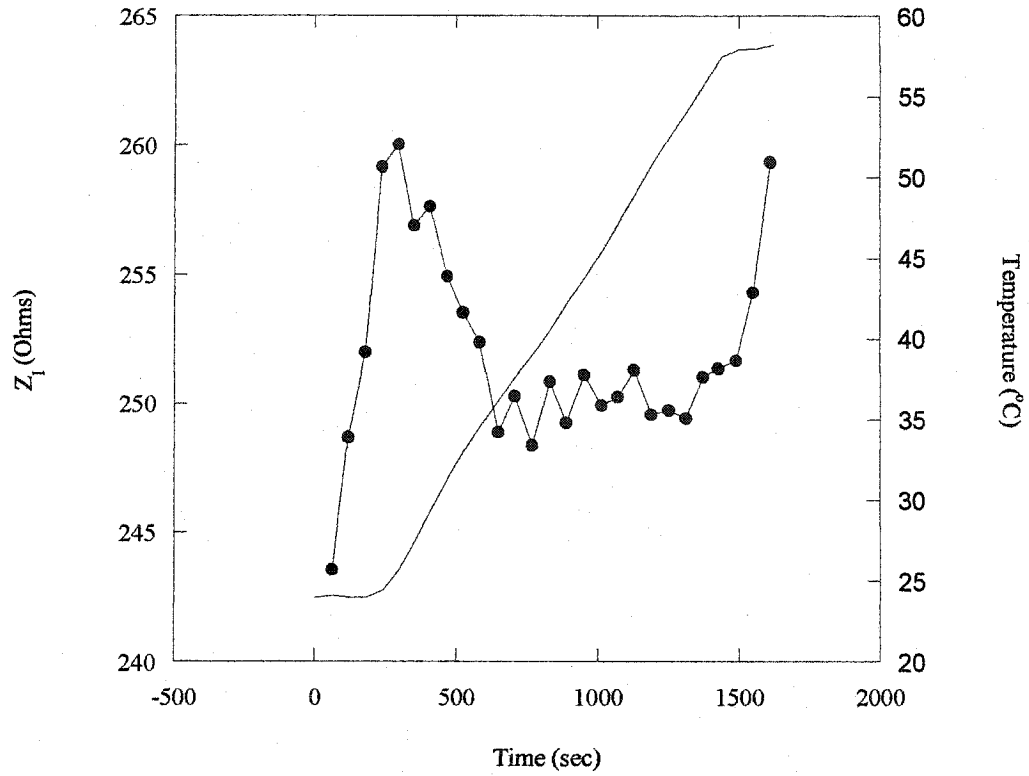

Figure 4.30 Change in impedance at -250mV for chip with just PNA probe layer and temperature ramp (plain line).

CHAPTER 5

CONCLUSIONS AND SUGGESTIONS FOR FUTURE WORK

5.1 Conclusions

Reproducible immobilization of ss-PNA probe layers was achieved through an epoxide/amine coupling reaction between the PNA amino linker and the epoxide group of GPTS, followed by hybridization with the complementary DNA sequences. There are two major components of a DNA biosensor that need to be optimized to ensure success of a biosensor: fabrication of the probe layer and signal transduction.

The first step is optimization of the functionalization method for attachment of the probe molecules. The silanization method was optimized. The silane mixture consisted of a 1% GPTS solution (mixture of ethanol, water, DPEA, GPTS). The optimal silanization time was determined to be four hours using the classical method of fluorescence. X-ray photoelectron spectroscopy confirmed the adequate functionalization of the surface and showed the coverage to be quite uniform.

Electrochemical impedance measurements are seen to provide a rapid, direct and sensitive approach for the detection of the immobilization and hybridization events, as corroborated by standard fluorescence measurements. These events are indicated by significant and reproducible variations in the semiconductor flat-band potential and out-of-phase impedances. Surface coverage of the probe PNA was 10^{13} molecules per cm^2 and 80% of the surface immobilized PNA have been hybridized.

The rate and extent of hybridization strongly depends on surface probe density. By

varying the reaction time of PNA with the solid support and by varying the probe solution concentration one can control the immobilized probe density. In the lowest probe density regimes, we found that the majority of the probes are hybridized (~100%), whereas at high probe density, the efficiencies drop to 80% and the kinetics are slower.

Two important requirements must be fulfilled in the operation of DNA biosensors. The biosensor must be very sensitive in the detection of the given nucleotide sequence. Our method is quite sensitive. We are able to detect the complementary DNA as low as 0.1ng/μL. In addition, the sensor must be highly specific, including detection of the change in a single nucleotide (point mutation, single-base mismatch). With this method we were able to detect a single-base mismatch. By measuring the change in impedance while applying a linear temperature ramp a single-base mismatch can be detected resulting in a lowering of the T_m by 12°C.

5.2 Suggestions for future work

For future work:

1. One major requirement for a successful biosensor is to have a well-oriented, not too dense probe layer that is highly selective and sensitive. Non-traditional approaches for the attachment of oligonucleotides to solid supports needs to be explored. One method is the use of PAMAM dendrimers which were developed by Tomalia et al. in the 1980s (104). Dendritic linker systems maximize immobilization capacity and hence increase the hybridization capacity by increasing the surface area available for binding of probe.

2. Further surface characterization of each fabrication step using atomic force microscopy.
3. Using this method to detect single-base mismatches by hybridizing the probe molecules with a mixture of perfectly matched and mismatched DNA.
4. Development of FET microarrays.

References

1. Cristopoulos, T. K. (1999) *Anal. Chem.* 71, 425R-438R.

2. Zhai, J., Hong, C. and Yang, R. (1997) *Biotechnol. Adv.* 15, 43-58.

3. Palacek, E., Fojta, M., Tomschick, M. and Wang, J. (1998) *Biosens. Bioelectron.* 13, 621-628.

4. Rowe-Taitt, C. A., Hazzard, J. W., Hoffman, K. E., Cras, J. J., Golden, J. P., Ligler, F. S. (2000) *Biosens. Bioelectron.* 15, 579-589.

5. Invitski, D., Abdel-Hamid, I., Atanasov, P., Wilkins, E., (1999) *Biosens. Bioelectron.* 14, 599-624.

6. Leonard, P., Stephen, H., Brennan, J., Dunne, L., John, Q., Chakraborty, T., O'Kennedy, R. (2003) *Enzyme and Microbial Tech.* 32, 3-13.

7. Baeumner, A., Cohen, R., Miksic, v., Min, J. (2003) *Biosens. Bioelectron.* 8 (4), 405-419.

8. Hartley, H. A. and Baumner, A. J. (2003) *Anal. Bioanal. Chem.* 376, 319-327.

9. Wang, J., Krause, R., Block, K., Musameh, M., Mulchandani, A., Schoning, M. J. (2003) *Biosens. Bioelectron.* 18, 255-260.

10. Kara, P., Meric, B., Zeytinoglu, A. and Ozsoz, M. (2004) *Anal. Chim. Acta,* 518, 1-2, 69-76.

11. Sato, Y., Fujimoto, K. and Kawaguchi, H. (2003) *Colloids and Surfaces B: Biointerfaces,* 27, 1, 23-31.

12. Yan, F., Erdem, A., Meric, B., Kerman, K., Ozsoz, M. and Sadik, O. A. (2001) *Electrochemistry Communications,* 3, 5, 224-228.

13. Wood, S. J. (1993) *Microchem. J.* 47, 330-337.

14. Persson, B., Stenhag, K., Nilsson, P., Larsson, A., Uhlen, M. and Nygren, P. A. (1997) *Anal. Biochem.* 246, 34-44.

15. Jordan, C. E., Frutos, A. G., Thiel, A. J. and Corn, R. M. (1997) *Anal. Chem.* 69, 4939-4947.

16. Nilsson, P., Persson, B., Larsson, A., Uhlen, M. and Nygren, P.A. (1997) *J. Mol. Recognit.* 10, 7-17.

17. Peterlinz, K. A. and Georgiadis, R. M. (1997) *J. Am. Chem. Soc.*119, 3401-3402.

18. Jensen, K. K., Orum, H., Nielsen, P. E. and Norden, B. (1997) *Biochemistry*, 36, 5072-5077.

19. Kai, E., Sawata, S., Ikebukuro, K., Iida, T., Honda, T. and Karube, I. (1999)*Anal. Chem.*71, 796-800.

20. He, L., Musick, M. D., Nicewarner, S. R., Salinas, F. G., Benkovic, S. J., Natan, M. J. and Keating, C. D. (2000) *J. Am. Chem. Soc.* 122, 9071-9077.

21. Nelson, B. P., Grimsrud, t. E., Liles, M. R., Goodman, R. M. and Corn, R. M. (2001) *Anal. Chem.* 73, 1-7.

22. Su, H., Kallury, K. M. R., Thompson, M. and Roach, A. (1994) *Anal. Chem.* 66, 769-777.

23. Su, H. and Thompson, M. (1995) *Biosens. Bioelectron.* 10, 329-340.

24. Cavic, B. A. and Thompson, M. (2000) *Anal. Chem.* 72, 1523-1531.

25. Fawcett, N., Evans, J., Chien, L. (1988) *Anal. Lett.* 21, 1099-1114.

26. Caruso, F., Rodda, E., Furlong, D., Nikura, K. and Okahata, Y. (1997) *Anal. Chem.* 69, 2043-2049.

27. Okahata, Y., Matsunobo, Y., Ijiro, K., Mukae, M., Murakami, A. and Makino, K. (1992) *J. Am. Chem. Soc.* 114, 8299-8300.

28. Towery, R. B., Fawcett, N. C., Zhang, P. and Evans, J. A. (2001) *Biosens. Bioelectron.* 16, 1-8.

29. Patolsky, F., Weizmann, Y. and Willner, I. (2002) *J. Am. Chem. Soc.* 124, 770-772.

30. Millan, K. M., Saraullo, A. and Mikkelsen, S. R. (1994) *Anal. Chem.* 66, 2943-2948.

31. Wang, J., Cai, X., Rivas, G. and Shiraishi, H. (1996) *Anal. Chim. Acta*, 326, 141-147.

32. Wang, J., Palacek, E., Nielsen, P. E., Rivas, G., Cai, X., Shiraishi, H., Dontha, N., Luo, D. and Farias, P. A. M. (1996) *J. Am. Chem. Soc.* 118, 7667-7670.

33. Mikkelsen, S. R. (1996) *Electroanalysis*,8, 15-19.

34. Wang, J., Cai, X., Rivas, G., Shiraishi, H. and Dontha, N. (1997) *Biosens. Bioelectron.* 12, 587-599.

35. Marraz, G., Chianela, I. And Mascini, M. (1999) *Biosens. Bioelectron.* 14, 43-51.

36. Chiti, G., Marraz, G. and Mascine, M. (2001) *Anal. Chim. Acta*, 427, 155-164.

37. Berney, H., Alderman, J., Lane, W. A. and Collins, J. K. (1997) *Sens. Actuators B*, 44, 578-584.

38. Patolsky, F., Zayats, M., Katz, E. and Willner, I. (1999) *Anal. Chem.* 71, 3171-3180.

39. Kharitonov, A. B., Shipway, A. N. and Willner, I. (1999) *Anal. Chem.* 71, 5441-5443.

40. Berggren, C., Stalhandske, P., Brundell, J. and Johansson, G. (1999) *Electroanalysis*, 11, 156-159.

41. Berney, H., West, J., Haefele, E., Alderman, J., Lane, W. and Collins, J. K. (2000) *Sens. Actuators B*, 68, 100-108.

42. Alfonota, L., Katz, E. and Willner, I. (2000) *Anal. Chem.*72, 927-935.

43. Souteyrand, E., Cloarec, J. P., Martin, J. R., Wilson, C., Lawrence, I., Mikkelsen, S. and Lawrence, M. F. (1997) *J. Phys. Chem. B*, 101, 2980-2985.

44. Martin, J. R., Souteyrand, E., Lawrence, M. F. and Mikkelsen, S. R. (2000) US Patent 6, 150, 106.

45. Cloarec, J. P., Deliagianis, N., Martin, J. R., Lawrence, I., Souteyrand, E., Polychronakos, C. and Lawrence, M. F. (2002) *Biosens. Bioelectron.* 17, 405-412.

46. Marquette, C., Lawrence, I., Polychronakos, C. and Lawrence, M. F. (2002) *Talanta*, 56, 763-768.

47. Egholm, M., Buchardt, O., Christensen, L., Behrens, C., Freler, S. M., Driver, D. A., Berg, R. H., Kim, S. K., Norden, B. and Nielsen, P. E. (1993) *Nature*, 365, 566-568.

48. Nielsens, P. E., Egholm, M. and Buchardt, O. (1994) *Bioconjugate Chem.* 5, 3-7.

49. Taylor, R. F. and Schultz, J. S. (1996) *Handbook of Chemical and Biological Sensors,* Institute of Physics Publishing, Bristol, UK.

50. Wang, J. (2000) *Nucleic Acids Research*, 28, 3011-3016.

51. Gooding, J. J. (2002) *Electroanalysis,* 14, 1149-1156.

52. Palacek, E., Fojta, M., Tomschik, M., Wang, J. (1998) *Biosens. Bioelectron.* 13, 621-628.

53. Moran, L. A., Scrimgeour, K. G., Horton, H. R., Ochs, R. S., Rawn, J. D. (1994) *Biochemistry*, Prentice-Hall, Inc., New Jersey.

54. Wang, J. (1998) *Biosens. Bioelectron.* 13, 757-762.

55. Nielsen, P. E. and Haaima, G. (1997) *Chemical Society Reviews*, 73-78.

56. Weiler, J., Gausepohl, H., Hauser, N., Jensen, O. N., and Hoheisel, J. D. (19xx) *Nucleic Acids Research*, 25, 2792-2799.

57. Eriksson, M. and Nielsen, P. E. (1996) *Quarterly Review of Biophysics*, 29, 4, 369-394.

58. Wang, J., Rivas, G., Cai, X., Chicharro, M., Parrado, C., Dontha, N., Begleiter, A., Mowat, M., Palacek, E., Nielsen, P. E. (1997b) *Anal. Chim. Acta*, 344, 111.

69. Macdonald, J. R. (1987) *Impedance Spectroscopy: Emphasizing Solid Materials and Systems*, John Wiley and Sons, Inc., New York.

60. Bard, A. J. and Faulkner, L. R. (2001) *Electrochemical methods: fundamentals and applications, 2nd edition,* Wiley, New York.

61. Finklea, H. (1988) *Semiconductor Electrodes,* Elsevier Science Publishers, Netherlands.

62. Kittel, C., (1976) *Introduction to Solid State Physics, 5th edition*, John Wiley & Sons, Inc., Canada.

63. Iler, R. K. (1979) *The Chemistry of Silica*, John Wiley & Sons.

64. Unger, K. K. (1979) *Porous silica, Journal of Chromatography Library*, 16, Elsevier Scientific Publishing Company.

65. Pludemann, E. P. (1991) *Silane Coupling Agents*, 2nd edition, Plenum Press.

66. Leyden, D. E. (1990) *Chemically modified surfaces, volume 1, "Silanes, surfaces and interfaces,"* Gordon & Breach Science Publishers.

67. McGovern, M. E., Kallury, K. M. R., Thompson, M. (1994) *Langmuir*, 10, 3607-3614.

68. Angst, D. L., Simmons, G. W. (1991) *Langmuir*, 7, 2236.

69. Blitz, J. P., Murthy, R. S. S., Leyden, D. E. (1988) *J. Colloid Interface Sci.* 121, 62.

70. Britcher, L. G., Kehoe, D. C., Matisons, J. G., Smart, R. St. C., Swincer, A. G. (1993) *Langmuir*, 9, 1609.

71. Kessel, C. R. (1991) *Langmuir*, 7, 532-538.

72. McGovern et al. (1994) *Langmuir*, 10.

73. Tripp, C. P., Hair, M. L. (1995) *Langmuir*, 11, 149-155.

74. Silberzan, P., Leger, L., Ausserre, D., Benattar, J. J. (1991) *Langmuir*, 7, 1647-1651.

75. Noll, W. (1968) *Chemstry and Technology of Silicones*, Academic Press, New York.

76. Corriu, R. J. P., Guerin, C. J. (1980) *Organomet. Chem.* 198, 231.

77. Sommer, L. H. (1965) *Stereochemistry, mechanism and silicon: An introduction to the dynamic stereochemistry and reaction mechanisms of silicon centers,* McGraw-Hill Inc., NY.

78. Blitz, J. P., Shreedhara Murthy, R. S., Leyden, D. E (1987) *J. Am. Chem. Soc.* 109, 7141-7145.

79. Burgener, M., Sanger, M., and Candrian, U. (2000) *Bioconjugate Chem.*11, 749-754.

80. Wang, J., Nielsen, P. E., Jiang, M., Cai, X., Fernandes, J. R., Grant, D. H., Ozsoz, M., Beglieter, A. and Mowat, M. (1997) *Anal. Chem.* 69, 5200-5202.

81. Skoog, D. A., Holler, F. J., Nieman, T. A. (1998) *Principles of Instrumental Analysis*, Harcourt Brace and Company, United States.

82. Riveiere, J. C. and Myhra, S. (1998) *Handbook of Surface and Interface Analysis*, Marcel Dekker, Inc., New York.

83. Lamture, J. B., Beattie, K. L., Burke, B. E., Eggers, M. D., Ehrlich, D. J., Fowler, R., Hollis, M. A., Kosicki, B. B., Reich, R. K. and Smith, S. R. (1994) *Nucleic Acids Res.* 22, 2121-2125.

84. Kallury, K. M. R., Krull, U. J., Thompson, M. (1988) *Anal. Chem.* 60, 169-172.

85. Reichl, R. and Gaukler, K. H. (1990) *Surf. Interface Anal.* 15, 211.

86. Laoharojanaphard, P., Lin, T. J., Stoffer, J. O. (1990) *J. Appl. Polymer Sci.* 40, 369.

87. Graham, M. J. (1995) *Corrosion Science*, 37, 9, 1377-1397.

88. Moulder, J. F. (Ed) (1992) *Handbook of X-ray Photoelectron Spectroscopy, 1st editions*, Elmer, Corporation, Eden Prairie, Minnesota.

89. Gooding, J. J. (2002) *Electroanalysis*, 14, 1149-1156.

90. Jensen, K. K., Orum, H., Nielsen, P. E., Norden, B. (1997) *Biochemistry*, 36, 5072-5077.

91. Peterson, A. W., Heaton, R. J., Georgiadis, R. M. (2001) *Nucleic Acids Res.* 29, 5163-5168.

92. Henry, M. R., Stevens, P. W., Sun, J., and Kelso, D. M. (1999) *Anal. Biochem.* 276, 204.

93. Zeng, J., Almadidy, A., Watterson, J., Krull, U. J. (2003) *Sens. Actuators A*, 90, 68.

94. Hagan, M. F., Chakraborty, A. K. (2004) *J. of Chemical Physics*, 120, 4958-4968.

96. Piunno, P. A. E., Watterson, J., Wust, C. C., Krull, U. J. (1999) *Anal. Chim. Acta.* 400, 73-89.

96. Watterson, J. H., Piunno, P. A. E., Wust, C. C., and Krull, U. J. (2000) *Langmuir*, 16, 4984-4992.

97. Nelson, J. W., Martin, F. H., Tinoco, I. (1981) *J. Biopolymers*, 20, 2509.

98. Marky, L. A. and Breslauer, K. J. (1987) *Biopolymers*, 26, 1601-1620.

99. Jensen, K. K., Orum, H., Nielsen, P. E., Norden, B. (1997) *Biochemistry*, 36, 5072-5077.

100. http://www. Biocorp. ca/

101. Howley, P. M., Israel, M. F., Law, M-F and Martin, M. A. (1979) *J. Biol. Chem.* 254, 4876-4883.

102. Nelson, J. W., Martin, F. H., Tinoco, I. (1981) *J. Biopolymers*, 20, 2509.

103. Su, H., Williams, P., Thompson, M. (1995) *Anal. Chem.* 67, 1010.

104. Tomalia, P. A., Naylor, A. M. and Goddard, W. A., Angew. Chem. Int. Fd. Engl. (1990), 29, 138-175.